Thermodynamics of Gross Neveu Models

Gökçe K. Başar, Ph.D.

University of Connecticut, 2011

We present the detailed properties of the phase diagrams of massless (1+1)-dimensional Gross-Neveu and Nambu-Jona-Lasinio models with discrete and continuous chiral symmetry by studying the exact, inhomogeneous solutions of the functional gap equation. We show that in addition to spontaneous breaking of continuous chiral symmetry, the Nambu-Jona-Lasinio model also exhibits translational symmetry breaking at finite density below a critical temperature. The spatially inhomogeneous phase, the "chiral spiral" is a periodic spiral in the chiral plane with a constant charge density. The mathematical method we develop to study the inhomogeneous phases, allows one to reduce the functional gap equation for the inhomogeneous condensate, to a nonlinear Schrödinger equation, which is exactly soluble. The general solution is a crystalline array of kinks and anti-kinks and includes as special cases all previously known real and complex condensate solutions to the gap equation. Furthermore, the associated Dirac equation is also soluble with this inhomogeneous chiral condensate, and the exact spectral

properties are derived. Analyzing the thermodynamic properties of these solutions, we show the stability of the chiral spiral phase against the more general "twisted kink crystal" solution of the gap equation. This situation should be contrasted with the Gross-Neveu model, which has a discrete chiral symmetry, and for which the phase diagram has a crystalline phase with a periodic kink crystal. Then we argue that the existence of the chiral spiral phase is ubiquitous in (1+1)-dimensional models exhibiting continuous chiral symmetry. We further develop a connection between the Ginzburg-Landau expansion of the thermodynamic grand potential and a well-known mathematical integrable hierarchy known as the Ablowitz-Kaup-Newell-Segur (AKNS) hierarchy.

Thermodynamics of Gross Neveu Models

Gökçe K. Başar

M.S., University of Connecticut, Storrs, CT, 2007

B.S., Middle East Technical University, Ankara, Turkey, 2006

A Dissertation

Submitted in Partial Fullfilment of the

Requirements for the Degree of

Doctor of Philosophy

at the

University of Connecticut

2011

APPROVAL PAGE

Doctor of Philosophy Dissertation

Thermodynamics of Gross Neveu Models

Presented by

Gökçe K. Başar, M.S.

Major Advisor

Gerald V. Dunne

Associate Advisor

Alex Kovner

Associate Advisor

Thomas C. Blum

University of Connecticut

2011

TABLE OF CONTENTS

LIST OF FIGURES

Chapter 1

Introduction

1.1 An overview of QCD at nonzero T and μ

Most of the matter that we see around us is made up of protons and neutrons which are members of a larger family called hadrons. The microscopic properties of hadronic matter are successfully described by the well established theory; Quantum Chromodynamics (QCD). However, the fundamental degrees of freedom of QCD are not protons or neutrons, but quarks and gluons. Quarks carry charges called the color charge and interact with each other by exchanging gluons in analogy to the way electrons interact with each other by exchanging photons, described by Quantum Electrodynamics (QED). Gluons themselves are also charged; therefore they self interact, as opposed to the photons which are neutral and do not self interact. Also, there are multiple "flavors" of quarks in the theory with different electrical charges and masses.

A striking feature of QCD is that, the coupling constant gets weaker at shorter length scales. This is the celebrated property called *asymptotic freedom*

[1]. As an immediate result of asymptotic freedom, perturbation theory can be safely used to investigate high energy processes and explain phenomena such as Bjorken scaling [2]; which seeded the idea of asymptotic freedom in the first place. Looking from the other side, the theory is strongly interacting at longer length scales or lower energies. The energy scale where the coupling is of the order unity is called Λ_{QCD} and it is approximately the size of a hadron ($\sim$1 fm^{-1}). In particular, this means the ground state of QCD and its low energy excitations are not accessible to perturbation theory. The low energy excitations are quasi-particles of quarks and gluons and they constitute the form of matter we see around: the hadrons. The hadronic states exhibit two phenomena: they are color-neutral and, compared to the mass of the quarks, they are heavy. The first phenomenon is called confinement. This confining nature of QCD says that single quarks or gluons do not exist as isolated states, because they carry color charge. It is still an open problem to derive confinement starting from the first principles of QCD. The second phenomenon is *chiral symmetry breaking*. In the limit where the quarks are massless, the QCD Lagrangian is invariant under a continuous symmetry called chiral symmetry. The vacuum ground state and its excitations, however, break that symmetry spontaneously by developing masses due to the interactions. Notably QCD with massless quarks is also scale invariant and the existence of this dynamically generated mass scale breaks the scale symmetry. This is known as dimensional transmutation, where the dynamics of a dimension-

free theory introduces a dimensionful parameter and the dimensionless coupling depends on the dimensionful parameter. In reality, the quarks have masses and the chiral symmetry is broken explicitly. Yet, the mass of the quasi-particle masses are vastly larger than quark masses[1]. This difference is again is related to chiral symmetry breaking.

At nonzero temperature and density, QCD has different phases with very different thermal and transport properties (see selected reviews [3] and the references therein). A very schematic phase diagram of QCD is shown below in Figure 1.1. The main order parameters characterizing the phases are confinement and chiral symmetry. In the confined phase, the phases are described by hadronic matter; whereas in the deconfined phase, they are described by quark matter. The chiral symmetry characterizes the excitation modes around the ground state.

At very high temperatures, entropy wins over order and the thermal ground state has all the symmetries of the Lagrangian. This phase is called the quark gluon plasma (QGP). The quasi-particles of the quark gluon plasma are weakly interacting, screened, deconfined quarks and gluons. The long range interactions between quarks are screened; hence the name "plasma". The screening length (also known as Debye length) is $1/g(T)T$ where g is the QCD coupling constant. As the temperature approaches the transition temperature, the QGP becomes

[1] The lightest quarks have masses at the order of 1 MeV; whereas the proton mass is 938 MeV.

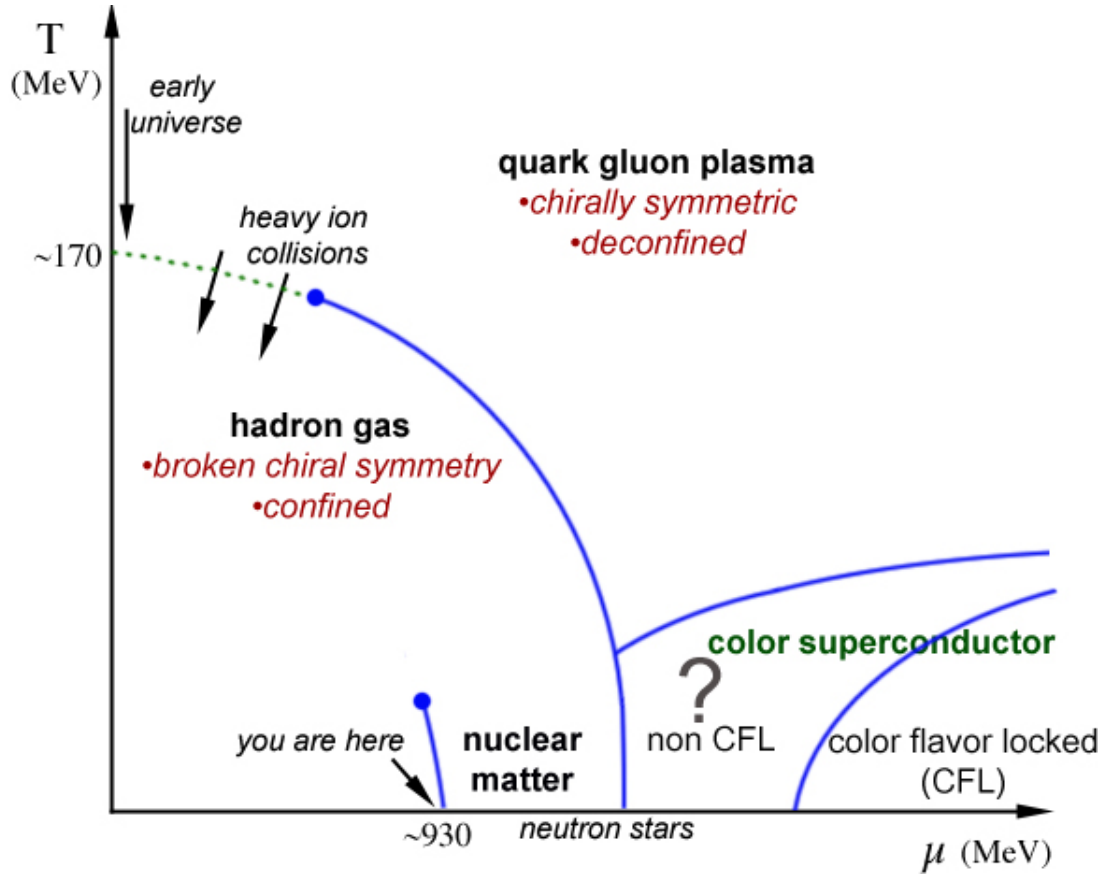

Fig. 1.1: A schematic phase diagram of QCD.

strongly coupled. The strongly coupled QGP is explored in heavy ion collision experiments at RHIC and LHC and has been shown to exhibit a set of rich and interesting properties such as a very low viscosity to entropy ratio putting it at the top of the list of the most perfect fluids. However the theoretical tools to investigate the properties of the strongly interacting QGP are very limited. Lattice QCD calculations provide solid information at zero density (i.e on the $\mu = 0$ axis), indicating a rapid crossover between the hadronic phase and QGP[4, 5]. The transition temperature is $T_c \sim 170$ MeV[4] where both the confinement-deconfinement

transition and chiral symmetry breaking happens. The crossover nature is due to the bare masses of the quarks where there is no total restoration of chiral symmetry. At nonzero μ however, lattice calculations suffer from the fermion sign problem which hinders the Euclidean computations. Analytical continuations [5] of the calculations with imaginary potential show that the crossover extends to the region of small μ near T_c. This is shown by the dashed green line in Fig. 1.1. It is hypothesized that the crossover ends with a second order critical point followed by a first order phase transition. One of the aims of the heavy ion collision experiments is to search for this critical point [6]. In addition to lattice QCD data, the AdS/CFT correspondence provides some useful insights into the strongly coupled QGP, such as the conjectured universal lower bound to the viscosity to entropy ratio [7].

In the regime of cold and extreme density, where the chemical potential $\mu_B \gg T$, quarks form Cooper pairs and these pairs condense, forming a superconducting phase. This is due to the famous Bardeen-Cooper-Schriffer (BCS) argument, stating that at low temperature and high enough chemical potential, the existence of any attractive interaction between the fermions will lower the free energy and cause the fermions near the Fermi surface to form pairs. In QCD, the Coulomb interaction between the quarks is already attractive and the BCS argument arises naturally in dense quark matter. Of course explicit theoretical calculations are limited to the region where $\mu_B \gg \Lambda_{QCD}$ where the quarks are

weakly interacting. In this regime, it is shown that (see for example [8]) the favored pairing pattern identifies the color and flavor of the paired quarks. This phase is called the color-flavor locked (CFL) phase and it is the phase where the symmetry is maximally broken. In the intermediate density regime $\mu_b \gtrsim \Lambda_{QCD}$, the situation is much less clear. There are many different possible symmetry breaking patterns for the quark matter and this is the region that hosts a number of different proposals for the preferred phase. It is also the relevant regime for the dynamics of neutron star cores, where the high density of nuclear matter overcomes the confining force leading to deconfined quark matter.

As the chemical potential approaches $\mu_B \sim \mathcal{O}(\text{GeV})$, the quark matter turns into nuclear matter, which is essentially a dilute Fermi liquid of protons and neutrons. This phase is known as the nuclear superfluid. Around $\mu_B \sim 930$ MeV$\equiv m_{proton}$, the nuclear liquid turns into a nuclear gas by a first order transition. As the temperature increases, the first order line ends with a second order critical point.

In general, in the intermediate regime of the QCD phase diagram where the phases are subject to strong coupling, our knowledge is very limited due to the lack of powerful theoretical and computational tools. The main aim of this dissertation is to address similar questions to chiral symmetry breaking and dimensional transmutation by studying simpler toy models; namely the Gross-Neveu and Nambu-Jona-Lasinio models. The advantage of this approach is that

we will be able to perform analytical calculations and study the mentioned physical phenomena in a controlled way. The outcome of our studies is expected to give some insights into these phenomena.

Throughout the rest of this chapter we review the basic properties of the Gross-Neveu and Nambu-Jona-Lasinio models following the original references [9, 10] and the references therein. In Chapter 2, we introduce a method to study translational symmetry breaking in these models in an analytical way. This chapter is mainly based on the publications [11, 12]. Then in Chapter 3 by studying the thermodynamical properties of the models, we demonstrate that inhomogeneous phases, in which translational symmetry is broken, appear in the associated phase phase diagrams. The results in this chapter are published in [13]. The last chapter, Chapter 4 is devoted to a particular application of our results to heavy ion collisions, which is published as [14]. Some technical ingredients, that we refer in the dissertation are summarized in Appendices A and B.

1.2 Gross-Neveu models as QCD-like models

A seminal work introducing the concept of dynamical symmetry breaking to particle physics is due to Nambu and Jona-Lasinio [9]. Inspired by the microscopic theory of superconductivity, Nambu and Jona-Lasinio (NJL) introduced a model where the mass of the fermion is generated dynamically through a self interaction

of the form:

$$\mathcal{L} = \bar{\psi}\, i\partial\!\!\!/\, \psi + \frac{G^2}{2}\left[(\bar{\psi}\psi)^2 + (\bar{\psi} i\gamma^5 \psi)^2\right] \tag{1.1}$$

In addition to the global U(1) gauge symmetry $\psi \rightarrow e^{i\theta}\,\psi$, this model has also a chiral U(1) symmetry $\psi \rightarrow e^{i\theta\gamma^5}\,\psi$. In superconductivity, the electrons form bound states (Cooper pairs) by attractive lattice interactions, and these bound states condense in the ground state. The low energy excitations of the system are the electron-hole quasi-particles with opposite charge and the same spin. The mixing between electrons and holes is due to the dynamically generated gap in the low energy spectrum. Furthermore, the condensation of Cooper pairs spontaneously breaks the U(1) gauge symmetry. As an immediate result; the photon becomes massive, a phenomenon known as the Meissner effect. The characteristic inverse mass scale is known as the London penetration depth.

In the Nambu Jona-Lasinio (in short NJL) model of nucleons, the self interaction causes fermion-anti fermion bound states to condense, generating a mass gap in the spectrum. The quasi-particles in this case are fermions with opposite chirality and the same charge. As opposed to the U(1) gauge symmetry, it is the axial (or chiral) U(1) symmetry which is spontaneously broken. Remarkably, this idea of treating the observed massive nucleons as quasi-particles of a manifestly chirally symmetric theory where the symmetry is broken dynamically, came long before QCD. However the NJL theory in 4 space-time dimensions is not renormalizable and an explicit cutoff has to be introduced in the calculations. The

existence of the cutoff destroys the Lorentz symmetry and makes the outcome of the theory less fundamental.

The second remarkable improvement came from the work of Gross and Neveu [10]. This was just after the introduction of non-abelian gauge theory as the theory of strong interactions. They considered the same type of theory with a scalar four-fermion interaction:

$$\mathcal{L}_{GN} = \bar{\psi}\, i\partial\!\!\!/\, \psi + \frac{g^2}{2}(\bar{\psi}\psi)^2 \tag{1.2}$$

in *two* space-time dimensions (which will be denoted as GN_2 hereafter). One important point is that there are N_f number of fermion flavors in the model, so that $\bar{\psi}\psi$ actually denotes:

$$\bar{\psi}\psi \equiv \sum_{a=1}^{N_f} \bar{\psi}_a \psi_a \tag{1.3}$$

For the sake of notational simplicity, we will suppress the flavor indices from now on. This theory has a *discrete* chiral symmetry:

$$\begin{aligned} &\psi \to \gamma^5 \psi \qquad , \qquad \bar{\psi} \to -\bar{\psi}\gamma^5 \\ &\Rightarrow \bar{\psi}\psi \to -\bar{\psi}\psi \end{aligned} \tag{1.4}$$

In two dimensions two important new things happen: the theory is renormalizable and it is asymptotically free. In fact, the GN_2 was the first example of an asymptotically free theory other than non-abelian gauge theory. Therefore, in addition to dynamical symmetry breaking, it also captures two other essential features of

QCD; renormalizability and asymptotic freedom. Moreover, it was also argued in [10] that all these phenomena are interrelated. Yet another significant point is that in two space-time dimensions, the coupling constant g is dimensionless and the theory is scale invariant. The dynamical mass generation breaks also the scale invariance. Recall that this is precisely the dimensional transmutation described above.

The original NJL model in *two* space-time dimensions (which will be denoted as NJL_2 hereafter):

$$\mathcal{L}_{NJL} = \bar{\psi}\, i\partial\!\!\!/\, \psi + \frac{g^2}{2}\left[(\bar{\psi}\psi)^2 + (\bar{\psi} i\gamma^5 \psi)^2\right] \tag{1.5}$$

with continuous chiral symmetry

$$\psi \to e^{i\theta\gamma^5}\,\psi \qquad , \qquad \bar{\psi} \to \bar{\psi}\, e^{i\theta\gamma^5} \tag{1.6}$$

was also investigated in the paper [10]. Again, there are N_f fermion flavors and $\bar{\psi}\psi \equiv \sum_{a=1}^{N_f} \bar{\psi}_a \psi_a \quad , \quad \bar{\psi}\gamma^5\psi \equiv \sum_{a=1}^{N_f} \bar{\psi}_a \gamma^5 \psi_a$

Now we quickly recapitulate the crucial properties of the GN_2 model. The same computations can be carried out almost identically in the NJL_2 model. We will point out the main difference between these two models later, at the end of this chapter. A very useful approach to investigate the symmetry breaking ground states of the theory is to make a Hubbard-Stratonovich transformation where a real auxiliary field Δ is introduced and the Gross-Neveu (GN_2) Lagrangian 1.2 is

re-expressed as:

$$\mathcal{L}_{GN} = \bar{\psi}\left(i\partial\!\!\!/ - \Delta\right)\psi - \frac{1}{2g^2}\Delta^2 \tag{1.7}$$

The auxiliary field Δ has no dynamics and can be eliminated by the classical equations of motion or a gaussian integration in the path integral to return back to 1.2. The advantage of studying the equivalent Lagrangian (1.7) is that it makes the spontaneous symmetry breaking self-evident. Notice that in order to maintain the discrete chiral symmetry (1.4) in the Lagrangian (1.7), Δ has to change sign along with (1.4). Therefore any state with $\Delta \neq 0$ breaks the chiral symmetry and is an example of spontaneous symmetry breaking.

To keep the discussion simple, we restrict ourselves to translationally invariant states and concentrate on chiral symmetry breaking in this chapter. Translational symmetry breaking, which constitutes a substantial part of this dissertation, will be introduced later when we consider these models at nonzero density. Semiclassically, the ground state of the theory is the minimum of the effective potential which is the sum of all irreducible diagrams that have an even number of external Δ legs with zero momentum, as shown in Figure 1.2. The dashed and solid lines represent Δ and fermion propagators respectively.

We now compute the potential action in the limit where the number of fermion flavors N_f is large. More precisely we let $N_f \to \infty$ by keeping the so called 't Hooft coupling $g^2 N_f$ finite.

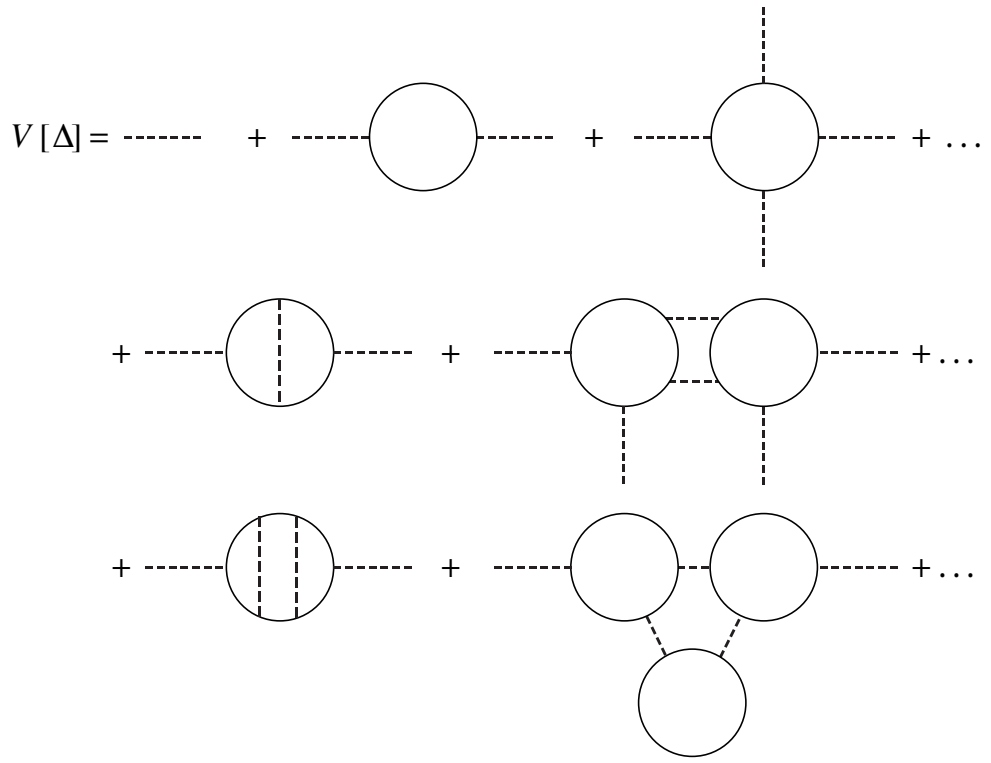

Fig. 1.2: Diagrammatic representation of the effective potential $V[\Delta]$.

1.2.1 Large N_f

The large N approach is a very powerful technique, invented by G. 't Hooft [15] in studying nonabelian gauge theories where $N \to \infty$ is the number of colors and used widely in many other models (for example see "$1/N$" in [16]). The basic idea is to reorganize the partition function as a series in $1/N$, where N is the number of fields. In principle, each term in the expansion is a resummation of a perturbation series; therefore the large N expansion provides substantial information beyond the perturbative regime. Even though this resummation cannot be performed

explicitly in QCD, it still is an important tool in studying it.[2] On the other hand, in the Gross-Neveu models, it is indeed possible to explicitly sum all the Feynman diagrams in leading order at $1/N$. As a result, all of our results are valid for *any* 't Hooft coupling $g^2 N_f$.

Returning to the GN_2 model, we see that a fermion loop carries a factor of N_f from the sum over fermion flavors and an internal Δ propagator carries a factor of $g^2 \propto 1/N_f$. Also, in any diagram with two or more loops, any loop has to be connected with at least two Δ propagators, due to irreducibility. As a result, at the leading order in the $1/N_f$ expansion, the effective potential has only one loop terms with no internal Δ propagators. These are the terms in the first line in Fig 1.2 and they are of order N_f. The examples in the second and third lines are of order N_f^0 and $1/N_f$ respectively and, so are sub-leading in the expansion.

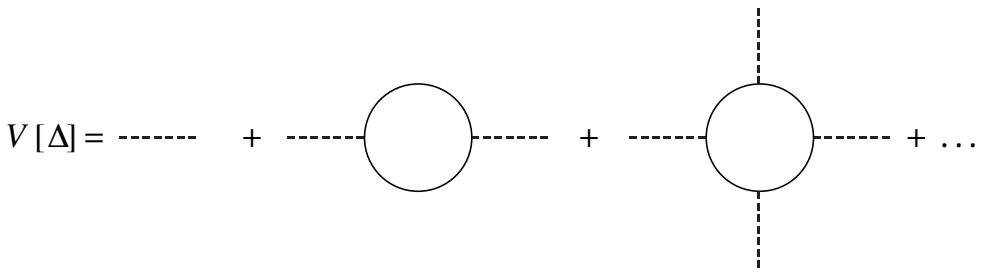

Fig. 1.3: $V[\Delta]$ to the leading order in $1/N_f$ expansion.

[2] Strictly speaking there are two separate large N limits in QCD; the limit where the number of quark flavors N_f is large or the number of colors N_c is large. Since asymptotic freedom depends nontrivially on both N_f and N_c, the physical results are sensitive to how these limits are taken.

This one loop effective action can be calculated straightforwardly [10, 16]. Here we perform the calculation in Euclidean space.

$$\begin{aligned} V[\Delta] &= \frac{1}{2g^2}\Delta^2 - N_f \sum_{n=1}^{\infty} \frac{(n-1)!}{n!} \int \frac{d^2k}{(2\pi)^2} \left(\frac{\Delta^2}{k^2}\right)^n \\ &= N_f \left[\frac{1}{2g^2 N_f}\Delta^2 - \int \frac{d^2k}{(2\pi)^2} \ln\left(1+\frac{\Delta^2}{k^2}\right)\right] \end{aligned} \tag{1.8}$$

Here the degeneracy factor $(n-1)!$ comes from the cyclic symmetry of a graph with n legs. Alternatively, the same result can be obtained by integrating out the fermions in the path integral:

$$\begin{aligned} \mathcal{Z} &= \int \mathcal{D}\Delta\mathcal{D}\bar{\psi}\mathcal{D}\psi \exp\left[i \int d^2x \left(\bar{\psi}\left(i\partial\!\!\!/ - \Delta\right)\psi - \frac{1}{2g^2}\Delta^2\right)\right] \\ &= \int \mathcal{D}\Delta \exp\left[-\frac{i}{2g^2}\int \Delta^2 + N_f \ln\det(i\partial\!\!\!/ - \Delta)\right] \\ &= \int \mathcal{D}\Delta \exp(i\, S[\Delta]) \end{aligned} \tag{1.9}$$

Here the effective action $S[\Delta]$ is recognized as $-V[\Delta]$[3] after a Wick rotation $k_0 \to ik_0$. Since $S[\Delta] \propto N_f$; as $N_f \to \infty$, the path integral will be dominated by the minimum of $V[\Delta]$.

1.2.2 Asymptotic freedom, dimensional transmutation and chiral symmetry breaking

The expression in (1.8) is UV divergent and has has to be regulated. We choose to regulate it by putting a cutoff Λ on the momentum integral. Hence we obtain

[3] Not that $\ln\det = \mathrm{tr}\ \ln$.

the effective potential (per flavor):

$$V[\Delta] = \Delta^2 \left[\frac{1}{2g^2 N_f} - \frac{1}{4\pi} \ln \left(\frac{\Lambda^2}{\Delta^2} + 3 \right) \right] \tag{1.10}$$

As usual, the cutoff dependence is absorbed in the coupling constant $g \equiv g(\Lambda)$[4] by imposing the condition that the effective potential is cutoff independent:

$$\begin{aligned} 0 &= \frac{d}{d\ln\Lambda} V[\Delta; g(\Lambda), \Lambda] \\ &= \frac{1}{\pi} + \frac{d}{d\ln\Lambda} \left(\frac{1}{g^2 N_f} \right) \end{aligned} \tag{1.11}$$

The renormalization group (RG) flow equation (1.11) describes how the coupling strength varies as the energy scale changes. Choosing a fixed, but arbitrary scale M_0, we see:

$$g^2 N_f(\Lambda) = \frac{g^2 N_f(M_0)}{1 + \frac{g^2 N_f(M_0)}{\pi} \ln \frac{\Lambda}{M_0}} \tag{1.12}$$

It is clear that as the energy scale Λ increases, the coupling strength gets weaker. This is the manifestation of asymptotic freedom. Alternatively, the negative sign in the beta function to the leading order:

$$\beta(g) = \frac{d\, g(\Lambda)}{d\ln\Lambda} = -\frac{g^3\, N_f}{2\pi} \tag{1.13}$$

is an indicator of the asymptotic freedom.

Another aspect of the RG flow (1.12) of the theory is dimensional transmutation. After renormalization, the effective potential (1.10) is written as:

$$V[\Delta] = \Delta^2 \left[\frac{1}{2g^2 N_f(M_0)} + \frac{1}{4\pi} \ln \left(\frac{\Delta^2}{M_0^2} - 3 \right) \right] \tag{1.14}$$

[4] Here what we actually mean is $g^2 N_f \equiv g^2 N_f(\Lambda)$, since it is the 't Hooft coupling which is nonzero and finite. But to keep the notation simple we stick with the notation $g(\Lambda)$.

It seems that $V[\Delta]$ depends on two parameters $g^2 N_f$ and M_0; however any change in the mass scale M_0 is compensated by the corresponding change in $g^2 N_f$. As a result, having both the coupling constant and M_0 is redundant. We fix M_0 such that $g^2 N_f(M_0) = \pi$. Therefore, the only parameter that the renormalized effective potential depends on is M_0:

$$V[\Delta] = \frac{\Delta^2}{4\pi}\left[\ln\left(\frac{\Delta^2}{M_0^2}\right) - 1\right] \tag{1.15}$$

The ground state of the theory is the minimum of the effective potential (1.15).

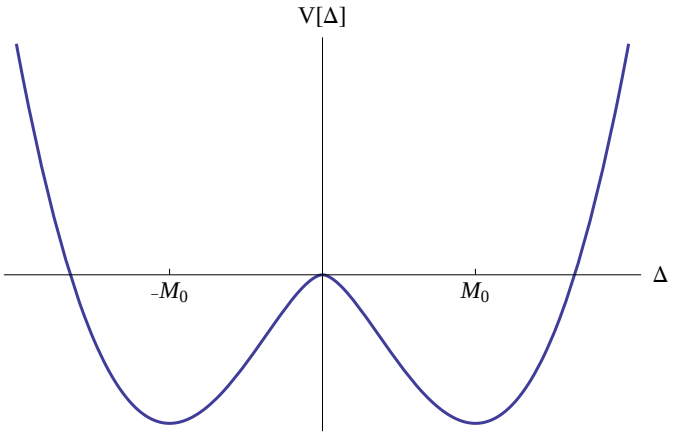

Fig. 1.4: Plot of the effective potential $V[\Delta]$.

The minimization condition is known as the *gap equation* in the literature.

$$\begin{aligned} 0 &= \frac{\delta V[\Delta]}{\delta \Delta}\Big|_{\Delta_0} \\ \Delta_0 = M_0 &= \Lambda\, e^{1-\frac{\pi}{g^2 N_f(\Lambda)}} \end{aligned} \tag{1.16}$$

Notice that the minimum is at a nonzero value of Δ [see Fig. 1.4]. As a result, we started with a scale invariant theory (1.2) with a dimensionless coupling constant g

and wound up with free massive fermions, with mass M_0, as low energy excitations. This mass is said to be dynamically generated by the dimensionless interaction: hence the name "dimensional transmutation". Moreover the appearance of the fermion mass obviously breaks the chiral symmetry (1.4). This is an example of the aforementioned dynamical symmetry breaking. Notably, being an explicit sum over all the one loop diagrams, the final result (1.16) depends on the coupling constant in a non-perturbative way and is valid for any value of the 't Hooft coupling.

Dimensional transmutation is a typical phenomenon in an asymptotically free theory. The coupling gets stronger at large distances (i.e, in the infrared or IR limit), and the vacuum ground state of the theory cannot be described perturbatively. As discussed in the previous section, this is also the case for QCD whose vacuum has neither massless gluons nor quarks with small bare masses; rather mesons and baryons as low energy excitations. The scale symmetry (in QCD with massless quarks) is also broken by Λ_{QCD} which is roughly the size of a nucleon.

1.2.3 Large N_f part 2: continuous symmetry breaking in 2d

We now focus on the distinguishing feature of the NJL_2 model; namely the *continuous* chiral symmetry breaking, which is absent in GN_2 model which exhibits *discrete* chiral symmetry breaking. Along the same lines as the previous chapter,

we introduce an auxiliary field Δ and write:

$$\mathcal{L}_{NJL} = \bar{\psi}\left(i\partial\!\!\!/ - \frac{1}{2}(1-\gamma^5)\Delta - \frac{1}{2}(1+\gamma^5)\Delta^*\right)\psi - \frac{1}{2g^2}|\Delta|^2 \tag{1.17}$$

Here the order parameter Δ is *complex*. Its real and imaginary parts are associated with scalar ($\bar{\psi}\psi$) and pseudoscalar ($\bar{\psi}\gamma^5\psi$) condensates respectively. The continuous chiral symmetry (1.6) is realized as $\Delta \to \Delta e^{2i\theta\gamma^5}$. Another way to express the coupling with the auxiliary field is:

$$\frac{1}{2}(1-\gamma^5)\Delta + \frac{1}{2}(1+\gamma^5)\Delta^* = M(x)e^{i\gamma^5\chi(x)} \tag{1.18}$$

where $\Delta(x) = M(x)e^{i\chi(x)}$. Naively, it might seem that the chiral symmetry breaking is identified with χ acquiring a nonzero vacuum expectation value and its fluctuations being the usual massless Goldstone excitations. However this is not possible in two space-time dimensions, a property known as the Coleman-Mermin-Wagner-Hohenberg theorem [17]. The fluctuations of the massless mode are logarithmic and grow in the infrared regime, destroying the long range order. To see this let us follow [18] and look at the two point correlation function:

$$\langle\bar{\psi}(1+\gamma^5)\psi(x)\bar{\psi}(1-\gamma^5)\psi(0)\rangle \sim \langle e^{-i\chi(x)}e^{i\chi(0)}\rangle \tag{1.19}$$

Since χ is a massless scalar field, the expectation value can easily be calculated.

$$\langle e^{-i\chi(x)}e^{i\chi(0)}\rangle \sim e^{-2\pi G(x)} \sim e^{-1/N_f \ln(|x|)} = |x|^{-1/N_f} \tag{1.20}$$

It is clear that long range order is precluded by the logarithmic behavior of the two dimensional propagator. However, the large N_f limit provides a way to sustain

long range order. Notice that:

$$e^{-1/N_f \ln(|x|)} = 1 - \frac{1}{N_f}\ln(|x|) + \mathcal{O}(1/N_f^2) \tag{1.21}$$

To leading order in the above expansion as $N_f \to \infty$, the two point correlator (1.18) takes a constant value indicating the existence of the long range order and chiral symmetry breaking. Physically, the large number of degrees of freedom suppresses the long range fluctuations. In general the power law type of behavior (1.20) of the order parameter is known as quasi-long range order. As opposed to the usual exponential decay, it decays much more slowly and the spatial size of the almost ordered region grows as N_f increases. The important implication is that in two space-time dimensions we can indeed study *continuum* chiral symmetry breaking in the large N_f limit.

Chapter 2

Inhomogeneous phases and their properties

At this chapter we introduce a new method to solve for the static and *inhomogeneous* ground states of GN_2 and NJL_2 models. Our method generalizes the previous works [19, 20, 21, 22] addressed the same problem by using various methods. As explained in Chapter 1, the ground states of the theory are the minima of an effective potential found by solving the functional gap equation. Our method allows one to reduce the *functional* gap equation (1.16) for inhomogeneous configurations into an ordinary differential equation which is further soluble. Further, we also present the solution of the associated Dirac equation and study the properties of the spinor solutions.

2.1 Effective action, gap equation, Hartree-Fock approximation

We start with setting the background of the problem, namely the inhomogeneous gap equation.

2.1.1 Gap equation

The partition function for the NJL_2 model is:

$$\mathcal{Z} = \int \mathcal{D}\bar{\psi}\mathcal{D}\psi \exp\left[i\int d^2x \left(\bar{\psi}i\not{\partial}\psi + \frac{g^2}{2}[(\bar{\psi}\psi)^2 + (\bar{\psi}i\gamma^5\psi)^2]\right)\right] \tag{2.1}$$

In the same manner as the discussion in the previous chapter (Section 1.2.3), we apply a Hubbard-Stratonovich transformation to get:

$$\begin{aligned}\mathcal{Z} &= \int \mathcal{D}\bar{\psi}\mathcal{D}\psi\mathcal{D}\Delta\mathcal{D}\Delta^* \exp\left[i\int d^2x \left(\bar{\psi}(i\not{\partial} - \frac{1}{2}(1-\gamma^5)\Delta - \frac{1}{2}(1+\gamma^5)\Delta^*)\psi \right.\right. \\ &\qquad \left.\left. -\frac{1}{2g^2}|\Delta|^2\right)\right] \\ &= \int \mathcal{D}\Delta\mathcal{D}\Delta^* \exp\left(i\, N_f\, S[\Delta,\Delta^*]\right)\end{aligned} \tag{2.2}$$

where Δ is a complex order parameter whose real and imaginary parts are associated with scalar ($\bar{\psi}\psi$) and pseudoscalar ($\bar{\psi}\gamma^5\psi$) condensates respectively. In the second line we integrated out the fermions and defined the action per flavor as:

$$S[\Delta,\Delta^*] = -\frac{1}{2g^2N_f}\int d^2x|\Delta^2| - i\,\ln\det\left(i\not{\partial} - \frac{1}{2}(1-\gamma^5)\Delta - \frac{1}{2}(1+\gamma^5)\Delta^*\right) \tag{2.3}$$

Here the trace is over both space-time and Dirac indices. In the large N_f limit, the partition function is dominated by the configurations which are the extrema of $S[\Delta,\Delta^*]$ in functional space. However, here we do not restrict ourselves to translationally invariant configurations as was done in the introduction. Using

the fact that $\ln\det = \mathrm{tr}\,\ln$, the gap equation can be written as:

$$\begin{aligned} 0 &= \frac{\delta S[\Delta,\Delta^*]}{\delta\Delta^*} \\ &= -\frac{1}{2g^2N_f}\Delta + i\,\frac{1}{2}\,\mathrm{tr}\left((1+\gamma^5)\frac{1}{i\partial\!\!\!/ - \frac{1}{2}(1-\gamma^5)\Delta - \frac{1}{2}(1+\gamma^5)\Delta^*}\right) \end{aligned} \quad (2.4)$$

If the condensate is constant, it is straightforward to evaluate the determinant and solve the gap equation as demonstrated in the previous chapter. When the condensate is inhomogeneous this is a much more difficult problem. Dashen, Hasslacher and Neveu [19] used inverse scattering to find kink-like static but spatially inhomogeneous condensates for the gap equation of the GN_2 model (where there is no pseudoscalar condensate, so Δ is real). Shei [20] extended this inverse scattering analysis to the chiral Gross-Neveu model, the NJL_2 model, and found a spatially inhomogeneous complex kink. A new approach to the inhomogeneous gap equation, based on the resolvent, was developed by Feinberg and Zee [21] and applied to the kink solutions of both the GN_2 and NJL_2 models. For the GN_2 model, Thies used a Hartree-Fock approach to find a periodic extension of the real kink solution, motivated by analogous inhomogeneous condensates in condensed matter systems [22]. Our approach will be to show that the complex gap equation (2.4) can be reduced in an elementary manner to a soluble form of the nonlinear Schrödinger equation. The general solution contains all previously known inhomogeneous condensates (real and complex), and yields a new crystalline extension of Shei's complex kink.

2.1.2 Hartree-Fock approximation

An alternative way to study the large N_f limit is the Hartree-Fock approach. To generate the expectation value of composite fermion fields, we introduce a complex current J:

$$\begin{aligned}\mathcal{Z}[J,J^*] &= \int \mathcal{D}\bar{\psi}\mathcal{D}\psi\mathcal{D}\Delta\mathcal{D}\Delta^* \exp\left[i\int d^2x \left(\bar{\psi}(i\partial\!\!\!/ - \frac{1}{2}(1-\gamma^5)(\Delta - J)\right.\right. \\ &\qquad \left.\left. -\frac{1}{2}(1+\gamma^5)(\Delta^* - J^*))\psi - \frac{1}{2g^2}|\Delta|^2\right)\right] \\ &= \int \mathcal{D}\Delta\mathcal{D}\Delta^* \exp\left[-i\frac{1}{2g^2}\int d^2x|\Delta + J|^2\right. \\ &\qquad \left. +N_f \,\mathrm{tr}\,\log\left(i\partial\!\!\!/ - \frac{1}{2}(1-\gamma^5)\Delta - \frac{1}{2}(1+\gamma^5)\Delta^*\right)\right]\end{aligned} \tag{2.5}$$

Here we shifted the integration variable as $\Delta \to \Delta + J$ in the path integral and integrated out the fermions. Then the complex chiral order parameter can be calculated as:

$$\langle\bar{\psi}\psi\rangle - i\langle\bar{\psi}i\gamma^5\psi\rangle = \frac{2}{i}\frac{\delta \ln \mathcal{Z}[J,J^*]}{\delta J^*}\Big|_{J=0} \tag{2.6}$$

After taking the large N_f limit the effective action is found to be:

$$\ln \mathcal{Z}[J,J^*] = -i\frac{1}{2g^2}\int d^2x|\Delta + J|^2 + N_f \,\mathrm{tr}\,\log\left(i\partial\!\!\!/ - \frac{1}{2}(1-\gamma^5)\Delta - \frac{1}{2}(1+\gamma^5)\Delta^*\right) \tag{2.7}$$

where Δ is evaluated on the gap equation (2.4), we obtain the self consistency relation:

$$\langle\bar{\psi}\psi\rangle - i\langle\bar{\psi}i\gamma^5\psi\rangle = -\frac{1}{g^2}\Delta \tag{2.8}$$

Here the spinors are solutions of the single particle Dirac equation, which is the equation of motion of (2.2):

$$\left(i\not{\partial} - -\frac{1}{2}(1-\gamma^5)\Delta - \frac{1}{2}(1+\gamma^5)\Delta^*\right)\psi = 0 \tag{2.9}$$

This is the standard Hartree-Fock approximation, used widely in many body theory, where the large numbers of degrees of freedom (in our case N_f) allows us to approximate the quartic self interaction with a mean-field potential (2.8). It should be emphasized that we consider inhomogeneous potentials in our analysis. Also the Hartree-Fock problem is completely local in our context. The reason is that the NJL model has a local self interaction instead of a Yukawa type coupling that typically occurs in many body problems, which leads to a non-local term in the Hartree-Fock Lagrangian. The locality can also be seen by coupling the fermions to a massive scalar [10]. At the limit where the mass of the scalar is infinite, the interaction becomes local since the scalar field do not propagate and we obtain the original NJL_2 model.

We choose Dirac matrices $\gamma^0 = \sigma_1$, $\gamma^1 = -i\sigma_2$, $\gamma^5 = \sigma_3$ to put the corresponding single particle Hamiltonian into the form of the standard Bogoliubov-

de Gennes (BdG) Hamiltonian of superconductivity [23]

$$H = \begin{pmatrix} -i\frac{d}{dx} & \Delta(x) \\ \Delta^*(x) & i\frac{d}{dx} \end{pmatrix} \tag{2.10}$$

The associated spectral equation

$$H\psi = E\psi \tag{2.11}$$

will be referred to as the Bogoliubov-de Gennes (BdG) equation.

2.2 A glimpse into finite temperature and density

Following the standard formalism [24] of investigating the thermal equilibrium properties of quantum field theories, we pass to imaginary time $t \to -i\tau$ and compactify on a circle with radius $\beta \equiv 1/T$. The Boltzmann constant k_B is embedded into the temperature T. The chemical potential μ enters through the addition of the term $\mu\psi^\dagger\psi$ to the Lagrangian. The fermions have anti-periodic boundary conditions under the identification $\tau = 0 \sim \beta$. Therefore the energy eigenvalues are pure imaginary, and quantized as:

$$\begin{aligned} \int \frac{d\omega}{2\pi} &\to \frac{1}{\beta}\sum_{n=-\infty}^{\infty} \\ \omega \equiv i\frac{\partial}{\partial t} &\to \omega_n = \frac{2\pi i}{\beta}\left(n + \frac{1}{2}\right) \end{aligned} \tag{2.12}$$

The tr ln part in the effective potential per flavor, $-S[\Delta,\Delta^*]/N_f$ (see (2.3)) then becomes:

$$\begin{aligned} & i\,\mathrm{tr}\,\ln\left(i\partial\!\!\!/ - \frac{1}{2}(1-\gamma^5)\Delta - \frac{1}{2}(1+\gamma^5)\Delta^* + \mu\gamma^0\right) \\ \to -\frac{1}{\beta}\sum_{n=-\infty}^{\infty}\left[-\omega_n + H - \mu\right] &= -\frac{1}{\beta}\,\mathrm{tr}\,\ln\left[\prod_{n=0}^{\infty}(-\omega_n^2 + (H-\mu)^2)\right] \end{aligned} \tag{2.13}$$

Here the trace is over spatial momentum and Dirac indices and H is the BdG Hamiltonian defined in (2.10). By the help of the product formula of cosh [101]:

$$\cosh(x) = \prod_{n=0}^{\infty}\left(1 + \frac{4x^2}{\pi^2(2n+1)^2}\right) \tag{2.14}$$

and dropping the terms independent of H, we get:

$$-\frac{1}{\beta}\mathrm{tr}\,\ln\left[\cosh\left(\frac{\beta(H-\mu)}{2}\right)\right] \;=\; -\frac{1}{2}\mathrm{tr}|H-\mu| - \frac{1}{\beta}\mathrm{tr}\,\ln\left(1+e^{-\beta|H-\mu|}\right) \tag{2.15}$$

The trace can be written explicitly as $\int dE\rho(E)$ with $\rho(E)$ being the density of states. The second term in (2.15) is the usual partition function of a generic fermion system. The first term is the vacuum free energy and formally UV divergent. We introduce an energy cutoff cutoff in the energy trace E_{min} and obtain:

$$\int_{E_min}^{\mu} dE\rho(E)(E-\mu) - \frac{1}{\beta}\int_{-\infty}^{\infty} dE\,\rho(E)\ln\left(1+e^{-\beta(E-\mu)}\right) \tag{2.16}$$

The first term contributes to the renormalization together with the $\frac{1}{2g^2}|\Delta|^2$ term. In the Hartree-Fock context, $\frac{1}{2g^2}|\Delta|^2$ corresponds to the double counting correction term.After absorbing the divergent piece in the second integral, the full grand

potential can be written compactly as:

$$\Psi[\Delta(x);T,\mu] = -\frac{1}{\beta}\int_{-\infty}^{\infty} dE\,\rho(E)\ln\left(1+e^{-\beta(E-\mu)}\right) + \frac{1}{2N_f g^2}\frac{1}{L}\int_0^L dx|\Delta(x)|^2 \quad . \tag{2.17}$$

2.3 Resolvent approach and the Nonlinear Schrödinger Equation

The key quantity in our approach is the coincident limit of Gor'kov Green's function, or the the "diagonal resolvent":

$$R(x;E) \equiv \langle x|\frac{1}{H-E}|x\rangle \quad . \tag{2.18}$$

The resolvent (2.18) is clearly a 2×2 matrix. For a static (but possibly spatially inhomogeneous) condensate, all spectral information is encoded in the resolvent. Indeed, the spectral function (or the density of states) characterizing the single-particle spectrum of fermions in the presence of the condensate $\Delta(x)$ is

$$\rho(E) = \frac{1}{\pi}\mathcal{I}m\,\mathrm{Tr}_{D,x}\left[R(x;E+i\epsilon)\right] \quad , \tag{2.19}$$

where the trace is a Dirac trace as well as a spatial trace. This fact follows trivially from the Sokhatsky-Weierstrass theorem:

$$\frac{1}{x-i\epsilon} = \mathcal{P}\left(\frac{1}{x}\right) + i\pi\delta(x) \tag{2.20}$$

It is also possible to read off the single particle spectrum of the fermions in the phase associated with the condensate, by investigating the analyticity structure

of the corresponding density of states. The bound states will show up as poles and the continuum states or bands will show up as branch cuts of $\rho(E)$.

Our first, very simple, observation is that the form of the BdG equation (2.11) places very strong constraints on the possible form of $R(x;E)$. For any static condensate $\Delta(x)$, $R(x;E)$ must satisfy the following algebraic conditions [these are explained in more detail in Appendix A]:

$$R = R^\dagger \tag{2.21}$$

$$\mathrm{tr}_D\left(R(x;E)\sigma_3\right) = 0 \tag{2.22}$$

$$\det R(x;E) = -\frac{1}{4} \quad . \tag{2.23}$$

Furthermore, $R(x;E)$ must satisfy the first-order differential equation

$$\frac{\partial}{\partial x}R(x;E)\,\sigma_3 = i\left[\begin{pmatrix} E & -\Delta(x) \\ \Delta^*(x) & -E \end{pmatrix}, R(x;E)\,\sigma_3\right] \tag{2.24}$$

simply as a consequence of the Dirac equation (2.11). In superconductivity, (2.24) is known as the Eilenberger equation [25, 26], and in mathematical physics as the Dik'ii equation [27]. These conditions (2.21)–(2.23), and the Eilenberger equation (2.24), all follow from the simple fact [26, 27, 28] that for the one-dimensional BdG equation, which involves derivatives with respect to the single variable x, the Green's function can be expressed as a product of two independent solutions to (2.11):

$$R(x;E) = \frac{1}{2iW}\left(\psi_1\psi_2^T + \psi_2\psi_1^T\right)\sigma_1 \tag{2.25}$$

where W is the Wronskian of two independent solutions $\psi_{1,2}$: $W = i\psi_1^T \sigma_2 \psi_2$.

The next step is to note that the gap equation provides further information about the possible form of the resolvent, and this is enough to motivate a specific ansatz form [11, 12]. There are two ways of viewing the gap equation (2.4) in terms of the resolvent. First, for a static condensate, recall that we can write the log det term in the effective action (2.3) as minus the grand canonical potential, in terms of the single-particle spectral function $\rho(E)$:

$$-\frac{1}{\beta}\int_{-\infty}^{\infty} dE\, \rho(E) \ln\left(1 + e^{-\beta(E-\mu)}\right) \quad . \tag{2.26}$$

All dependence on $\Delta(x)$ resides in the spectral function $\rho(E)$, via (2.19). Therefore, inserting this into the gap equation (2.4), this relates $\Delta(x)$ to the *diagonal* entries of $R(x;E)$. Further, as a consequence of the condition (2.22), these diagonal entries are equal. So, the simplest natural solution to the gap equation is for the diagonal entries of $R(x;E)$ to be linear in $|\Delta(x)|^2$. A second way to view the gap equation is to evaluate the functional derivative in (2.4), which for a static condensate leads to:

$$\Delta(x) = -iNg^2 \mathrm{tr}_{D,E}\left[\gamma^0\left(\mathbf{1} + \gamma^5\right) R(x;E)\right] \tag{2.27}$$

The Dirac trace then relates the *off-diagonal* entries of $R(x;E)$ to $\Delta(x)$. Since R is hermitean, these off-diagonal entries are complex conjugates of one another.

Summarizing, $R(x;E)$ must be a hermitean 2×2 matrix with equal diagonal entries, such that [after the spatial and energy trace] the variation of the diagonal

terms is proportional to $\Delta(x)$, and with off-diagonal terms linear in $\Delta(x)$, after the energy trace. This suggests taking the resolvent to be of the form

$$R(x;E) = \mathcal{N}(E) \begin{pmatrix} a(E) + |\Delta(x)|^2 & b(E)\Delta(x) \\ b(E)\Delta^*(x) & a(E) + |\Delta(x)|^2 \end{pmatrix} \tag{2.28}$$

where $a(E)$, $b(E)$ and $\mathcal{N}(E)$ are functions of E, independent of x, and are to be determined. However, this ansatz cannot describe inhomogeneous condensates because the only solution of this form consistent with (2.23) is a condensate with constant magnitude, independent of x. Indeed, taking Δ to be constant (and by a global chiral rotation, real), $\Delta = M$, the solution to (2.21)–(2.24) is simply

$$R(x;E) = \frac{1}{2\sqrt{M^2 - E^2}} \begin{pmatrix} E & M \\ M & E \end{pmatrix} \tag{2.29}$$

as is familiar. This example also illustrates that the hermiticity condition (2.21) must of course be interpreted with the appropriate $i\epsilon$ prescription for the energy.

To find inhomogeneous condensates, extend the ansatz (2.28) to include a first derivative term in the off-diagonal entries:

$$R(x;E) = \mathcal{N}(E) \begin{pmatrix} a(E) + |\Delta(x)|^2 & b(E)\Delta(x) - i\Delta'(x) \\ b(E)\Delta^*(x) + i\Delta'^*(x) & a(E) + |\Delta(x)|^2 \end{pmatrix} \quad . \tag{2.30}$$

This is the simplest extension of (2.28) that is consistent with the various algebraic constraints and with the Eilenberger equation (2.24). Indeed, substituting the ansatz (2.30) into the Eilenberger equation (2.24), we see that the diagonal entry of this equation is identically satisfied, while the off-diagonal entry implies that

$\Delta(x)$ must satisfy the following nonlinear Schrödinger equation (NLSE) [and its complex conjugate]:

$$\Delta'' - 2|\Delta|^2\,\Delta + i\,(b-2E)\,\Delta' - 2\,(a-Eb)\,\Delta = 0 \quad . \tag{2.31}$$

Two comments are in order. First, it is not immediately obvious that $R(x;E)$ in (2.30) can satisfy the normalization condition (2.23) for an inhomogeneous condensate, since

$$\det R(x;E) = \mathcal{N}^2\left\{|\Delta|^4 - |\Delta'|^2 + (2a-b^2)|\Delta|^2 + ib\,(\Delta'\Delta^* - \Delta\Delta^{*\prime}) + a^2\right\} \tag{2.32}$$

Remarkably, the NLSE (2.31) implies that $(\det R(x;E))$ is constant:

$$\begin{aligned}\frac{d}{dx}\left(\frac{\det R(x;E)}{\mathcal{N}^2}\right) &= \left(2|\Delta|^2 + 2a - b^2\right)\left(|\Delta|^2\right)' - \Delta''\Delta^{*\prime} + ib\Delta''\Delta^* + c.c. \\ &= 0 \end{aligned} \tag{2.33}$$

where we have used the fact that the NLSE (2.31) implies that $(\Delta''\Delta^{*\prime} + \Delta'\Delta^{*\prime\prime}) = (2|\Delta|^2 + 2a - 2Eb)\,(|\Delta|^2)'$, and that $(\Delta''\Delta^* - \Delta^{*\prime\prime}\Delta) = -i(b-2E)\,(|\Delta|^2)'$. Since $\det R(x;E)$ is constant, the normalization in (2.23) can be achieved by suitable choice of $\mathcal{N}(E)$. Second, while the ansatz (2.30) automatically satisfies the x dependence of the gap equation in its form coming from (2.26) [because the trace of R is, by construction, linear in $|\Delta|^2$], it doesn't satisfy the other form of the gap equation (2.27), until the energy trace is performed. This is because of the $\Delta'(x)$ terms in the off-diagonal. The energy trace puts a consistency condition on the solution:

$$0 = \mathrm{tr}_E\left(\mathcal{N}(E)\right) \equiv \int \frac{dE}{2\pi}\frac{\mathcal{N}(E)}{1+e^{\beta(E-\mu)}} \tag{2.34}$$

Thus, we have reduced the very difficult problem of solving the functional gap equation (2.4) for a self-consistent condensate $\Delta(x)$ to the much simpler problem of solving the NLSE for $\Delta(x)$. In fact, the NLSE (2.31) is explicitly soluble, as is discussed in the following sections, in which we describe first the real solutions [relevant for the GN_2 model], and then the complex solutions [relevant for the NJL_2 model].

2.4 Solutions of the Nonlinear Schrödinger Equation

In this Section we examine the solutions of the NLSE (2.31) extensively. We first start with the most general solution, the twisted kink crystal, and demonstrate how all the previously known complex and real solutions arise as special cases of the most general solution. We also recapitulate the main properties of these previously known solutions in the context of NLSE and resolvent approach.

2.4.1 Twisted kink crystal condensate

The most general solution to the NLSE (2.31) describes a crystalline condensate [11, 12]. It is a periodic array of kinks that also rotate in the chiral plane, as illustrated in Figure 2.4.1. In the figure, the solution is the red line and the background envelope is to emphasize the modulation in its amplitude. The *single* chirally-twisted kink was originally found by Shei [20] using inverse scattering techniques, and subsequently studied in a resolvent approach by Feinberg and Zee

[21]. The periodic array of such twisted kinks can be expressed in terms of the

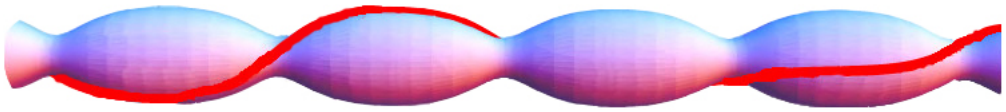

Fig. 2.1: The twisted kink crystal condensate (2.35).

elliptic functions:

$$\begin{aligned}\Delta(x) &= -\lambda A e^{2iqx}\frac{\sigma(\lambda A\, x + i\mathbf{K}' - i\theta/2)}{\sigma(\lambda A\, x + i\mathbf{K}')\sigma(i\theta/2)} \\ &\quad \times \exp\left[i\lambda A\, x\,(-i\,\zeta(i\theta/2) + i\,\mathrm{ns}(i\theta/2)) + i\,\theta\eta_3/2\right] \qquad (2.35)\end{aligned}$$

where sc=sn/cn, nd=1/dn are Jacobi elliptic functions, and the functions σ and ζ are the Weierstrass sigma and zeta functions [101, 102, 103, 104], chosen to have real and imaginary half-periods: $\omega_1 = \mathbf{K}(\nu)$, and $\omega_3 = i\,\mathbf{K}' \equiv i\mathbf{K}(1-\nu)$. $\mathbf{K}$ is the elliptic integral of the first kind definded as $\mathbf{K}(\nu) \equiv \int_0^{\pi/2}\left(1-\nu\,\sin^2 t\right)^{-1/2} dt$. Both periods are therefore controlled by a single [real] elliptic parameter $0 \leq \nu \leq 1$. Note that $\eta_3 = \zeta(i\mathbf{K}')$ is pure imaginary. The parameter λ sets the overall scale of the condensate, and $1/\lambda$ sets the length scale of the crystal. Later, we will use units in which the vacuum mass of the fermion is 1, so that λ sets the scale relative to the vacuum fermion mass. The angular parameter θ takes values in the range $\theta \in [0, 4\mathbf{K}'(\nu)]$. The [real] constant A is a function of θ and the elliptic parameter ν:

$$A = A(\theta,\nu) = -2i\,\mathrm{sc}(i\theta/4;\nu)\,\mathrm{nd}(i\theta/4;\nu) \qquad (2.36)$$

For brevity we will usually suppress the explicit dependence of the elliptic functions on the elliptic parameter ν. The final parameter q is an overall phase parameter that affects the chiral angle through which the condensate rotates over one period $L = \frac{2\mathbf{K}}{\lambda A}$:

$$\Delta(x+L) = e^{2i\varphi}\Delta(x) \quad ; \quad \varphi = \mathbf{K}\left(-i\,\zeta(i\theta/2) + i\,\mathrm{ns}(\theta/2) - \frac{\eta\theta}{2\mathbf{K}} + \frac{2q}{\lambda A}\right) \tag{2.37}$$

where $\eta \equiv \zeta(\mathbf{K})$ is real. Thus the general solution is specified by four real parameters: a scale parameter λ, a phase parameter q, an angular parameter θ, and the elliptic parameter ν.

It is also useful to visualize the condensate (2.35) in terms of its amplitude and phase: $\Delta = M\,e^{i\chi}$. The modulus squared is a bounded periodic function, with period $2\mathbf{K}/A$:

$$M^2 \equiv |\Delta(x)|^2 = \lambda^2 A^2\left(\mathcal{P}\left(\lambda A x + i\mathbf{K}'\right) - \mathcal{P}\left(i\theta/2\right)\right) \tag{2.38}$$

Here we used the quasi-periodicity property (B.2) of the σ function, together with the product identity (B.12) relating the σ and $\mathcal{P}$ functions. The phase χ can be expressed as

$$\chi(x) = \lambda A(-i\,\zeta(i\theta/2) + i\,\mathrm{ns}(i\theta/2))x + \frac{i}{2}\ln\left(\frac{\sigma(\lambda A x + i\mathbf{K}' + i\theta/2)}{\sigma(\lambda A x + i\mathbf{K}' - i\theta/2)}\right) + \frac{\eta_3\theta}{2} + 2q \tag{2.39}$$

The amplitude and phase are plotted in Figure 2.2, for $\theta = 1.6$ and $\nu = 0.95$. Note that the amplitude is periodic while the phase changes by 2φ over each period.

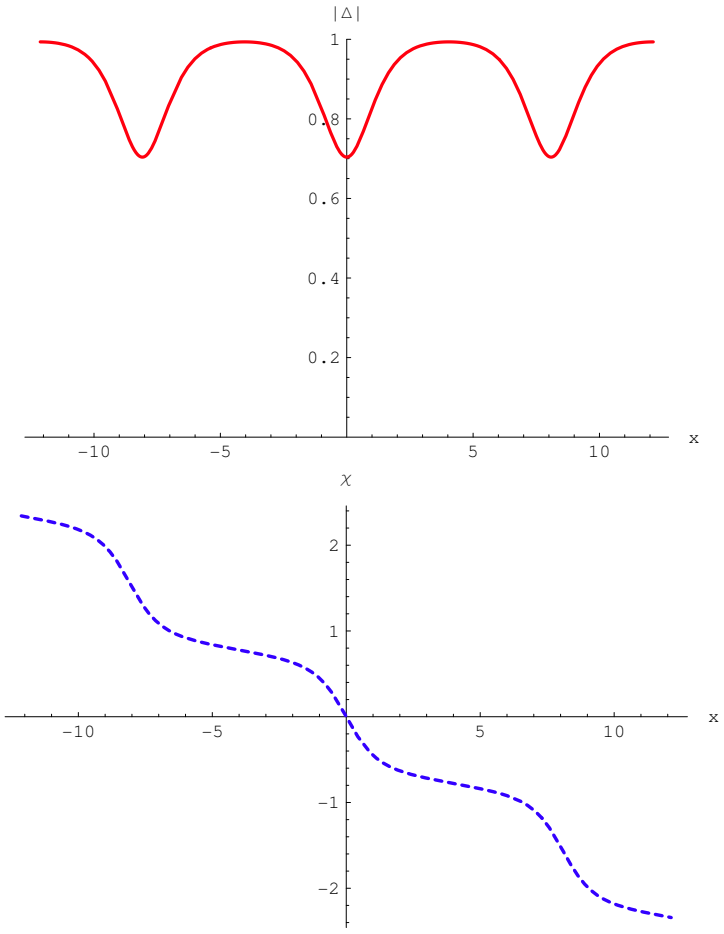

Fig. 2.2: Plots of the amplitude $M(x)$ and phase $\chi(x)$ of the complex kink crystal condensate (2.35).

The complex crystalline condensate in (2.35) satisfies the NLSE:

$$\Delta'' - 2\,|\Delta|^2\,\Delta - i\,\left(2\lambda A\, i\,\mathrm{ns}(i\theta/2) - 2q\right)\Delta' - \lambda^2 A^2\left(3\,\mathcal{P}(i\theta/2) - \mathrm{ns}^2(i\theta/2)\right)\Delta = 0 \tag{2.40}$$

Comparing this equation with the NLSE (2.31) we can extract the functions $a(E)$, $b(E)$ and $\mathcal{N}(E)$ appearing in (2.30), thereby determining the *exact* diagonal resolvent. These parameters also parametrize the energy spectrum of fermions in such a condensate background, which has two gaps, with band edges $E_1 \le E_2 \le E_3 \le E_4$ as shown in the first plot of Figure 2.3:

$$\begin{aligned} E_1 &= q - \lambda \\ E_2 &= q + \lambda(-1 + 2\,\mathrm{nc}^2(i\theta/4)) \\ E_3 &= q + \lambda(-1 + 2\,\mathrm{nd}^2(i\theta/4)) \\ E_4 &= q + \lambda \end{aligned} \tag{2.41}$$

Thus, in terms of the single particle fermion spectrum, the role of the four parameters is as follows: λ determines the overall energy scale; q determines the overall offset; while θ and ν determine the location and width of the band that lies in the gap between the "outer" edges E_1 and E_4. The simple linear dependence of the energy spectrum on the parameters λ and q is a direct consequence of the form of the Hamiltonian (2.10), and reflects the an important scale and shift symmetry described in detail in Section 3.1.

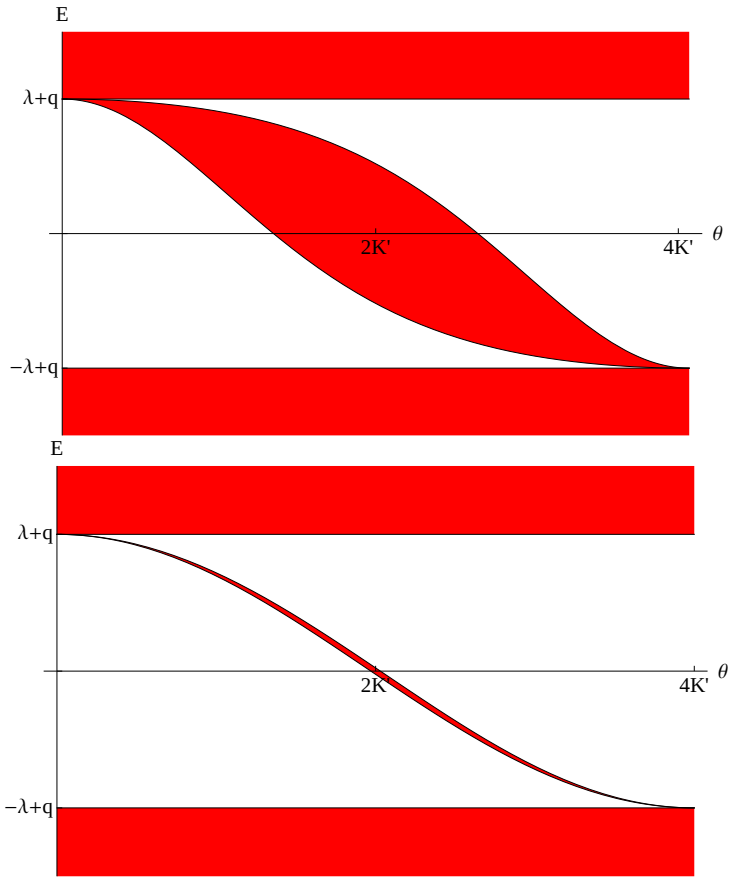

Fig. 2.3: Plots of the single-particle fermion spectrum (2.41) for the complex kink crystal condensate.

We can roughly think of the parameter θ as setting the offset location of the band inside the gap, while the parameter ν, together with θ, plays the role of determining the period of the crystal, and hence the width of the band. This can be seen in Figure 2.3, where the first and second plots are for $\nu = 0.1$ and $\nu = 0.9$ respectively. In terms of the band edges, the resolvent functions $a(E)$, $b(E)$ and

$\mathcal{N}(E)$ that appear in the resolvent (2.30) take the following simple form:

$$\begin{aligned} a(E) &= 2E^2 - \left(\sum_{j=1}^{4} E_j\right) E + \frac{1}{8}\left\{\left(\sum_{j=1}^{4} E_j\right)^2 - \sum_{i<j}^{4}(E_i - E_j)^2\right\} \\ b(E) &= 2E - \sum_{j=1}^{4} E_j \\ \mathcal{N}(E) &= \frac{i}{4\sqrt{\prod_{j=1}^{4}(E - E_j)}} \end{aligned} \tag{2.42}$$

Here the normalization $\mathcal{N}(E)$ is fixed by the property $\det R = -\frac{1}{4}$. From (2.19), we also have an explicit exact expression for the density of states of fermions in the presence of such a twisted kink condensate field, following from the trace of the resolvent. Within the bands:

$$\rho(E) = \frac{1}{2\pi} \frac{a(E) + \lambda^2 Z}{\sqrt{\prod_{j=1}^{4}(E - E_j)}} \tag{2.43}$$

Here we have defined the function $Z(\theta, \nu)$ in terms of the normalized average of $|\Delta(x)|^2$ over one period:

$$Z(\theta, \nu) \equiv \frac{1}{\lambda^2}\langle|\Delta(x)|^2\rangle = -A(\theta, \nu)^2 \left(\mathcal{P}(i\theta/2) + \frac{\eta}{\mathbf{K}}\right) \tag{2.44}$$

with $\mathcal{P}$ being the Weierstrass $\mathcal{P}$ function. Thus, the density of states $\rho(E)$ is an explicitly known function of the energy E, depending parametrically on the four parameters λ, q, θ and ν that characterize the solution (2.35) to the gap equation. This parametric dependence enters through the band edge energies E_j in (2.41), and through the function Z defined in (2.44).

2.4.2 Single twisted kink condensate

Shei [20] found a solution to the gap equation for the NJL_2 model, in which both the scalar and pseudoscalar condensates have a kink-like form:

$$\begin{aligned} \mathcal{R}e[\Delta(x)] &= \lambda \left[\cos^2(\theta/2) + \sin^2(\theta/2) \tanh\left(\lambda \sin\left(\theta/2\right)\, x\right)\right] \\ \mathcal{I}m[\Delta(x)] &= -\frac{\lambda}{2} \sin(\theta) \left[1 - \tanh\left(\lambda \sin\left(\theta/2\right)\, x\right)\right] \end{aligned} \tag{2.45}$$

where $\theta \in [0, 2\pi]$ is a parameter. This complex kink (2.45) has also been extensively studied in the resolvent approach by Feinberg and Zee [21]. This solution follows as a special case of the general solution (2.35) as the period of the crystal goes to infinity. This limit is approached as $\nu \to 1$. Using the properties of the Weierstrass functions (see Appendix B), $\Delta(x)$ in (2.35) reduces to:

$$\Delta(x) = \lambda \frac{\cosh\left(\lambda \sin\left(\theta/2\right)\, x - i\theta/2\right)}{\cosh\left(\lambda \sin\left(\theta/2\right)\, x\right)} e^{i\theta/2} \quad . \tag{2.46}$$

which is precisely Shei's solution (2.45). This complex form is plotted in Figure 2.4 with $\theta = 3\pi/2$, illustrating how the kink winds around zero without the amplitude vanishing. The kink is the solid [red] line, and the surface is shown simply to illustrate that both the amplitude and the phase are changing. This also illustrates the role of the parameter $\theta \in [0, 2\pi]$ as the net rotation angle of the kink as x goes from $-\infty$ to $+\infty$:

$$\Delta(x = +\infty) = e^{-i\theta} \Delta(x = -\infty) \tag{2.47}$$

Observe that when $\theta = \pi$, the complex kink (2.46) is in fact real, and reduces to the familiar real kink solution (see Section 2.4.5); this real kink changes its

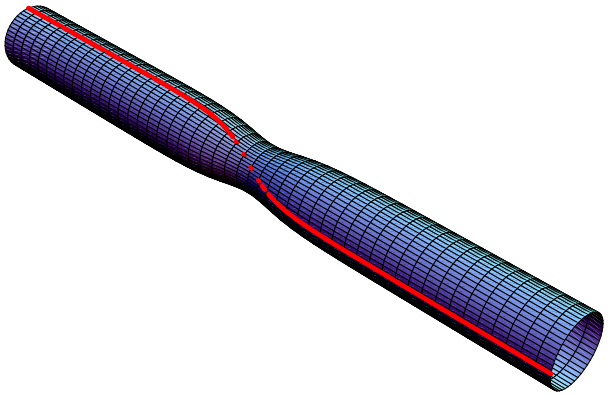

Fig. 2.4: Plot of the complex kink condensate.

sign [i.e., rotates through π] in passing from $x = -\infty$ to $x = +\infty$. Another useful representation of this kink is in terms of the magnitude and phase $\Delta(x) = M(x)e^{i\chi(x)}$:

$$M^2(x) = \lambda^2 \left[1 - \sin^2(\theta/2)\,\mathrm{sech}^2\left(\lambda \sin(\theta/2)\; x\right)\right] \tag{2.48}$$

$$\chi(x) = \arctan\left(\frac{\sin\theta}{\cos\theta + e^{2\lambda x \sin(\theta/2)}}\right) \tag{2.49}$$

This form is illustrated in Figure 2.5. The condensate amplitude $M(x)$ [solid, red curves] approaches m at $x = \pm\infty$, and equals $m\cos(\theta/2)$ at the kink center $x = 0$. The phase $\chi(x)$ [dashed, blue, curves] winds from θ to 0 as x ranges from $x = -\infty$ to $x = +\infty$. The plots are for $\theta = \pi/10$, $\theta = \pi/2$, and $\theta = 9\pi/10$. The complex kink condensate (2.46) satisfies the NLSE:

$$\Delta'' - 2\,|\Delta|^2\,\Delta - 2\,i\,\lambda\,\cos(\theta/2)\;\Delta' + 2\lambda^2\Delta = 0 \tag{2.50}$$

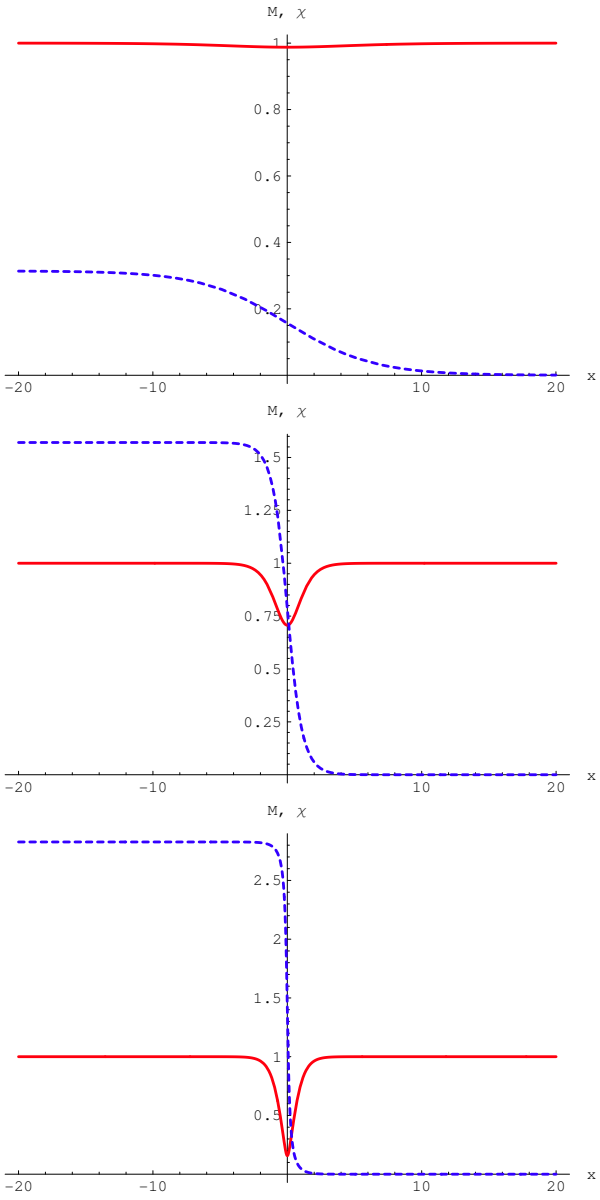

Fig. 2.5: Plots of the amplitude M and phase χ of the complex kink condensate.

From this NLSE, we deduce the exact diagonal resolvent to be of the form (2.30) with

$$\begin{aligned} a(E) &= 2E^2 - 2\,\lambda\,\cos(\theta/2)E - \lambda^2 \\ b(E) &= 2E - \lambda\,\cos(\theta/2) \\ \mathcal{N}(E) &= \frac{1}{4(E - \lambda\,\cos\,(\theta/2))\sqrt{\lambda^2 - E^2}} \end{aligned} \tag{2.51}$$

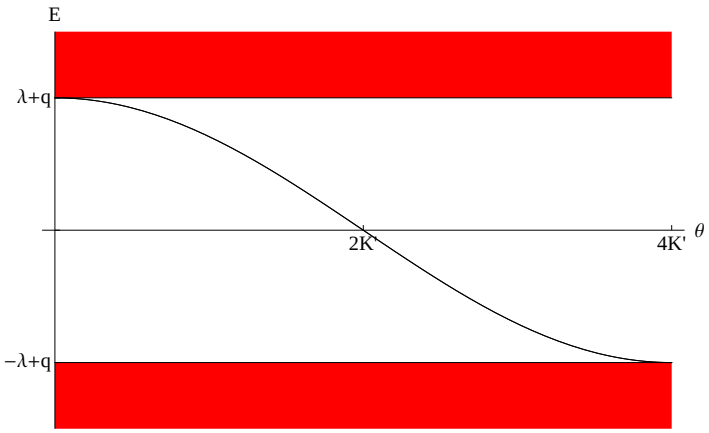

Fig. 2.6: Plot of the fermion single-particle spectrum for the single complex kink.

The spectrum of the associated BdG equation (2.11) has positive and negative energy continua starting at $E = \pm\lambda$, together with a single bound state located at $E = \lambda\,\cos\,(\theta/2)$. The bound state is the remnant of the band in the spectrum of the twisted crystal (2.41) condensate. Here the band contracts to a single bound state, with $E_2 = E_3 = \lambda\cos\,(\theta/2)$. When $\theta = \pi$, where this complex kink reduces to the standard real kink, the bound state is a zero mode. But for other values of θ the single bound state lies asymmetrically inside the gap, as

plotted in Figure 2.6. As θ goes from 0 to 2π, one state moves from the positive to the negative energy continuum. As is clear from the previous subsection, we can always multiply the complex kink solution (2.46) by a plane-wave factor e^{2iqx}, which has the net effect of displacing the fermion spectrum by q, with the corresponding simple modifications to the resolvent functions $a(E)$, $b(E)$ and $\mathcal{N}(E)$ in (2.51).

At this stage we have shown that Shei's complex kink condensate (2.46) solves the NLSE, and we have found the corresponding exact diagonal resolvent (2.30) with $a(E)$, $b(E)$ and $\mathcal{N}(E)$ given in (2.51). This agrees with the spectral properties derived from inverse scattering [20]. Shei further showed [20] that this complex condensate solves the gap equation provided a further restriction is applied to the winding parameter θ. This condition states that $\theta/(2\pi)$ is equal to the filling fraction $\frac{n}{N}$, in the large flavor limit, of the single bound state in the gap by n flavors, with $\frac{n}{N}$ fixed as $N \to \infty$ [20, 21]:

$$\frac{\theta}{2\pi} = \frac{n}{N} \tag{2.52}$$

In fact, this is the same condition (2.34) that arises from demanding that the coefficient of the $\Delta'(x)$ term in (2.27) vanishes after the energy trace, a necessary requirement to satisfy the gap equation.

2.4.3 Spiral condensate

An important special case of the general solution (2.35) is the degenerate case when the bound band of the fermion spectrum shrinks and merges with the upper or lower continuum, so that the spectrum has just a single gap. This occurs when the angular parameter takes values at its extreme limits: $\theta = 0$ [which implies that $E_2 = E_3 = E_4$, so that the bound band merges with the upper continuum], or $\theta = 4\mathbf{K}'$ [which implies that $E_1 = E_2 = E_3$, so that the bound band merges with the lower continuum] (see Fig 2.3). The general twisted kink crystal condensate (2.35) reduces to a single plane wave

$$\Delta = \lambda\, e^{2iqx} \tag{2.53}$$

which is clearly a solution to the NLSE (2.31). For this condensate the amplitude

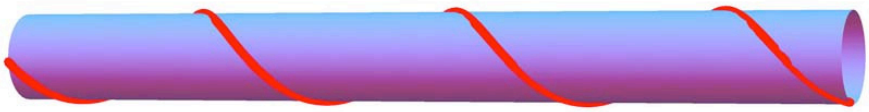

Fig. 2.7: The spiral condensate (2.53).

is constant, while the phase rotates at a constant rate, set by q, as shown in Figure 2.7. The fermion energy spectrum has just one gap, of width 2λ, centered at q; that is, the band edges lie at $E_1 = q - \lambda$, and $E_4 = q + \lambda$. Correspondingly, the resolvent trace has a simplified form, and the spectral function within the

continuum bands is simply:

$$\rho(E) = \frac{1}{\pi} \frac{|E-q|}{\sqrt{\lambda^2 - (E-q)^2}} \tag{2.54}$$

which we recognize as the spectral function of a constant condensate $\Delta = \lambda$, shifted in energy by q.

2.4.4 Real kink crystal condensate

Another important special case of the general solution (2.35) is the case where the condensate is real [relevant for the GN_2 model]. For a real condensate Δ, the phase parameter vanishes; $q = 0$, and the angular parameter θ takes its midpoint value $\theta = 2\mathbf{K}'(\nu)$. Thus the real kink crystal is described by just two parameters, the scale λ and the elliptic parameter ν:

$$\Delta(x) \;=\; \lambda \left(\frac{2\sqrt{\nu}}{1+\sqrt{\nu}} \right) \mathrm{sn}\left(\frac{2\lambda\, x}{1+\sqrt{\nu}}; \nu \right) \tag{2.55}$$

Over one period, $L = \frac{2\mathbf{K}(\tilde{\nu})}{\lambda}$, the condensate changes sign [that is, it rotates through an angle $2\varphi = -\pi$], as shown in Figure 2.8. This change of sign corresponds to the *discrete* chiral symmetry of the GN_2 model, while the phase rotation (2.37) of the general kink crystal condensate (2.35) through an arbitrary angle is associated with the *continuous* chiral symmetry of the NJL_2 model. The real kink crystal describes the inhomogeneous condensate of the crystalline phase of the GN_2 model [22], and its thermodynamics will be discussed below in Section 3.4. In addition to the crystalline phase of the Gross-Neveu model [22], this

solution also describes, a polaron crystal in polymer physics [29], a spin Peierls cuprate $CuGeO_3$[31], and a periodic pair potential in inhomogeneous superconductors [32, 33, 34, 35, 36]. The periodic condensate (2.55) satisfies the NLSE

$$\Delta'' - 2\,\Delta^3 + (1+\nu)\left(\frac{2\lambda}{1+\sqrt{\nu}}\right)^2 \Delta = 0 \quad . \tag{2.56}$$

Thus, we deduce:

$$a(E) \;=\; 2E^2 - 2\lambda^2 \frac{1+\nu}{(1+\sqrt{\nu})^2} \tag{2.57}$$

$$b(E) \;=\; 2E \tag{2.58}$$

$$\mathcal{N}(E) \;=\; \frac{1}{4}\frac{1}{\sqrt{\lambda^2 - E^2}\,\sqrt{E^2 - \lambda^2(\frac{1-\sqrt{\nu}}{1+\sqrt{\nu}})^2}} \tag{2.59}$$

This periodic condensate is plotted in Figure 2.8 for elliptic parameter $\nu = 0.99$

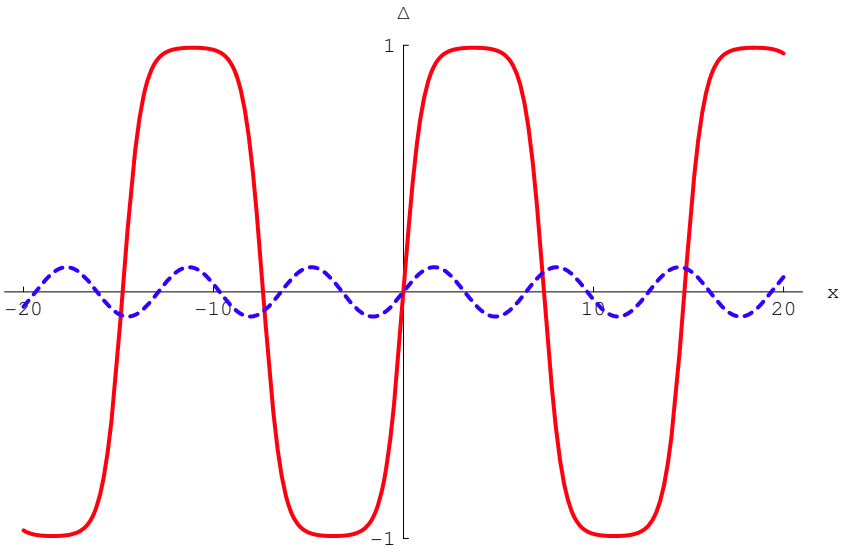

Fig. 2.8: The real kink crystal condensate (2.55).

[solid, red curve], and for $\nu = 0.1$ [dashed, blue curve]. For small ν the condensate

has the Larkin-Ovchinikov-Fulde-Ferrell (LOFF)[37] form of a small amplitude sinusoidal condensate, while for $\nu \to 1$ the condensate resembles an array of kinks and anti-kinks. Note that over the period $x \in [-\frac{\mathbf{K}(\nu)(1+\sqrt{\nu})}{2\lambda}, \frac{\mathbf{K}(\nu)(1+\sqrt{\nu})}{2\lambda}]$, the condensate is shaped like a single kink. This reflects the expansion of the Jacobi sn function in terms of an array of periodically displaced tanh functions:

$$\mathrm{sn}(x;\nu) = \frac{\pi}{2\sqrt{\nu}\,\mathbf{K}'} \sum_{n=-\infty}^{\infty} (-1)^n \tanh\left(\frac{\pi}{2\mathbf{K}'}(x - 2n\mathbf{K})\right) \tag{2.60}$$

where we use the standard notation $\mathbf{K}'(\nu) \equiv \mathbf{K}(1-\nu)$. In the infinite period limit ($\nu \to 1$), the interval $[-\frac{\mathbf{K}(\nu)(1+\sqrt{\nu})}{2m}, \frac{\mathbf{K}(\nu)(1+\sqrt{\nu})}{2m}]$ maps to the whole real line, and $\mathbf{K}' \to \pi/2$, and so the kink crystal (2.55) reduces to a single kink condensate.

It is worth noting that this periodic kink crystal (2.55) can be written in an equivalent, but different looking, form, by use of a Landen transformation [101, 102, 103, 104] of the Jacobi functions. That is, by rescaling the elliptic parameter ν together with the argument λx, we can write

$$\Delta(x) = \lambda\,\tilde{\nu}\,\frac{\mathrm{sn}\,(\lambda\,x;\tilde{\nu})\,\mathrm{cn}\,(\lambda\,x;\tilde{\nu})}{\mathrm{dn}\,(\lambda\,x;\tilde{\nu})} \qquad ; \qquad \tilde{\nu} \equiv \frac{4\sqrt{\nu}}{(1+\sqrt{\nu})^2} \quad . \tag{2.61}$$

This is the form in which this periodic kink solution is presented by Thies *et al* [22] on the crystalline phase of the Gross-Neveu model, while the form (2.55) was used in the condensed matter literature in [29, 32, 33, 34, 35]. The spectrum of the associated BdG equation (2.11) has positive and negative energy continua starting at $E = \pm\lambda$, together with a single bound band in the middle of the gap, with band edges at $E = \pm\left(\frac{1-\sqrt{\nu}}{1+\sqrt{\nu}}\right)\lambda$. This band lies symmetrically in the center

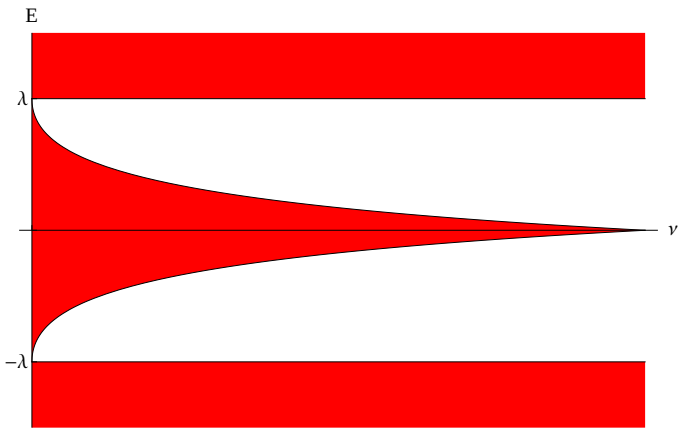

Fig. 2.9: The band spectrum of the real kink crystal.

of the gap. The spectrum is plotted in Figure 2.9 as a function of the elliptic parameter ν. Notice that there is just one bound band in the energy gap, and when $\nu \to 1$ [the infinite period limit], the bound band at the center of the gap contracts smoothly to the single bound zero mode of the kink condensate. The particular scaling in (2.55) fixes the continuum band edges to $\pm\lambda$.

2.4.5 Single real kink condensate

A well known nontrivial solution to the gap equation is the single (real) kink which is the infinite period limit ($\nu \to 1$) of the kink crystal (2.55) [19]:

$$\Delta(x) = \lambda \, \tanh(\lambda \, x) \tag{2.62}$$

This satisfies the NLSE

$$\Delta'' - 2\,\Delta^3 + 2\lambda^2\Delta = 0 \quad , \tag{2.63}$$

and so we deduce the exact diagonal resolvent to be of the form (2.30) with

$$\begin{aligned} a(E) &= 2E^2 - \lambda^2 \\ b(E) &= 2E \\ \mathcal{N}(E) &= \frac{1}{4}\frac{1}{E\sqrt{\lambda^2 - E^2}} \end{aligned} \tag{2.64}$$

The spectrum of the associated BdG equation (2.11) has positive and negative energy continua starting at $E = \pm\lambda$, together with a single bound state located at $E = 0$, at the center of the gap. This mid-gap zero mode has many important consequences in a variety of branches of physics [38] and can be seen here to arise in the limit where the bound band shrinks to a single state when the period becomes infinite.

2.4.6 Homogeneous condensate

If the condensate is constant, then by a global chiral rotation it can be taken to be real:

$$\Delta(x) = \lambda \tag{2.65}$$

This clearly satisfies the NLSE (2.31), and we find

$$\begin{aligned} a(E) &= 2E^2 - \lambda^2 \\ b(E) &= 2E \\ \mathcal{N}(E) &= \frac{1}{4}\frac{1}{E\sqrt{\lambda^2 - E^2}} \end{aligned} \tag{2.66}$$

The spectrum of the associated BdG equation (2.11) is that of a free fermion with mass λ, with positive and negative energy continua starting at $E = \pm\lambda$, the mass scale being set by the amplitude of the condensate.

2.5 Solutions of the Dirac-Bogoluibov-de Gennes equation

2.5.1 Spinor wavefunctions

Remarkably, not only is it possible to solve the NLSE (2.31) exactly, we can also solve exactly the associated BdG equation [39]. In the previous sections we described the spectrum; here we present the explicit spinor solutions and express the spectral information in a more compact and useful form. Also we set $\lambda = 1, q = 0$ for simplicity. This is equivalent to setting $E_1 = -E_4 = 1$ in the energy spectrum (2.41). This point will be explored in more detail in Section 3.1. We write the BdG equation (2.11) as

$$\begin{pmatrix} -i\frac{d}{dx} & \Delta(x) \\ \Delta^*(x) & i\frac{d}{dx} \end{pmatrix} \psi = E\psi \tag{2.67}$$

The solutions for the real condensates in Sections 2.4.4, 2.4.5 are well known [19, 21]. For the complex plane wave, $\Delta(x) = \lambda e^{2iqx}$, the solutions are simply chiral rotations of free spinors, and are discussed for example in [40]. For Shei's complex kink condensate (2.46), the spinor solutions are given in [20, 55]. For the complex kink crystal (2.35), the two independent spinor solutions can be written

as

$$\psi_+ = -\sqrt{\frac{A}{2|dk/d\alpha|}}e^{i\eta_3\alpha}\begin{pmatrix} \frac{\sigma(Ax+i\mathbf{K}'-i\alpha-i\theta/4)}{\sigma(Ax+i\mathbf{K}')\,\sigma(i\alpha+i\theta/4)}e^{\frac{iAx}{2}[-i\zeta(i\theta/2)+i\,\mathrm{ns}(i\theta/2)]+i\theta\eta_3/4+i\pi/4} \\ \frac{\sigma(Ax+i\mathbf{K}'-i\alpha+i\theta/4)}{\sigma(Ax+i\mathbf{K}')\,\sigma(i\alpha-i\theta/4)}e^{-\frac{iAx}{2}[-i\zeta(i\theta/2)+i\,\mathrm{ns}(i\theta/2)]-i\theta\eta_3/4-i\pi/4} \end{pmatrix} \times \exp\left[(-\frac{iAx}{2}[i\zeta(i\alpha+i\theta/4)+i\zeta(i\alpha-i\theta/4)]\right]$$

$$\psi_- = \sqrt{\frac{A}{2|dk/d\alpha|}}e^{-i\eta_3\alpha}\begin{pmatrix} \frac{\sigma(Ax+i\mathbf{K}'+i\alpha-i\theta/4)}{\sigma(Ax+i\mathbf{K}')\,\sigma(i\alpha-i\theta/4)}e^{\frac{iAx}{2}[-i\zeta(i\theta/2)+i\,\mathrm{ns}(i\theta/2)]+i\theta\eta_3/4+i\pi/4} \\ \frac{\sigma(Ax+i\mathbf{K}'+i\alpha+i\theta/4)}{\sigma(Ax+i\mathbf{K}')\,\sigma(i\alpha+i\theta/4)}e^{-\frac{iAx}{2}[-i\zeta(i\theta/2)+i\,\mathrm{ns}(i\theta/2)]-i\theta\eta_3/4-i\pi/4} \end{pmatrix} \times \exp\left[\frac{iAx}{2}[i\zeta(i\alpha+i\theta/4)+i\zeta(i\alpha-i\theta/4)]\right] \tag{2.68}$$

Here, α is a spectral parameter that characterizes the energy and momentum of these solutions, and k is the momentum, defined below in (2.73). Notice that $\psi_\pm$ differ from one another by the sign of α.

To relate the energy eigenvalue E to the spectral parameter α, we substitute these forms into the BdG equation (2.67), and make use of the Weierstrass function identity (B.13). This identity immediately shows that these are indeed solutions, and determines the energy to be

$$\begin{aligned} E(\alpha) &= \frac{A}{2}[i\,\zeta(i\alpha-i\theta/4)-i\,\zeta(i\alpha+i\theta/4)+i\,\zeta(i\theta/2)+i\,\mathrm{ns}(i\theta/2)] \\ &= -1+2\left(\frac{\mathcal{P}(i\theta/4)-\mathcal{P}(i\mathbf{K}')}{\mathcal{P}(i\theta/4)-\mathcal{P}(i\alpha)}\right) \end{aligned} \tag{2.69}$$

where A is given by (2.36). The spectral parameter α appearing in the spinor solutions (2.68), is defined on the vertical edges, $0 \le i\alpha \le i\mathbf{K}'(\nu)$, $\mathbf{K}(\nu) \le i\alpha \le \mathbf{K}(\nu)+i\mathbf{K}'(\nu)$, of the fundamental rectangle shown in Figure 2.10. Only on these

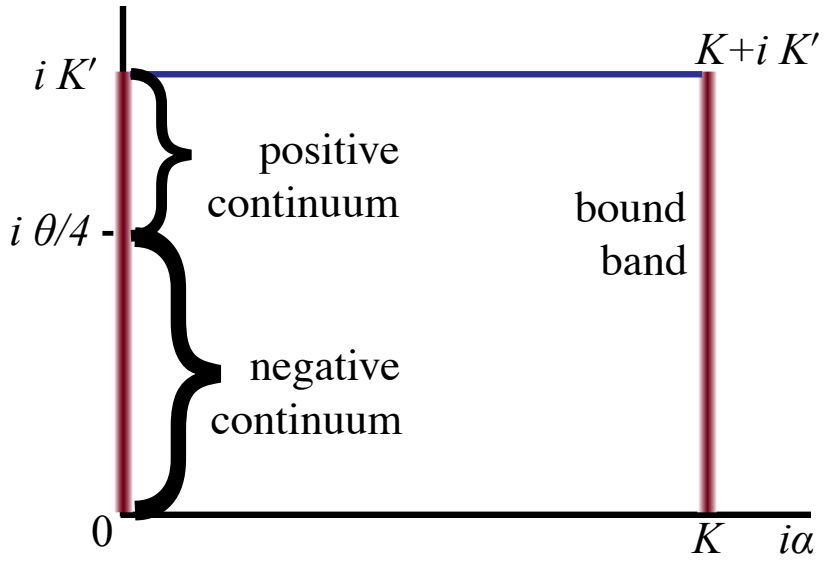

Fig. 2.10: The fundamental rectangle for the spectral parameter $i\alpha$.

edges of the fundamental rectangle are the spinor wavefunctions in (2.68) bounded, and is the energy $E(\alpha)$ real. The bound band is characterized by $\mathbf{K}(\nu) \leq i\alpha \leq \mathbf{K}(\nu) + i\mathbf{K}'(\nu)$, while the positive and negative energy continua are characterized by $0 \leq i\alpha \leq i\mathbf{K}'(\nu)$. The point $\alpha = \theta/4$ represents $E = \pm\infty$, depending on the side of approach. The vertices of the rectangle correspond to the band edges [compare with equation (2.41)]:

$$\begin{aligned} E_1 &= E(i\alpha = 0) = -1 \\ E_2 &= E(i\alpha = \mathbf{K}) = -1 + 2\,\mathrm{nc}^2(i\theta/4) \\ E_3 &= E(i\alpha = \mathbf{K} + i\mathbf{K}') = -1 + 2\,\mathrm{nd}^2(i\theta/4) \\ E_4 &= E(i\alpha = i\mathbf{K}') = +1 \end{aligned} \tag{2.70}$$

The right-hand boundary of the fundamental rectangle corresponds to the bound

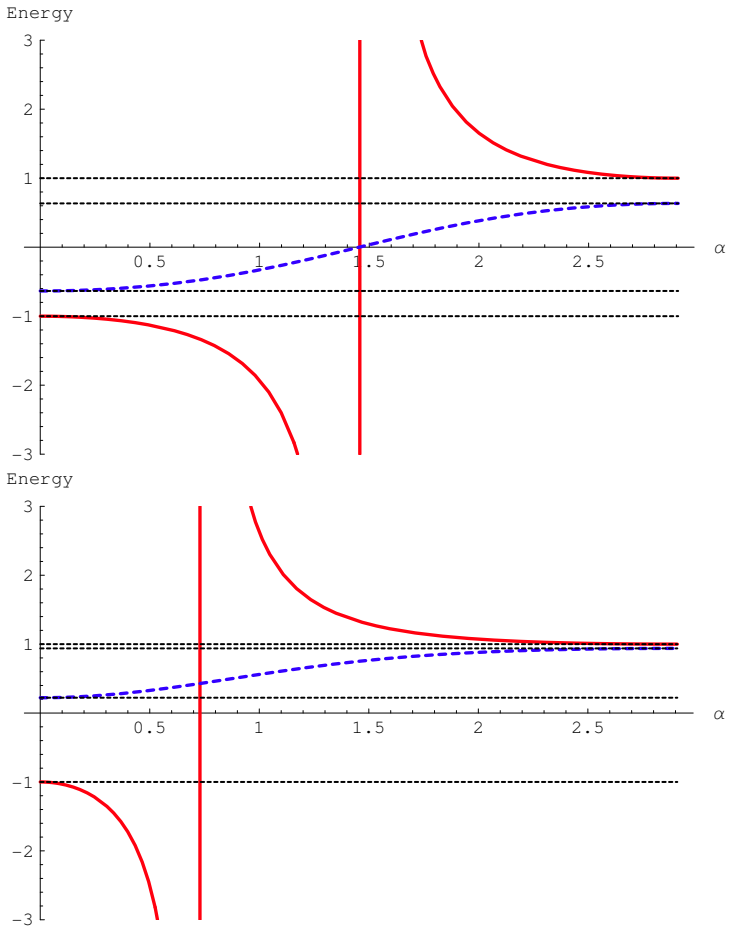

Fig. 2.11: Energy $E(\alpha)$ from (2.69) as a function of the spectral parameter α.

band, while the left-hand boundary corresponds to the positive and negative energy continua. The point $\alpha = \theta/4$ is associated with the point at infinity; the bottom of the Dirac sea is approached as $\alpha \to \theta/4$ from below, and the top of the positive energy continuum as $\alpha \to \theta/4$ from above. This is depicted in Figure 2.11. The solid [red] curves show the continuum energies, while the dashed [blue] curves show the energy in the bound band. The horizontal dashed lines denote the band edge energies E_1, E_2, E_3 and E_4 from (2.70), and the vertical [red] line gives

the asymptote to $E = \mp\infty$ at $\alpha = \theta/4$, as discussed in the text. These curves are for elliptic parameter $\nu = 0.05$. The first plot is for $\theta = 2\mathbf{K}' = 5.82$, so that the band is symmetric about the origin. The second plot is for $\theta = \mathbf{K}' = 2.91$, so the band is asymmetrically offset from the origin.

To identify the momentum associated with these solutions, we recall that the quasiperiodic winding (2.37) of the condensate in (2.35) implies that the BdG hamiltonian (2.10) is invariant under a period shift, up to a global chiral rotation through the winding angle φ:

$$H\,(x+L) \;\; = \;\; e^{i\gamma_5\varphi}\,H\,(x)\;e^{-i\gamma_5\varphi} \tag{2.71}$$

Using the quasiperiodicity properties of the Weierstrass functions (B.2), we see that under a period shift, the spinors in (2.68) acquire a chiral rotation and a Bloch phase:

$$\psi_\pm(x+L) \;\; = \;\; e^{\pm ikL}e^{i\varphi\gamma_5}\psi_\pm(x) \tag{2.72}$$

where φ is the winding angle defined in (2.37). The Bloch momentum k is expressed in terms of the spectral parameter α as:

$$k(\alpha) = -\frac{A}{2}\left[i\,\zeta(i\alpha + i\theta/4) + i\,\zeta(i\alpha - i\theta/4) + 2\eta\alpha/\mathbf{K}\right] \tag{2.73}$$

This is the relativistic version of Bloch's theorem. The momentum is real for α taking values on the vertical edges of the fundamental rectangle, and is plotted in Figure 2.12. The first plot shows the momentum in the positive and negative

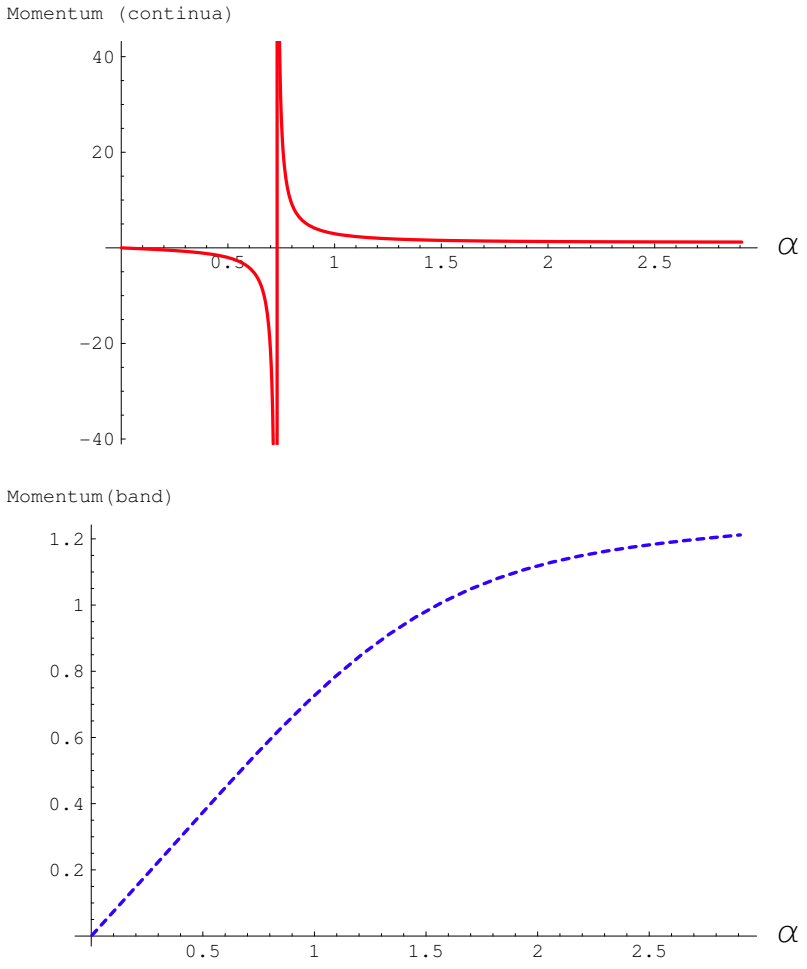

Fig. 2.12: Momentum as a function of the spectral parameter α.

continua and in the second plots shows it in the bound band. Note that $dk/d\alpha$ is negative in the continuum and positive in the bound band. These plots are for $\nu = 0.05$ and $\theta = \mathbf{K}'$, as in the second figure in Figure 2.11. The vertical [red] line in the first plot gives the asymptote to $k = \mp\infty$ at $\alpha = \theta/4$, as discussed in the text. Since $k(\alpha)$ is odd in α, we see that $\psi_\pm$ in (2.68) are positive and negative momentum solutions.

2.5.2 Density of states

In this Section we present an efficient characterization of the density of states, and show how this relates to the resolvent in (2.30). In the previous section both the energy E and the momentum k were expressed in terms of the spectral parameter α. Now consider the derivatives of the energy and momentum with respect to the spectral parameter α. From (2.69) and (2.73) we see that

$$\begin{aligned} \frac{dE}{d\alpha} &= -\frac{A}{2}\left[\mathcal{P}\left(i\alpha + i\theta/4\right) - \mathcal{P}\left(i\alpha - i\theta/4\right)\right] \\ \frac{dk}{d\alpha} &= -\frac{A}{2}\left[\mathcal{P}\left(i\alpha + i\theta/4\right) + \mathcal{P}\left(i\alpha - i\theta/4\right) + 2\eta/\mathbf{K}\right] \end{aligned} \tag{2.74}$$

The significance of these expressions becomes clearer once we write the resolvent functions $a(E)$, $b(E)$ and $\mathcal{N}(E)$ in (2.42) as functions of α (instead of E):

$$a(\alpha) = \frac{A^2}{2}[2\mathcal{P}(i\theta/2) - \mathcal{P}(i\alpha + i\theta/4) - \mathcal{P}(i\alpha - i\theta/4)] \tag{2.75}$$

$$b(\alpha) = A[i\zeta(i\alpha - i\theta/4) - i\zeta(i\alpha + i\theta/4) + i\zeta(i\theta/2) - i\mathrm{ns}(i\theta/2)] \tag{2.76}$$

$$\mathcal{N}(\alpha) = \frac{\mp i}{A^2[\mathcal{P}(i\alpha + i\theta/4) - \mathcal{P}(i\alpha - i\theta/4)]} \tag{2.77}$$

Here the upper sign in $\mathcal{N}$ is for the continuum states, and the lower sign is for the band. Thus, we recognize $dE/d\alpha$ as

$$\frac{dE}{d\alpha} = \mp\frac{2}{A}\sqrt{(E^2-1)(E-E_2)(E-E_3)} \quad . \tag{2.78}$$

And $dk/d\alpha$ can be written as

$$\frac{dk}{d\alpha} = -A\left[\mathcal{P}\left(i\theta/2\right) - a(\alpha)/A^2 + \eta/\mathbf{K}\right] \quad , \tag{2.79}$$

which is negative in the continuum and positive in the band [see Figure 2.12]. Consequently, the density of states can be expressed as

$$\begin{aligned}\frac{dk}{dE} &= \frac{dk}{d\alpha}\Big/\frac{dE}{d\alpha} \\ &= \mp\frac{[a(E) - A^2\mathcal{P}(i\theta/2) - A^2\eta/\mathbf{K}]}{2\sqrt{(E^2-1)(E-E_2)(E-E_3)}}\end{aligned} \tag{2.80}$$

When $\theta = 2\mathbf{K}'$, which is the GN_2 limit [i.e., with a real condensate], this density of states reduces to

$$\frac{dk}{dE} = \mp\frac{E^2 - \frac{\mathbf{E}(\tilde{\nu})}{\mathbf{K}(\tilde{\nu})}}{\sqrt{(E^2-1)(E^2-(1-\tilde{\nu}))}} \quad , \quad \tilde{\nu} \equiv \frac{4\sqrt{\nu}}{(1+\sqrt{\nu})^2} \tag{2.81}$$

where $\mathbf{E}$ and $\mathbf{K}$ are the complete elliptic integrals [101, 102]. This density of states (2.81) is precisely that found for the single-band finite-gap Schrödinger system of the GN_2 model [22]. The result in (2.43) generalizes this density of states to the general complex crystalline condensate (2.35).

The density of states (2.43) has been derived from the energy and momentum of the spinor solutions in (2.68). For consistency, we compare this with the trace of the resolvent (2.30) over one period:

$$\begin{aligned}\frac{1}{L}\int_L \mathrm{tr}_D\, R(x;E)dx &= \frac{A}{2\mathbf{K}}\int_{-\mathbf{K}/A}^{+\mathbf{K}/A} 2\mathcal{N}(E)\left(a(E) + |\Delta(x)|^2\right)dx \\ &= \frac{A\mathcal{N}(E)}{\mathbf{K}}\int_{-\mathbf{K}/A}^{+\mathbf{K}/A} dx\left[a(E) + A^2\left(\mathcal{P}(Ax + i\mathbf{K}') - \mathcal{P}(i\theta/2)\right)\right] \\ &= \frac{[a(E) - A^2\mathcal{P}(i\theta/2) - A^2\eta/\mathbf{K}]}{2\sqrt{(1-E^2)(E-E_2)(E-E_3)}} \quad ,\end{aligned} \tag{2.82}$$

where we have used the integral

$$\int_{-\mathbf{K}/A}^{+\mathbf{K}/A} \mathcal{P}(Ax + i\mathbf{K}')dx = -\frac{2\eta}{A} \quad . \tag{2.83}$$

This illustrates the consistency of our resolvent ansatz (2.30) with the spectral properties of the associated BdG equation.

2.5.3 Consistency condition and fermion bilinears

Recall that, in order order to solve the gap equation (2.27)

$$\Delta(x) = -2ig^2 N_f \mathrm{tr}_E \left[\mathcal{N}(E)\left(b(E)\Delta(x) - i\Delta'(x)\right)\right] \tag{2.84}$$

we first need to show that the coefficient of $\Delta'(x)$ on the right-hand-side vanishes once the energy trace is taken:

$$\mathrm{tr}_E \left[\mathcal{N}(E)\right] = 0 \tag{2.85}$$

This computation is greatly simplified by converting it into an integral over the spectral parameter α. Recalling (2.78) and the normalization factor in (2.42) we have

$$\mathcal{N}(E) \;=\; \pm\frac{i}{2A}\frac{d\alpha}{dE} \quad . \tag{2.86}$$

We assume that the negative energy continuum is fully occupied, and that the band inside the gap is partially occupied, by a fraction ξ. Then we can express (2.85) as

$$\begin{aligned} 0 &= \frac{i}{2\pi A}\left\{\int_0^{\theta/4} d\alpha - \int_{-i\mathbf{K}}^{-i\mathbf{K}+\xi\,\mathbf{K}'} d\alpha\right\} \\ &= \frac{i}{2\pi A}(\theta/4 - \xi\,\mathbf{K}') \end{aligned} \tag{2.87}$$

Thus, θ must satisfy the condition:

$$\frac{\theta}{4\mathbf{K}'} = \xi = \text{filling fraction.} \tag{2.88}$$

The consistency condition (2.88) is shown in Figure 2.13.

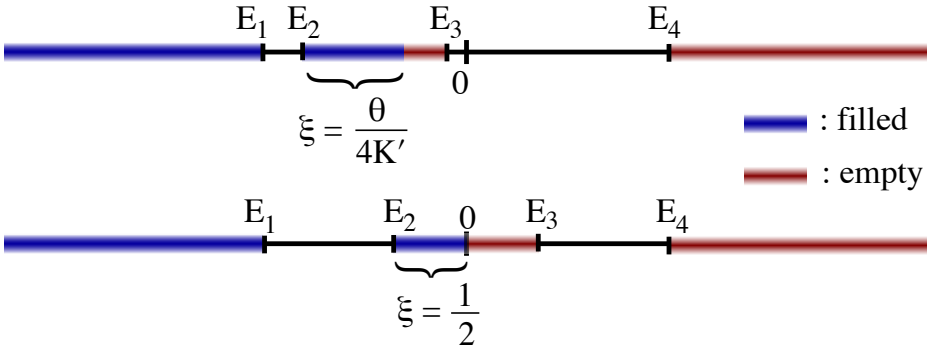

Fig. 2.13: The occupation of single-particle fermionic states.

To appreciate this condition, we consider some special limiting cases. In the real [GN_2] limit, where $\theta = 2\mathbf{K}'$, this corresponds to filling the band half-way. Since the band is symmetrically placed about zero energy, this corresponds precisely to filling all the negative energy states, as in the conventional GN_2 model analysis [10, 19]. For the single kink, which is obtained in the infinite period limit, the bound state is half occupied [38].

For general θ, in the infinite period limit, where $\mathbf{K}' \to \pi/2$, we recover Shei's condition (2.52) that $\theta/2\pi$ is the fractional filling of the bound state in the gap. Note that in this case, the fractional filling of this state is conventionally interpreted [20, 21] in terms of the filling of the level by a fixed fraction $\frac{n}{N_f}$ of the fermion flavors, with this fraction kept fixed in the infinite N_f limit. At finite

period, it is thermodynamically more natural to consider a fraction of the band being occupied by all flavors, as above. As the band contracts to a single bound state in the infinite period limit, we smoothly tend to the situation of having the level partially filled, while maintaining consistency with the gap equation for any period.

The other condition required for the gap equation (2.84) to be satisfied is that

$$-2ig^2 N_f \mathrm{tr}_E \left[\mathcal{N}(E)\, b(E)\right] = 1 \quad . \tag{2.89}$$

This is the standard vacuum gap equation for the renormalization of the coupling [10, 19, 20, 21].

Alternatively, given the spinor solutions of the BdG equation, we can reconstruct the expectation values $\langle\bar{\psi}(x)\psi(x)\rangle$ and $-\langle\bar{\psi}(x)i\gamma^5\psi(x)\rangle$, to verify that they correspond to the real and imaginary parts of condensate $\Delta(x)$. From (2.68), we find

$$\begin{aligned}
\bar{\psi}_k(x)\psi_k(x) - i\,\bar{\psi}_k(x)i\gamma^5\psi_k(x) &= \psi_k^\dagger(x)(\gamma^0+\gamma^1)\psi_k(x) \\
&= \frac{iA}{|dk/d\alpha|}\exp\left[-2i\eta_3\alpha + iAx\left(-i\zeta(i\theta/2) + i\mathrm{ns}(i\theta/2)\right)\right] \\
&\quad\times\frac{\sigma(Ax+i\mathbf{K}'+i\alpha-i\theta/4)\sigma(Ax-i\mathbf{K}'-i\alpha-i\theta/4)}{\sigma(Ax+i\mathbf{K}')\sigma(-i\alpha-i\theta/4)\sigma(i\alpha-i\theta/4)\sigma(Ax-i\mathbf{K}')} \\
&= \frac{i}{|dk/d\alpha|}\left[\zeta(Ax+i\mathbf{K}') - \zeta(Ax+i\mathbf{K}'-i\theta/2)\right. \\
&\qquad\left. +\zeta(i\alpha-i\theta/4) - \zeta(i\alpha+i\theta/4)\right]\,\Delta(x) \\
&= \frac{1}{|dk/d\alpha|}\frac{1}{A}\left[b(E)\,\Delta(x) - i\Delta'(x)\right]
\end{aligned} \tag{2.90}$$

where the subscript k on ψ_k emphasizes that these are spinor solutions of a given momentum k. In deriving (2.90) we have used the product identity (B.13) for the Weierstrass sigma function.

Thus, for a given momentum k, $\bar{\psi}_k(x)\psi_k(x) - i\,\bar{\psi}_k(x)i\gamma^5\psi_k(x)$ has the same x dependence as the upper off-diagonal entry of the resolvent, which appears in the gap equation (2.84). To compute the expectation value we trace over the N_f flavors and integrate over momentum:

$$\begin{aligned}\langle\bar{\psi}(x)\psi(x)\rangle - i\langle\bar{\psi}(x)i\gamma^5\psi(x)\rangle &= N_f\int\frac{dk}{2\pi}\left[\bar{\psi}_k(x)\psi_k(x) - i\,\bar{\psi}_k(x)i\gamma^5\psi_k(x)\right] \\ &= \frac{N_f}{2\pi A}\int d\alpha\,\mathrm{sgn}\left(\frac{dk}{d\alpha}\right)\left[b(\alpha)\Delta(x) - i\Delta'(x)\right]\end{aligned} \tag{2.91}$$

Thus we have precisely the same integrals as were evaluated above to show that the gap equation is satisfied. The vanishing of the coefficient of $\Delta'(x)$ leads to the same relation (2.88) between the filling fraction and θ, while the the coefficient of $\Delta(x)$ is again the vacuum gap equation (2.89) expressing the renormalization of the coupling constant g^2N_f.

As a side remark, in the GN_2 case where there is no pseudoscalar condensate, the spinors satisfy:

$$\bar{\psi}_k(x)\psi_k(x) = \frac{1}{|dk/d\alpha|}\frac{1}{A}b(k)\,\Delta(x) \tag{2.92}$$

Therefore; the spinors not only solve the Hartree-Fock equation $(i\partial\!\!\!/ - f(k)\langle\bar{\psi}\psi\rangle)\psi_k =$

0, but also the nonlinear Dirac equation:

$$(i\partial\!\!\!/ - f(k)\bar{\psi}_k\psi_k)\psi_k = 0 \tag{2.93}$$

Here $f(k) = |dk/d\alpha|A/b(k)$ is the momentum dependent coefficient given in (2.92). Moreover, in addition to the static, inhomogeneous solutions we discussed, there are also genuinely time dependent solutions of this nonlinear Dirac equation [41, 42]. One class of these time dependent solutions describes scattering multi kink (antikink) solutions. Another class describes kinks (antikinks) in a type of oscillatory motion, known as breathers. There is an elegant connection between the nonlinear Dirac equation (2.93) and classical string theory on AdS_3 [42, 43] where the inhomogeneous phases in the GN_2 model are mapped to certain excitation modes of closed strings.

2.5.4 Charge density and axial anomaly

An important property of the twisted crystal phase is that while the condensate $\Delta(x)$ is spatially inhomogeneous, the expectation value of the charge density is spatially uniform. From the explicit spinor solutions in (2.68) we find:

$$\psi_k^\dagger(x)\psi_k(x) = \frac{1}{|dk/d\alpha|}\frac{1}{A}\left(|\Delta(x)|^2 + a(\alpha)\right) \tag{2.94}$$

For a given single particle state of momentum k, the charge density $\psi_k^\dagger(x)\psi_k(x)$ is spatially inhomogeneous, but this inhomogeneity is washed out by integrating

over k, so that the expectation value is uniform:

$$\frac{d}{dx}\langle\psi^\dagger(x)\psi(x)\rangle = 0 \tag{2.95}$$

Indeed, for a given k, the charge density $\psi_k^\dagger(x)\psi_k(x)$ has spatial inhomogeneity determined by $|\Delta(x)|^2$, the magnitude squared of the condensate. But the coefficient of this x-dependent term in (2.94) is precisely the same as the coefficient of the $\Delta'(x)$ term in (2.90). We just saw above that this term vanishes [when the energy trace is taken], in order to satisfy the gap equation. Thus, the very same condition (2.88) that ensures that the gap equation is satisfied also shows that $\langle\psi^\dagger(x)\psi(x)\rangle$ is uniform.

There is another, more physical, way to understand this fact [44]. It expresses the conservation of axial charge in the NJL_2 model. Recall that the NJL_2 system has two conserved currents: the first is the charge current $j^\mu = \bar\psi\gamma^\mu\psi$, and the second is the axial current $j_5^\mu = \bar\psi\gamma^\mu\gamma^5\psi$. In $1+1$ dimensions these are related by $j_5^\mu = \epsilon^{\mu\nu}j_\nu$. For static but spatially inhomogeneous condensates, charge current conservation is automatically satisfied. Axial current conservation is more interesting. For a static condensate,

$$\frac{\partial}{\partial x^\mu}\langle j_5^\mu(x)\rangle = \frac{d}{dx}\langle\psi^\dagger(x)\psi(x)\rangle \tag{2.96}$$

so axial charge conservation requires a uniform charge expectation value, as was found above (2.95) from the single-particle spectral properties. Another way to see this is to observe that we can express the expectation value of the axial current

in terms of the resolvent

$$\langle j_5^\mu \rangle \;=\; tr_{E,D}\left(\gamma^0\gamma^\mu\gamma^5 R(x;E)\right) \tag{2.97}$$

Taking the spatial derivative and using the Eilenberger equation (2.24), we find

$$\begin{aligned}\frac{d}{dx}\langle j_5^1\rangle &= tr_{E,D}\left(\partial_x R(x;E)\right)\\ &= 2\,\mathcal{R}e[\Delta(x)]\langle\bar\psi(x)i\gamma^5\psi(x)\rangle - 2\,\mathcal{I}m[\Delta(x)]\langle\bar\psi(x)\psi(x)\rangle\end{aligned} \tag{2.98}$$

Thus, once again, the gap equation ensures that axial current conservation is satisfied. Interestingly, it is encoded into the Eilenberger equation (2.24). In the following section 3.1 we will revisit this property for nonzero chemical potential μ.

On the other hand, in the GN_2 model, which has just a discrete chiral symmetry, there is no axial current conservation and $\mathcal{I}m[\Delta(x)] = 0$. Then the Eilenberger equation (2.24) again expresses the correct relation

$$\partial_\mu\langle j_5^\mu\rangle = 2\Delta(x)\langle\bar\psi(x)i\gamma^5\psi(x)\rangle \tag{2.99}$$

and $\langle\bar\psi(x)\psi(x)\rangle$, $\Delta(x)$ and $\langle\bar\psi(x)i\gamma^5\psi(x)\rangle$ are all inhomogeneous.

Chapter 3

Thermodynamics of NJL_2 and GN_2 models

In this chapter we study the phase structure of the $\mathrm{NJL}_2$and GN_2 systems at nonzero temperature and chemical potential. Our starting point is the solution of the corresponding gap equation that was analysed in the previous chapter. Recall that the most general solution (2.35) depends on four parameters characterizing the scale (λ), phase (q), period (ν) and twist (θ). The thermodynamic ground state (for given values of T and μ) is the minima of the grand canonical potential with respect to these four parameters. At the end of the minimization, all of the parameters; hence the shape of the condensate and the energy associated with the single particle fermion, will be determined by T and μ.

We start by exploiting the symmetries of the Bogoluibov-deGennes Hamiltonian and derive a general result on the minimization with respect to λ and q that holds for *any* condensate Δ. Then using this general result we will show that the thermodynamically favored phase of the NJL_2system is the spiral condensate introduced in (2.4.3) and the twisted crystal (2.35) is thermodynamically unstable. Next, we will revisit the phase diagram of the GN_2 model [22] in order to

compare and contrast with the NJL_2 one.

Consequently, we will show that the Ginzburg-Landau expansions of these models can be mapped to certain integrable hierarchies. This mapping provides special properties to the expansions allowing them to be soluble to all orders. We demonstrate how the inhomogeneous phases appear near the tricritical point in the Ginzburg Landau approximation. This analysis suggests new approaches to the Ginzburg-Landau expansion in the higher dimensional models where it may be the only viable approach.

The chapter will be concluded with a general overview of the phase diagrams NJL_2 and GN_2 models focusing on the underlying physical phenomena; namely chiral symmetry breaking and the Peierls instability.

3.1 Symmetries and thermodynamics

In this Section we describe a simple but important symmetry property of the Bogoliubov-de Gennes equation (2.67), that has important consequences for the thermodynamical analysis. The Bogoliubov-de Gennes equation (2.67) admits a family of solutions obtained by rescaling and phase shifting (i.e. making a *linear* local chiral rotation) a given solution:

$$\begin{aligned} \Delta(x) &\to \lambda\, \Delta(\lambda\, x)\, e^{2iqx} \\ \psi(x) &\to e^{iqx\gamma_5} \lambda^{1/2}\, \psi(\lambda\, x) \end{aligned} \tag{3.1}$$

which generates all the linear transformations acting on the energy spectrum:

$$E \to \lambda\, E + q \quad . \tag{3.2}$$

Acting on the band edges, $E_i \to \lambda E_i + q$, the effect of the transformation on the density of states is:

$$\rho(E) \to \rho\left(\frac{E-q}{\lambda}\right) \quad . \tag{3.3}$$

Since this symmetry defines a family of solutions spanned by parameters λ and q, the minimization of the grand potential with respect to them provides valuable information concerning the thermodynamic properties of the NJL_2 model. Furthermore, being a symmetry of the Hamiltonian with a generic order parameter Δ, the results of this minimization are global. In particular, the functional space of solutions of the complex NLSE is spanned by four parameters λ, q, θ and ν.The above result means that we can first carry out the minimization with respect to the scale and phase parameters λ and q, and then with respect to the two remaining parameters θ and ν.

It is crucial that the phase parameter q does not exist in GN_2 system. The reason is that the phase parameter is due to the chiral U(1) symmetry of the NJL_2 model, which does not exist in GN_2 . Instead, it has a discrete $\mathcal{Z}_2$ symmetry whose effect on the energy spectrum is the charge conjugation symmetry:

$$E \to -E \tag{3.4}$$

Consequently, as opposed to the offset freedom in the NJL_2 energy spectrum

(3.2), any phase in the GN_2 system has a symmetric energy spectrum. This is an important property and has a direct effect on the phase diagram of the GN_2 model as we will study explicitly. In fact, the underlying reason for the vast difference in the phase diagrams of NJL_2 and GN_2 models is this difference of the chiral symmetry.

We will show that the grand potential has an anomalous dependence on λ and q which makes the minimization carry non-trivial physical information. Physically, the nontrivial λ dependence is due to the breaking of conformal symmetry due to the dimensional transmutation, and the q dependence is due to the chiral U(1) symmetry breaking.

It is useful to define the "unscaled" and "unshifted" spectrum to be the one with $\lambda = 1$ and $q = 0$, so that $E_1 = -1$, and $E_4 = 1$ (in units where the vacuum fermion mass is 1). All other spectral functions can be generated from this basic solution using the simple transformation (3.3). The corresponding density of states will be written as

$$\hat{\rho}(E) = \frac{1}{2\pi} \frac{\Big(2E^2 - (\hat{E}_2 + \hat{E}_3)E - (\hat{E}_3 - \hat{E}_2)^2/4 - 1 + Z\Big)}{\sqrt{(E^2-1)(E-\hat{E}_2)(E-\hat{E}_3)}} \tag{3.5}$$

where $Z = Z(\theta, \nu)$ is defined in (2.44), and

$$\begin{aligned} \hat{E}_2 &= -1 + 2\,\mathrm{nc}^2(i\theta/4;\nu) \\ \hat{E}_3 &= -1 + 2\,\mathrm{nd}^2(i\theta/4;\nu) \end{aligned} \tag{3.6}$$

Importantly, $\hat{\rho}(E)$ depends parametrically only on the two remaining parameters,

θ and ν. This separation of parametric dependences has important consequences for the minimization of the thermodynamic grand potential (2.17) with respect to the parameters. Now, we analyse the transformation properties of various thermodynamic quantities:

3.1.1 Transformation properties of thermodynamic quantities

We begin our discussion with the grand canonical potential $\Psi[\hat{\Delta}(x); T, \mu]$ for the unscaled/unshifted condensate $\hat{\Delta}(x)$, obtained from (2.35) by setting the scale parameter $\lambda = 1$, and the phase parameter $q = 0$. The grand potential is formally divergent in the UV region and has to be renormalized, as is well known [10, 19, 22]. At finite density and nonzero temperature, it is convenient to separate the single particle contribution as

$$\begin{aligned} -\frac{1}{\beta}\int_{-\infty}^{\infty} dE\,\hat{\rho}(E)\ln(1+e^{-\beta(E-\mu)}) &= \int_{E_{\min}}^{\mu} dE\,\hat{\rho}(E)(E-\mu) \\ &\quad -\frac{1}{\beta}\int_{-\infty}^{\infty} dE\,\hat{\rho}(E)\ln(1+e^{-\beta|E-\mu|}) \end{aligned} \tag{3.7}$$

where $E_{\min} = -\Lambda/2 - Z/\Lambda + \ldots$, in terms of the momentum cutoff $\Lambda/2$. Only the first term, the zero temperature expression, in (3.7) is divergent. We isolate the divergent terms using the large E behaviour of the density of states (3.5):

$$\hat{\rho}(E) \approx 1 + \frac{Z}{2E^2} + \ldots \tag{3.8}$$

It should be kept in mind that these leading and sub-leading terms in the asymptotic behaviors of the density of states and dispersion relation are not limited to the

solutions of the gap equation but true for any condensate Δ with $Z =< |\hat{\Delta}|^2 >$. The quickest way to see this is by analyzing the heat kernel expansion of the Bogoluibov-de Gennes Hamiltonian, which will be studied later in this section in terms of the Ginzburg-Landau expansion. The divergent part is

$$\Psi_{\rm div} = -\frac{\Lambda^2}{8\pi} - \frac{\Lambda\mu}{2\pi} - \frac{Z}{2\pi}\ln\Lambda \quad . \tag{3.9}$$

The quadratically and linearly divergent terms are absorbed by definition of the renormalized energy and baryon number densities, and the logarithmically divergent term is canceled by the double counting correction [22]

$$\frac{1}{2N_f g^2}\frac{1}{L}\int_0^L |\hat{\Delta}(x)|^2 dx = \frac{Z}{2\pi}\ln\Lambda \tag{3.10}$$

where we have used vacuum gap equation $\frac{\pi}{N_f g^2} = \ln\Lambda$. Hence the finite renormalized grand canonical potential is

$$\begin{aligned}\Psi_{\rm ren}[\hat{\Delta}(x);T,\mu] &= \int_{E_{\rm min}}^{\mu} dE\,\hat{\rho}(E)(E-\mu) - \frac{1}{\beta}\int_{-\infty}^{\infty} dE\,\hat{\rho}(E)\ln(1+e^{-\beta|E-\mu|}) \\ &\quad + \frac{\Lambda^2}{8\pi} + \frac{\Lambda\mu}{2\pi} + \frac{Z}{2\pi}\ln\Lambda \end{aligned} \tag{3.11}$$

Now we can analyse the effect of the transformation (3.3) on the *renormalized* grand canonical potential for the general condensate

$$\Delta(x) = \lambda\,\hat{\Delta}(\lambda\,x)\,e^{2iqx} \quad . \tag{3.12}$$

The finite temperature (f.t.) contribution [the 2nd term on the r.h.s. of Eq. (3.11)] has the following simple scaling behaviour,

$$\begin{aligned}\Psi_{\rm ren}[\lambda\,\hat{\Delta}(\lambda x)\,e^{2iqx};T,\mu]\Big|_{\rm f.t.} &= -\frac{1}{\beta}\int_{-\infty}^{\infty} dE\,\hat{\rho}\left(\frac{E-q}{\lambda}\right)\ln(1+e^{-\beta|E-\mu|}) \\ &= -\frac{\lambda^2}{\hat{\beta}}\int_{-\infty}^{\infty} dE\,\hat{\rho}(E)\ln(1+e^{-\hat{\beta}|E-\hat{\mu}|}) \\ &= \lambda^2\,\Psi_{\rm ren}[\hat{\Delta}(x);\hat{T},\hat{\mu}]\Big|_{\rm f.t.} \end{aligned} \tag{3.13}$$

with the rescaled variables

$$\begin{aligned}\hat{\mu} &= \frac{\mu-q}{\lambda} \\ \hat{\beta} &= \frac{1}{\hat{T}} \;=\; \lambda\beta \end{aligned} \tag{3.14}$$

For the zero temperature contribution (z.t.) in (3.11), we start from the expression,

$$\Psi_{\rm ren}[\lambda\,\hat{\Delta}(\lambda x)\,e^{2iqx};T,\mu]\Big|_{\rm z.t.} = \int_{E^\lambda_{\rm min}}^{\mu} dE\,\hat{\rho}\left(\frac{E-q}{\lambda}\right)(E-\mu)+\frac{\Lambda^2}{8\pi}+\frac{\Lambda\mu}{2\pi}+\frac{\lambda^2 Z}{2\pi}\ln\Lambda \tag{3.15}$$

where $E^\lambda_{\rm min}=-\Lambda/2-\lambda^2 Z/\Lambda$. Here, due to the regularization, the scaling relation analoguous to Eq. (3.13) develops anomalous terms akin to the chiral U(1) and scale anomalies,

$$\Psi_{\rm ren}[\lambda\,\hat{\Delta}(\lambda x)\,e^{2iqx};T,\mu]\Big|_{\rm z.t.} = \lambda^2\;\Psi_{\rm ren}[\hat{\Delta}(x);\hat{T},\hat{\mu}]\Big|_{\rm z.t.}+\frac{Z}{2\pi}\lambda^2\ln\lambda+\lambda^2\frac{\hat{\mu}^2}{2\pi}-\frac{\mu^2}{2\pi} \tag{3.16}$$

Being renormalization effects, the extra terms are independent of temperature. As mentioned, the scale anomaly, reflected by the $\lambda^2\ln\lambda$ term is an expected result

of dimensional transmutation which breaks the conformal symmetry of the theory in the quantum level. The other two terms are the remnants of the chiral U(1) anomaly. Combining Eqs. (3.13) and (3.16), we see that the renormalized grand potential for the general condensate in (3.12), is

$$\Psi_{\rm ren}[\lambda\,\hat{\Delta}(\lambda x)\,e^{2iqx};T,\mu] = \lambda^2\left(\hat{\Psi}_{\rm ren} + \frac{Z}{2\pi}\ln\lambda + \frac{\hat{\mu}^2}{2\pi}\right) - \frac{\mu^2}{2\pi} \tag{3.17}$$

with the shorthand notation

$$\hat{\Psi}_{\rm ren} \equiv \Psi_{\rm ren}[\hat{\Delta}(x);\hat{T},\hat{\mu}]. \tag{3.18}$$

For the sake of compactness in the notation, we will drop the subscript "ren" from now on, and work exclusively with the physical renormalized thermodynamic quantities.

The grand canonical potential is related to the density ρ, [not to be confused with the density of states $\rho(E)$!], the entropy s, and the free energy u:

$$\Psi = u - \mu\rho - Ts \tag{3.19}$$

Thus we can obtain expressions for the effect of the scaling and phase shifting transformation on the renormalized ρ, s and u as follows:

From the basic relation $\rho = -\frac{\partial\Psi}{\partial\mu}$, we write $\frac{\partial}{\partial\mu} = \frac{1}{\lambda}\frac{\partial}{\partial\hat{\mu}}$, and act on (3.17) to obtain:

$$\begin{aligned}\rho &= \lambda^2(-\frac{1}{\lambda}\frac{\partial\hat{\Psi}}{\partial\hat{\mu}} - \frac{1}{\lambda}\frac{\hat{\mu}}{\pi}) + \frac{\mu}{\pi} \\ &= \lambda\,\hat{\rho} + \frac{q}{\pi}\end{aligned} \tag{3.20}$$

From the basic relation $s = -\frac{\partial \Psi}{\partial T}$, we write $\frac{\partial}{\partial T} = \frac{1}{\lambda}\frac{\partial}{\partial \hat{T}}$, and act on (3.17) to obtain:

$$\begin{aligned} s &= \lambda^2(-\frac{1}{\lambda}\frac{\partial \hat{\Psi}}{\partial \hat{T}}) \\ &= \lambda\, \hat{s} \end{aligned} \tag{3.21}$$

The transformation property of the energy density now follows directly from the relation (3.19):

$$\begin{aligned} u &= \Psi + \mu\rho + Ts \\ &= \lambda^2 \left(\hat{u} + \frac{Z}{2\pi} \ln \lambda \right) + \lambda\, q\, \hat{\rho} + \frac{q^2}{2\pi} \end{aligned} \tag{3.22}$$

We are now in a position to work out the minimization of the grand potential with respect to scale and chiral phase parameters λ and q.

3.1.2 Minimization of the grand potential Ψ with respect to the phase parameter q

The minimization of Ψ with respect to q can be transformed into minimization with respect to the chemical potential, due to the symmetry (3.3). We write $\frac{d}{dq} = -\frac{1}{\lambda}\frac{d}{d\hat{\mu}}$, and differentiate Ψ in (3.17) with respect to $\hat{\mu}$:

$$0 = -\frac{d\Psi}{d\hat{\mu}} = \lambda^2 \left(-\frac{\partial \hat{\Psi}}{\partial \hat{\mu}} - \frac{\hat{\mu}}{\pi} \right) = \lambda^2 \left(\hat{\rho} - \frac{\hat{\mu}}{\pi} \right) \tag{3.23}$$

So the q minimization implies

$$\pi \hat{\rho} = \hat{\mu} \tag{3.24}$$

Recalling (3.20) and (3.14), this means that after minimizing with respect to the phase parameter q, the (period averaged) number density is simply proportional to the chemical potential:

$$\rho = \frac{\mu}{\pi} \tag{3.25}$$

As mentioned above, this remarkable fact is independent of the form of the (complex) condensate, and simply follows from the transformation property (3.1) of the BdG Hamiltonian and its effect on the renormalized grand potential, as reflected in (3.17). Note, again, that such a relation between ρ and μ *does not arise* in the GN_2 model, where the condensate is real and there is no phase invariance parameter q.

Another way to obtain this result directly from the existence of continuous chiral symmetry is through the axial anomaly. We can identify the chemical potential with a slowly varying electrostatic potential:

$$\mu \equiv eA_0(x) \tag{3.26}$$

Then, repeating the steps in section (2.5.4), the 1+1 dimensional form of the axial anomaly for static configurations, dictates:

$$\begin{aligned} \partial_\alpha J_5^\alpha &= \frac{e}{\pi}\epsilon^{\alpha\beta}\partial_\alpha A_\beta \\ \frac{d}{dx}\langle\bar{\psi}\gamma^5\gamma^1\psi\rangle &= \frac{e}{\pi}\frac{d}{dx}\left(\frac{\mu}{e}\right) \end{aligned} \tag{3.27}$$

which, using the identity $\gamma^5\gamma^1 = \gamma^0$ and vacuum renormalization condition $\rho = 0$

at zero chemical potential, leads to the desired result:

$$\langle\bar{\psi}\gamma^0\psi\rangle = \frac{\mu}{\pi} \tag{3.28}$$

Alternatively, in the first reference in [46] it is shown, directly from the path integral à la Fujikawa, that $\langle\bar{\psi}\gamma^0\psi\rangle$ develops an anomalous term which is equal to μ/π.

3.1.3 Minimization of the grand potential Ψ with respect to the scale parameter λ

From (3.17), it follows that Ψ depends on the scale λ explicitly, and also implicitly though the dependence of $\hat{\Psi} \equiv \Psi[\hat{\Delta}; \hat{T}, \hat{\mu}]$ on $\hat{T} = T/\lambda$, and on $\hat{\mu} = (\mu - q)/\lambda$. Thus we can write

$$\begin{aligned}\frac{d\Psi}{d\lambda} &= 2\lambda\left(\hat{\Psi} + \frac{Z}{2\pi}\ln\lambda\right) + \frac{Z\lambda}{2\pi} + \lambda^2\left(-\frac{\hat{T}}{\lambda}\right)\frac{\partial\hat{\Psi}}{\partial\hat{T}} + \lambda^2\left(-\frac{\hat{\mu}}{\lambda}\right)\frac{\partial\hat{\Psi}}{\partial\hat{\mu}} \\ &= 2\lambda\left(\hat{\Psi} + \frac{Z}{2\pi}\ln\lambda + \frac{Z}{4\pi} + \frac{1}{2}\hat{T}\hat{s} + \frac{1}{2}\hat{\mu}\hat{\rho}\right)\end{aligned} \tag{3.29}$$

Since $\hat{\Psi} = \hat{u} - \hat{T}\hat{s} - \hat{\mu}\hat{\rho}$, we can express the minimization condition $\frac{d\Psi}{d\lambda} = 0$ in terms of the free energy as:

$$\hat{u} = -\frac{Z}{4\pi} - \frac{Z}{2\pi}\ln\lambda + \frac{1}{2}\hat{\mu}\hat{\rho} + \frac{1}{2}\hat{T}\hat{s} \tag{3.30}$$

If we impose also the condition (3.24) arising from the minimization with respect to the phase parameter q, we obtain the condition

$$\hat{u} = -\frac{Z}{4\pi} - \frac{Z}{2\pi}\ln\lambda + \frac{\hat{\mu}^2}{2\pi} + \frac{1}{2}\hat{T}\hat{s} \tag{3.31}$$

Alternatively, we can express these conditions in terms of the thermodynamic quantities for the general condensate $\Delta(x)$ in (3.12). Without using the condition (3.25) arising from the q minimization, the λ minimization condition (3.30) can be written as

$$u = -\frac{Z\lambda^2}{4\pi} + \frac{1}{2}\mu\,\rho + \frac{1}{2}Ts + \frac{q}{2}\left(\rho - \frac{\mu}{\pi}\right) \tag{3.32}$$

After imposing the condition (3.25) arising from the q minimization, the last term vanishes and we obtain

$$u = -\frac{Z\lambda^2}{4\pi} + \frac{\mu^2}{2\pi} + \frac{1}{2}Ts \tag{3.33}$$

These conditions must hold for any form of the condensate $\Delta(x)$, and will prove very useful in studying the phase diagram of both the NJL_2 and GN_2 models.

3.1.4 Transformation property of the consistency condition

The final technical ingredient before studying the thermodynamics is the effect of the transformation (3.1) on the consistency condition (2.34). Note that the consistency condition (2.34) must be satisfied also at finite T and μ, for the gap equation to hold. Thus, the energy trace involves the thermodynamical Fermi factor, as in (2.34). As with the grand potential, density, entropy and free energy, it is useful to express the consistency condition in terms of the condensate $\hat{\Delta}(x)$ obtained by setting the scale $\lambda = 1$, and phase $q = 0$. All we need to know is the effect of the transformation (3.2) on $\mathcal{N}(E)$. From the form of (2.42) it is clear

that

$$\mathcal{N}(E) = \frac{1}{\lambda^2}\hat{\mathcal{N}}\left(\frac{E-q}{\lambda}\right) \tag{3.34}$$

where

$$\hat{\mathcal{N}}(E) \equiv \frac{i}{4\sqrt{(E^2-1)(E-\hat{E}_2)(E-\hat{E}_3)}} \tag{3.35}$$

Hence we can write the consistency condition as

$$\int \frac{dE}{2\pi}\frac{\hat{\mathcal{N}}(E)}{1+e^{\hat{\beta}(E-\hat{\mu})}} = 0 \tag{3.36}$$

Note that this integral is finite, even at $T = 0$, and no renormalization is required. The effect of this condition is to express one of the four parameters λ, q, θ and ν, in terms of the others, in a manner depending on T and μ.

3.2 Thermal properties of the chiral spiral

We start our analysis by investigating the thermodynamics of the spiral condensate:

$$\Delta(x) = \lambda\, e^{2iqx} \tag{3.37}$$

For this condensate, $\hat{\Delta}(x) = 1$, (i.e., the vacuum fermion mass in our units), and so the thermodynamics is simply that of a constant condensate of unit magnitude. The fermion spectrum is now symmetric about 0, and so we can immediately write an expression for the corresponding grand potential $\hat{\Psi}$:

$$\hat{\Psi} = -\frac{1}{4\pi} - \frac{\hat{T}}{\pi}\int_1^\infty dE \frac{E}{\sqrt{E^2-1}} \ln((1+e^{-\hat{\beta}(E-\hat{\mu})})(1+e^{-\hat{\beta}(E+\hat{\mu})})) \tag{3.38}$$

The full grand potential Ψ for the spiral condensate (3.37) is then obtained using (3.17). Next we minimize the full grand potential Ψ with respect to q and λ.

3.2.1 Minimization with respect to the phase parameter q

At $T = 0$, we see from (3.38) that $\hat{\Psi} = -\frac{1}{4\pi}$, independent of $\hat{\mu}$, so that $\hat{\rho} = 0$. Therefore, the condition (3.24), arising from the minimization with respect to q, implies that $\hat{\mu} = 0$ at $T = 0$. In other words, $q = \mu$, so that the chemical potential lies at the center of the gap in the single-particle fermionic spectrum. With $q = \mu$, the spiral condensate (3.37) is the "chiral spiral" solution proposed in [47]. At nonzero temperature, the q minimization condition (3.24) can be written explicitly as

$$\begin{aligned} \hat{\mu} = \pi\hat{\rho} &= \pi \frac{\partial \hat{\Psi}}{\partial \hat{\mu}} \\ &= 2\sinh(\hat{\beta}\hat{\mu}) \int_1^\infty dE \frac{E}{\sqrt{E^2-1}} \frac{e^{\hat{\beta}E}}{(1+e^{\hat{\beta}(E-\hat{\mu})})(1+e^{\hat{\beta}(E+\hat{\mu})})} \end{aligned} \tag{3.39}$$

At low temperatures, $T \ll 1$, the main contribution to the energy integrals in (3.39) comes from near the upper band edge $E = 1$. So we approximate the density of states as:

$$\hat{\rho}(E) \approx \frac{1}{\sqrt{2}\sqrt{E-1}} \tag{3.40}$$

and (3.39) becomes

$$\begin{aligned} \hat{\mu} &\approx \sqrt{2}\sinh(\hat{\beta}\hat{\mu}) \int_1^\infty dE \frac{1}{\sqrt{E-1}} e^{\hat{\beta}E} e^{-\hat{\beta}(E-\hat{\mu})} e^{-\hat{\beta}(E+\hat{\mu})} \\ &= \sqrt{\frac{2\pi T}{\lambda}}\, e^{-\hat{\beta}}\, \sinh(\hat{\beta}\hat{\mu}) \end{aligned} \tag{3.41}$$

This also requires $\hat{\mu}$=0, leading again to the chiral spiral solution with $q = \mu$. Indeed, it is easy to verify numerically that the finite temperature equation (3.39) has a solution only at $\hat{\mu} = 0$, for all temperature T. Another argument in favor of $\mu = q$ at all temperatures is that instead of minimizing with respect to q, we can minimize with respect to $\hat{\mu}$. Since $\hat{\Psi}$ is symmetric under $\hat{\mu} \to -\hat{\mu}$, there must be a stationary point at $\hat{\mu} = 0$, i.e., $\mu = q$. That it is a minimum can easily be seen by looking at the sign of the 2nd derivative (Taylor expansion of the integrand). Other minima (which could only come in pairs) are ruled out numerically.

Thus, we conclude that the minimization of the grand potential with respect to the phase parameter q leads to $q = \mu$ for all temperature T, so μ always lies at the center of the gap. As should be clear from this discussion, this fact can be traced directly to the phase transformation symmetry in (3.1). This point will be further explained in Section 3.6 in terms of Peierls instability.

Another immediate consequence of $q = \mu$ is that the grand potential for the chiral spiral has a simple μ dependence. This follows because (3.24) with $\hat{\mu} = 0$ implies that $\hat{\Psi}$ is independent of the chemical potential μ. Indeed, when $\hat{\mu} = 0$, the grand potential (3.38)can then be written as

$$\hat{\Psi} = -\frac{1}{4\pi} - \frac{2\hat{T}}{\pi} \int_1^\infty dE \frac{E}{\sqrt{E^2 - 1}} \ln(1 + e^{-\hat{\beta}E}) \tag{3.42}$$

Then the general relation (3.17) implies that for the chiral spiral condensate the

full grand potential is

$$\Psi = \frac{\lambda^2}{4\pi}\left(\ln\lambda^2 - 1\right) - \frac{2\lambda T}{\pi}\int_1^\infty dE \frac{E}{\sqrt{E^2-1}}\ln(1+e^{-\hat{\beta}E}) - \frac{\mu^2}{2\pi} \tag{3.43}$$

Thus, the grand potential for the chiral spiral has a simple μ dependence, and it is clear that $\rho = -\partial\Psi/\partial\mu = \mu/\pi$. At this point we see that the λ dependence is completely decoupled from μ; therefore there cannot be any phase transitions along the μ axis.

3.2.2 Minimization with respect to the scale parameter λ

From (3.43) it follows that the scale parameter λ is determined only by T, independent of the chemical potential μ. Indeed, minimizing (3.43) with respect to λ, we obtain the equation for the thermal mass scale $\lambda(T)$:

$$0 = \lambda\frac{\ln\lambda}{\pi} - \frac{2T}{\pi}\int_1^\infty dE \frac{E}{\sqrt{E^2-1}}\ln(1+e^{-\hat{\beta}E}) + \lambda\frac{2}{\pi}\int_1^\infty dE \frac{E^2}{\sqrt{E^2-1}}\frac{1}{1+e^{\hat{\beta}E}} \tag{3.44}$$

It is a simple exercise to show that this is equivalent to the general λ minimization condition (3.33), expressed in terms of the entropy and the free energy. At $T = 0$, (3.44) reduces to $\lambda\ln\lambda = 0$, which implies that $\lambda(T = 0)$=1, and the grand potential is simply

$$\Psi_{\min}^{T=0} = -\frac{1}{4\pi} - \frac{\mu^2}{2\pi} \tag{3.45}$$

For small but nonzero temperature, the scale parameter λ receives an exponentially small finite T correction, found by approximating the energy integrals in

(3.44):

$$\lambda(T) \sim 1 - \sqrt{2\pi T} e^{-1/T} \qquad , \qquad T \ll 1 \tag{3.46}$$

Applying the same approximation to the minimized grand potential in (3.43) we find the leading small T correction to the grand potential:

$$\begin{aligned} \Psi_{\rm min}^{T\ll 1} &\sim \frac{\lambda^2}{4\pi}(\ln\lambda^2 - 1) - \sqrt{\frac{2T^3}{\pi}} e^{-1/T} - \frac{\mu^2}{2\pi} \\ &\sim -\frac{1}{4\pi} - \frac{\mu^2}{2\pi} - \sqrt{\frac{2T^3}{\pi}} e^{-1/T} \end{aligned} \tag{3.47}$$

For general T, the temperature dependent mass scale $\lambda(T)$ can be obtained numerically from (3.44). The scale $\lambda(T)$ decreases monotonically from the value $\lambda = 1$ at $T = 0$, and vanishes at a critical temperature

$$T_c = \frac{e^\gamma}{\pi} \approx 0.566933 \tag{3.48}$$

At this temperature, $T = T_c$, the system undergoes a phase transition to a massless phase. Obviously, this phase transition is independent of the chemical potential μ, as follows from the fact that $\lambda(T)$ is independent of μ. We can trace this fact directly to the simple form (3.43) of the grand potential for the chiral spiral condensate, after minimization with respect to the scale parameter q.

Just below T_c the dependence of λ on T is nonanalytic, as can be seen from the following argument. After integrating by parts the second integral in (3.44), and expanding the Fermi factor we obtain

$$0 = \ln\lambda + 2\sum_{n=1}^{\infty}(-1)^{n+1}\int_1^\infty dE \frac{1}{\sqrt{E^2-1}} e^{-n\hat{\beta}E} = \ln\lambda + 2\sum_{n=1}^{\infty}(-1)^{n+1} K_0(n\hat{\beta}) \tag{3.49}$$

where $K_0(x)$ is the modified Bessel function. To obtain the critical exponent near the phase transition, we analyse this equation near small values of λ. Since $\hat{\beta} = \lambda/T$ we expand the Bessel functions around zero:

$$0 = \ln\lambda + 2\sum_{n=1}^{\infty}(-1)^{n+1}\left[-\ln\left(\frac{n\lambda}{2T}\right) - \gamma - \frac{n^2\lambda^2}{4T^2}\left(\ln\left(\frac{n\lambda}{2T}\right) + \gamma - 1\right)\right] \quad (3.50)$$

Here γ is Euler's constant. The n sums can be evaluated in terms of the Riemann zeta function, leading to

$$0 = \ln(T\pi) - \gamma - \frac{14\zeta'(-2)\lambda^2}{4T^2} \quad (3.51)$$

In particular, at the phase transition where $\lambda = 0$, the critical temperature is found to be $T_c = e^{\gamma}/\pi$, and to the leading order in $(T_c - T)$, for $T < T_c$, the critical exponent is found as 1/2:

$$\lambda(T) = \sqrt{\frac{2T_c}{-7\zeta'(-2)}}\sqrt{T_c - T} + \cdots \approx 3.06\sqrt{T_c(T_c - T)} + \ldots \quad (3.52)$$

The full dependence of λ to T is shown in Fig. 3.1

Thus, for the spiral condensate (3.37), the thermodynamic phase diagram is given in Figure 3.2, showing the phase transition at $T = T_{\rm tc} = e^{\gamma}/\pi \approx 0.5669$, independent of μ. After minimizing the grand potential we learn that in the region $T < T_c$, the pitch angle q of the spiral condensate is directly proportional to the chemical potential, $q = \mu$, independent of T, while the amplitude $\lambda(T)$ is just a function of temperature [vanishing at T_c], independent of μ.

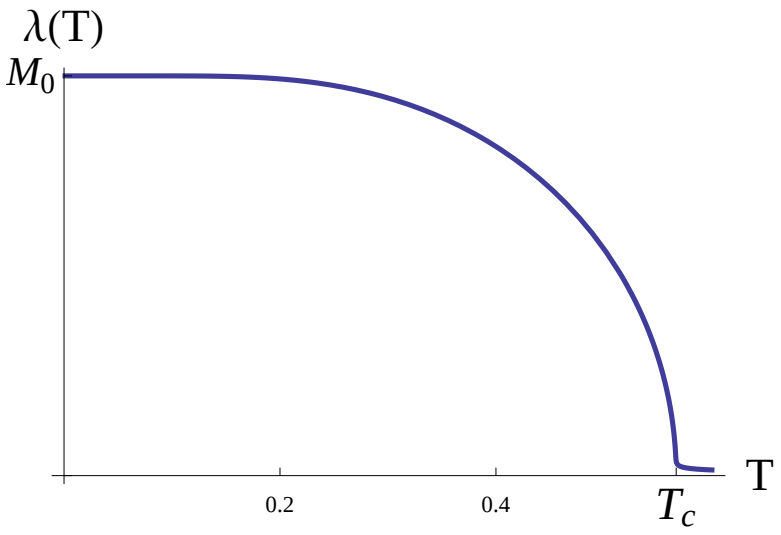

Fig. 3.1: The thermal mass scale λ as a function of T.

3.3 Instability of the twisted kink crystal

In this section we develop results for the thermodynamics of the NJL_2 model with the twisted kink crystal condensate, that is the general solution of the inhomogeneous gap equation. Recall that the twisted kink crystal condensate (2.35) is characterized by 4 parameters: the scale parameter λ, the phase parameter q, an angular parameter θ, and the elliptic parameter ν. We first consider the situation analytically at $T = 0$, then at nonzero T. In each case, we show that this crystal phase is unstable against the chiral spiral and never favored. The physical reasoning is given in Section 3.6.

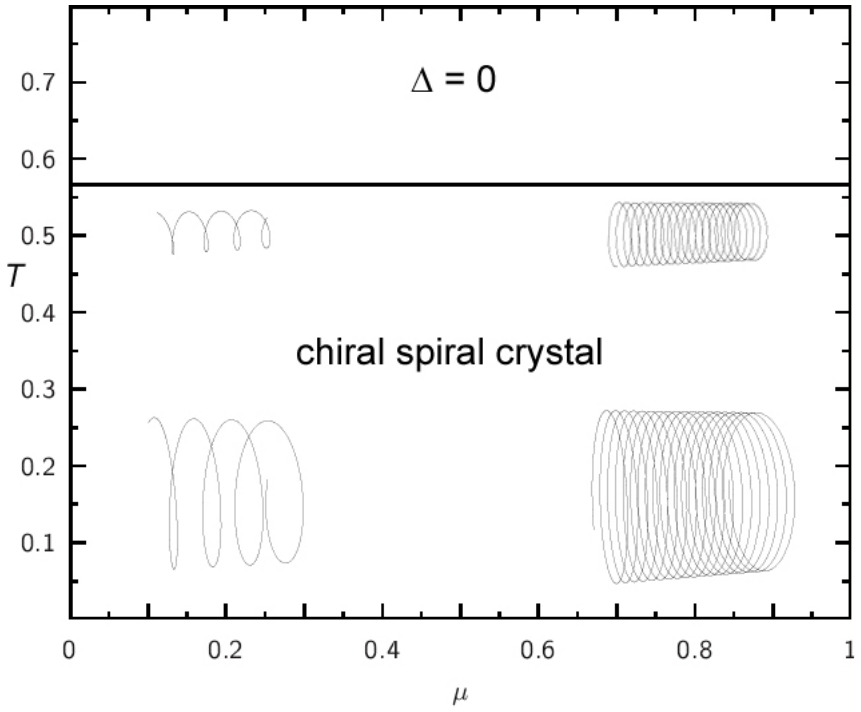

Fig. 3.2: The phase diagram of the NJL_2 model.

3.3.1 Twisted kink crystal at $T = 0$

At $T = 0$ there are some significant simplifications. First of all, the Fermi factor becomes a step function that acts as a cutoff of the energy integrals. Thus, in the consistency condition (3.36), we use

$$\frac{1}{1 + e^{\hat{\beta}(E-\hat{\mu})}} \to \Theta(\hat{\mu} - E) \tag{3.53}$$

If we assume that $\hat{\mu}$ is in the upper gap, then both the lower continuum and the bound band are completely filled. Thus the consistency condition (3.36) reads

$$0 = \int_{-\infty}^{-1} dE\, \mathcal{N}(E) + \int_{E_2}^{E_3} dE\, \mathcal{N}(E) = \frac{1}{2A}\left(\frac{\theta}{4} - \mathbf{K}'\right) \tag{3.54}$$

Therefore, the consistency condition forces $\theta = 4\mathbf{K}'$, which is precisely the spiral condensate case. In this limit, the band shrinks and joins the negative energy continuum, leaving just the single-gap spectrum of the spiral condensate. Then the q minimization leads to $q = \mu$ as described in the previous section, and we find the preferred condensate to be the chiral spiral. Similarly, if we assume that $\hat{\mu}$ is in the lower gap, then we get $\theta = 0$, that is also the spiral condensate limit; in this limit the bound band joins to the positive energy continuum. Once again, minimization with respect to the phase parameter q leads to $q = \mu$, so the condensate is the chiral spiral.

The only other possibility is $\hat{\mu}$ lying inside the bound band. In this case the consistency condition (3.36) leads to an expression for the Fermi energy:

$$\hat{E}_F = \hat{E}_F(\theta, \nu) = \mathrm{nc}\,(i\theta/2; \nu) \tag{3.55}$$

On the other hand, at $T = 0$, this Fermi energy is simply the chemical potential. Minimization with respect to the phase parameter q leads to the relation $\hat{\mu} = \pi\,\hat{\rho}$. We can evaluate the density obtained by filling up to the Fermi energy $\hat{E}_F(\theta, \mu)$:

$$\hat{\rho} = \hat{\rho}(\theta, \nu) = \frac{1}{\pi}\frac{1}{\mathrm{cn}(i\theta/2; \nu)}\left(\frac{\mathrm{cn}(i\theta/2; \nu) - \mathrm{dn}(i\theta/2; \nu)}{\mathrm{cn}(i\theta/2; \nu) + \mathrm{dn}(i\theta/2; \nu)}\right) \tag{3.56}$$

The simultaneous solution of these two conditions, namely $\hat{E}_F = \pi\hat{\rho}$, has the unique solution $\theta = 2\mathbf{K}'$, for all ν, as can be seen from Figure 3.3 , where $\theta \equiv$

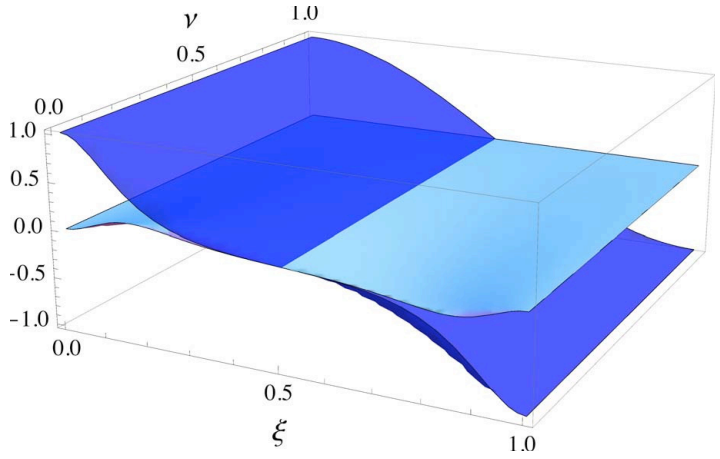

Fig. 3.3: Plot of $\pi\hat{\rho}(\xi,\nu)$ [light blue surface] and $\hat{E}_F(\xi,\nu)$ [darker blue surface].

$4\mathbf{K}'\xi$. The surfaces intersect at $\xi = 1/2$, which means $\theta = 2\mathbf{K}'$. Evaluating the free energy for this solution we obtain the following function of the remaining parameters λ and ν:

$$\mathcal{E} = \mathcal{E}(\lambda,\nu) = \frac{2\lambda^2}{\pi(1+\sqrt{\nu})^2}\left[\frac{\nu}{2} + \left(1 - \frac{\mathbf{E}(\nu)}{\mathbf{K}(\nu)}\right)\left(\ln\left(\frac{2\lambda}{1+\sqrt{\nu}}\right) - 1\right)\right] + \frac{\mu^2}{2\pi} \tag{3.57}$$

Minimizing $\mathcal{E}(\lambda,\nu)$ with respect to ν, we find that we are forced to $\nu = 1$, which means

$$\mathcal{E}(\lambda,\nu=1) = \frac{\lambda^2}{4\pi}\left(\ln\lambda^2 - 1\right) + \frac{\mu^2}{2\pi} \tag{3.58}$$

from which we recognize the $T = 0$ grand potential (3.43) of the chiral spiral solution. Thus, once again, the minimization forces us to the chiral spiral condensate solution, at $T = 0$.

3.3.2 Twisted kink crystal at $0 < T \ll 1$

The minimization of the grand potential at $T = 0$ shows that the preferred twisted kink crystal configuration is the chiral spiral, with the chemical potential sitting in the middle of the gap (i.e $\hat{\mu} = (\mu - q)/\lambda = 0$). For this solution, the angular parameter θ takes the values 0 or $4\mathbf{K}'$. We will consider the latter case [a similar argument applies for the other choice]. Intuitively, it is unlikely that a crystalline phase which is not favored at $T = 0$ to form at nonzero T, due to its relatively low entropy. We will now show that this is indeed the case. Consider the stability of this chiral spiral for T nonzero but small. If we change T slightly away from 0, then the consistency condition that sets the angular parameter $\theta = 4\mathbf{K}'$, will also change slightly, and the preferred value of θ will shift away from $4\mathbf{K}'$. We write $\theta = 4\mathbf{K}' - 4\epsilon$, where $\epsilon \ll \hat{T} \ll 1$. This changes the single-particle spectrum by producing a very narrow band very close to the lower band edge $\hat{E}_1 = -1$. With $\theta = 4\mathbf{K}' - 4\epsilon$, the band edges (3.6) and from (2.44), the averaged amplitude $Z(\theta, \nu) = \langle |\hat{\Delta}(x)|^2 \rangle$ take the form :

$$\begin{aligned} \hat{E}_2(\theta, \nu) &\approx -1 + 2\nu\epsilon^2 + \dots \\ \hat{E}_3(\theta, \nu) &\approx -1 + 2\epsilon^2 + \dots \\ Z(\theta, \nu) &\approx 1 - h(\nu)\epsilon^2 + \dots \end{aligned} \tag{3.59}$$

where $h(\nu) = 2\nu - 2 + 4\mathbf{E}(\nu)/\mathbf{K}(\nu)$. We now calculate the small T correction to the grand potential $\hat{\Psi}$ for this configuration. As usual, we split the grand potential

into zero temperature and finite temperature parts. For small T, we use the fact that $\ln(1+e^{-|\hat{\beta}(E-\hat{\mu})|}) \approx e^{-|\hat{\beta}(E-\hat{\mu})|} \approx e^{-\hat{\beta}|E|}$ (recall that $\hat{\mu}=0$ for $T=0$).

$$\begin{aligned}
\hat{\Psi} &\approx \int_{-\infty}^{-1} dE\hat{\rho}(E)(E-\hat{\mu}) + \int_{E_2}^{E_3} dE\hat{\rho}(E)(E-\hat{\mu}) \\
&\quad -T\left(\int_{-\infty}^{-1} dE\,\hat{\rho}(E)e^{\hat{\beta}E} + \int_{1}^{\infty} dE\,\hat{\rho}(E)e^{-\hat{\beta}E} + \int_{E_2}^{E_3} dE\,\bar{\rho}(E)e^{\hat{\beta}E}\right) \\
&= <\hat{\Psi}>_{T=0} -Te^{-\hat{\beta}}\left(\int_0^{\infty} dx\,\hat{\rho}(-x-1)e^{-\hat{\beta}x} + \int_0^{\infty} dx\,\hat{\rho}(x+1)e^{-\hat{\beta}x}\right. \\
&\qquad \left. + \int_{2\nu\epsilon^2}^{2\epsilon^2} dx\,\hat{\rho}(x-1)e^{\hat{\beta}x}\right) \qquad (3.60)
\end{aligned}$$

In the small T limit, the continuum integrals are dominated by the region $x \approx 0$ (i.e near the band edges). The spectral function around the band edges has the behavior:

$$\int_0^{\infty} dx\,\hat{\rho}(-x-1)e^{-\hat{\beta}x} = \sqrt{\frac{T}{2\pi}} - \epsilon\,\frac{1}{\mathbf{K}(\sqrt{\nu})} \qquad (3.61)$$

$$\int_0^{\infty} dx\,\hat{\rho}(x+1)e^{-\hat{\beta}x} \approx \sqrt{\frac{T}{2\pi}} + O(\epsilon^2) \qquad (3.62)$$

Note that the lower continuum leads to an O(ϵ) correction, while the upper continuum leads to an O(ϵ^2) correction. The band integral also leads to an O(ϵ) correction. This can be seen by changing the integration variable $x \to \epsilon^2 x$:

$$\begin{aligned}
\int_{2\nu\epsilon^2}^{2\epsilon^2} dE\,\hat{\rho}(x-1)e^{\hat{\beta}x} &= \epsilon\int_{2\nu}^{2} dx\,e^{\hat{\beta}x\epsilon^2}\frac{-x-(1+\nu)-h(\nu)/2}{\pi\sqrt{x(x-2\nu)(2-x)}} \\
&\approx \epsilon\int_{2\nu}^{2} dx\,\frac{2-x-2\mathbf{E}(\nu)/\mathbf{K}(\nu)}{\pi\sqrt{x(x-2\nu)(2-x)}} \equiv \epsilon\,L(\nu) \qquad (3.63)
\end{aligned}$$

An important observation is that this function $L(\nu) < 0$ for all $\nu \in [0,1]$.

Finally, we use the general transformation of the grand potential (3.17) to deduce the grand potential for the twisted kink crystal. Since after minimization,

$\hat{\psi}_{T=0} = -1/(4\pi)$, the small T correction to λ does not contribute to the full grand potential Ψ (as in (3.47)), and the full grand potential is found to be:

$$\Psi \approx \left(-\frac{1}{4\pi} - \frac{\mu^2}{2\pi} - \sqrt{\frac{2T^3}{\pi}} e^{-1/T} \right) + \epsilon \left(\frac{1}{\mathbf{K}(\sqrt{\nu})} - L(\nu) \right) T e^{-1/T} + \dots \quad (3.64)$$

The first term in parentheses is just the low T grand potential for the chiral spiral, as in (3.47). Since $L(\nu)$ is always negative, and $\mathbf{K}(\sqrt{\nu})$ is always positive, we see that the system is unstable with respect to the opening of a gap near the lower continuum edge. In other words, at small T the minimization of the grand potential reduces the general twisted kink crystal condensate to the chiral spiral condensate, just as at $T = 0$.

3.3.3 Numerical results for the thermodynamics of the twisted kink crystal condensate

The previous two sections have shown that at $T = 0$ and for small T, the chiral spiral condensate is the thermodynamically preferred form of the more general twisted kink crystal condensate. We have also checked this conclusion numerically at various locations on the phase diagram, and we find that throughout the phase diagram the chiral spiral is the thermodynamically preferred limit of the general twisted kink crystal solution of the inhomogeneous gap equation. This analysis is possible because we have an explicit closed form expansion for the renormalized grand potential (3.11).

3.4 Thermodynamics of the real kink crystal and the GN_2 model

Initially, the phase diagram of the NJL_2 and GN_2 models was studied assuming homogeneous condensates [48, 49], but this assumption does not capture certain aspects of the true physical phase diagram as we have seen for the NJL_2 model. Now we turn into GN_2 model. The phase diagram of the GN_2 model, is by now well understood; both analytically [22], on the lattice [50, 51] and through Monte-Carlo simulations [52, 53, 54]. But we revisit it here briefly, with a new perspective. It is shown in Figure 3.4. The tricritical point is at $\mu_{\mathrm{tc}} = 0.608$ and $T_{\mathrm{tc}} = 0.318$. In the region of $\mu > 2/\pi$, the massless and massive phases are separated by a crystalline phase. The analysis of this dissertation shows that the key to understanding the phase diagram of the NJL_2 model is the behavior (3.17) of the renormalized grand potential under the rescaling and shifting transformation (3.1). But in the GN_2 model there is no pseudoscalar interaction, so the condensate is real. Thus, there is no symmetry corresponding to a phase rotation of the condensate. In other words, $q \equiv 0$. The angular parameter θ in the solution (2.35) of the inhomogeneous gap equation is also zero, as the condensate cannot wind by an arbitrary phase as it goes through one period. Furthermore, there is no need to impose any consistency condition on the solution of the gap equation: since the pseudoscalar condensate $\mathcal{I}m(\Delta)$ is identically zero, there is no condition arising from its variation, which means that the off-diagonal terms in (2.27) play no role. Thus, the general solution (2.35) of the inhomogeneous gap equation simplifies to

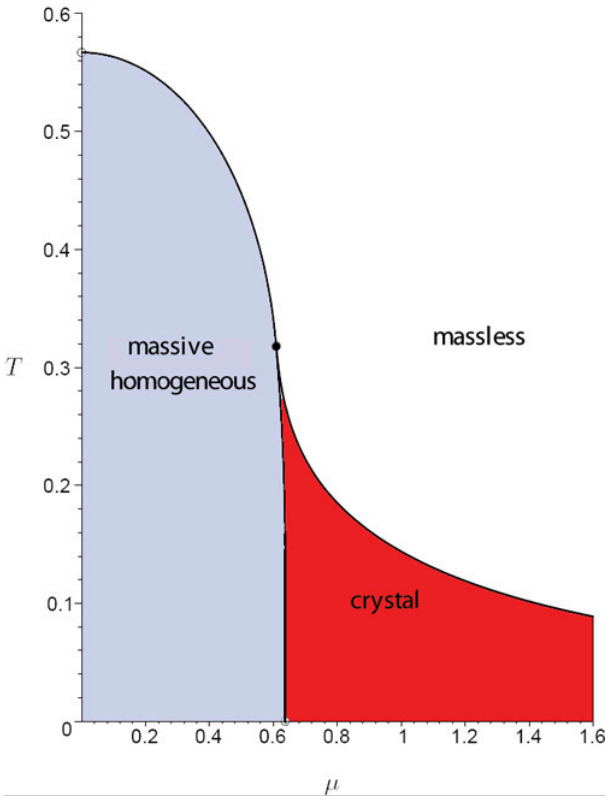

Fig. 3.4: Phase diagram of the GN_2 model.

the real kink crystal solution in (2.55), which depends on just two parameters, the scale λ and the elliptic parameter ν. Concerning the grand potential, the key formula is now (3.17), with q set to 0:

$$\Psi_{\rm ren}[\lambda\,\hat{\Delta}(\lambda x);T,\mu] \;=\; \lambda^2\left(\hat{\Psi}_{\rm ren}[\hat{\Delta}(x);T/\lambda,\mu/\lambda]+\frac{Z}{2\pi}\ln\lambda\right) \qquad (3.65)$$

The last term reflects the anomalous behavior of the grand potential under the rescaling of the condensate by λ.

3.4.1 Real kink crystal at $T = 0$

From previous work [22], we know explicit expressions for the thermodynamical quantities at $T = 0$ as functions of the elliptic parameter ν. For $\lambda = 1$, the density is

$$\hat{\rho} = \frac{1}{2\,\mathbf{K}(\tilde{\nu})} \qquad , \qquad \tilde{\nu} \equiv \frac{4\sqrt{\nu}}{(1+\sqrt{\nu})^2} \tag{3.66}$$

The free energy is

$$\hat{\mathcal{E}} \;=\; \frac{Z(\tilde{\nu})}{4\pi}\,(\ln\tilde{\nu} - 1) + \frac{1}{2\pi}\frac{\mathbf{E}(\tilde{\nu})}{\mathbf{K}(\tilde{\nu})} \tag{3.67}$$

where

$$Z(\tilde{\nu}) \;=\; 2\left(1 - \frac{\tilde{\nu}}{2} - \frac{\mathbf{E}(\tilde{\nu})}{\mathbf{K}(\tilde{\nu})}\right) \tag{3.68}$$

The function $\mathbf{E}(\tilde{\nu})$ is the complete elliptic integral of the second kind [104]. Thus we can write the $T = 0$ grand potential as

$$\begin{aligned} \Psi &= \mathcal{E} - \mu\,\rho \\ &= \lambda^2\,(f_1(\tilde{\nu}) + f_2(\tilde{\nu})\,\ln\lambda) - \mu\,\lambda\,f_3(\tilde{\nu}) \end{aligned} \tag{3.69}$$

where

$$f_1(\tilde{\nu}) \;\equiv\; \frac{Z(\tilde{\nu})}{4\pi}\,(\ln\tilde{\nu} - 1) + \frac{1}{2\pi}\frac{\mathbf{E}(\tilde{\nu})}{\mathbf{K}(\tilde{\nu})} \tag{3.70}$$

$$f_2(\tilde{\nu}) \;\equiv\; \frac{Z(\tilde{\nu})}{2\pi} \tag{3.71}$$

$$f_3(\tilde{\nu}) \;\equiv\; \frac{1}{2\mathbf{K}(\tilde{\nu})} \tag{3.72}$$

Minimizing Ψ with respect to λ and $\tilde{\nu}$ leads to two equations:

$$\begin{aligned} \frac{\partial \Psi}{\partial \lambda} &= 2\lambda \left(f_1 + \frac{1}{2} f_2 + f_2 \ln \lambda \right) - \mu f_3 = 0 \\ \frac{\partial \Psi}{\partial \tilde{\nu}} &= \lambda \left\{ \lambda \left(f_1' + f_2' \ln \lambda \right) - \mu f_3' \right\} = 0 \end{aligned} \tag{3.73}$$

Simultaneous solution of these conditions leads to a complicated-looking expression for $\ln \lambda$, that actually simplifies dramatically:

$$\begin{aligned} \ln \lambda &= \frac{f_3 f_1' - 2 f_3' (f_1 + f_2/2)}{2 f_2 f_3' - f_3 f_2'} \\ &= -\frac{1}{2} \ln \tilde{\nu} \end{aligned} \tag{3.74}$$

In showing this remarkable reduction we use the property

$$\frac{\partial Z}{\partial \tilde{\nu}} = \frac{(Z - \tilde{\nu})^2}{4\tilde{\nu}(1 - \tilde{\nu})} \tag{3.75}$$

Inserting this result for λ back into the minimization conditions (3.73) we find the minimized values at $T = 0$:

$$\mu(\tilde{\nu}) = \frac{2\mathbf{E}(\tilde{\nu})}{\pi \sqrt{\tilde{\nu}}} \tag{3.76}$$

$$\lambda(\tilde{\nu}) = \frac{1}{\sqrt{\tilde{\nu}}} \tag{3.77}$$

The critical value of chemical potential, $\mu_c = \frac{2}{\pi}$, corresponding to the baryon mass [10, 19, 50], is obtained at $\tilde{\nu} = 1$, in agreement with known results [22].

3.4.2 Real kink crystal at $T \ll 1$

At nonzero temperature, the minimization with respect to λ and $\tilde{\nu}$ leads to T dependent expressions for the chemical potential and the scale factor λ, as functions

of the elliptic parameter $\tilde{\nu}$, generalizing the $T = 0$ expressions (3.76, 3.77). This can be done numerically, as in [22], but here we find analytic expressions valid in the small T limit. First, we note that the $T = 0$ chemical potential in (3.76) lies

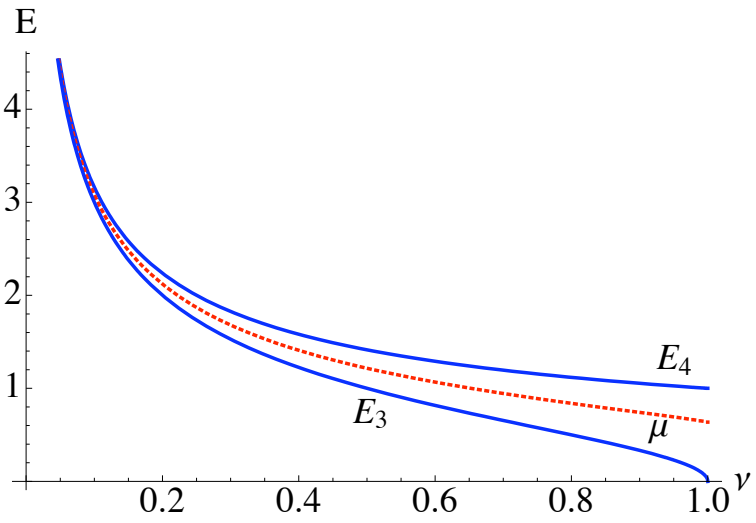

Fig. 3.5: Plot of the chemical potential [center line], and the band edge energies, as a function of the elliptic parameter $\tilde{\nu}$.

in the upper gap [see Figure 3.5],

$$E_3(\tilde{\nu}) = \lambda(\tilde{\nu})\sqrt{1-\tilde{\nu}} \leq \mu(\tilde{\nu}) \leq E_4(\tilde{\nu}) = \lambda(\tilde{\nu}) \tag{3.78}$$

and moreover, it is slightly closer to the upper band edge, E_4, than to the lower band edge, E_3. Since μ is in the gap, at small T there is an exponentially small factor in the corrections to thermodynamic quantities going like

$$\exp[-|\mu - \text{nearest band edge}|/T] \tag{3.79}$$

Furthermore, for all $\tilde{\nu}$, μ is closer to E_4 than to E_3. Thus, we can write as a leading approximation

$$\begin{aligned}
\Psi &= -T \int dE\, \rho(E)\, \ln\left(1 + e^{-\beta(E-\mu)}\right) && (3.80)\\
&= \Psi_{T=0} - T \int dE\, \rho(E)\, \ln\left(1 + e^{-\beta|E-\mu|}\right) && (3.81)\\
&\sim \Psi_{T=0} - T e^{-\beta(E_4-\mu)} \int_{E_4}^{\infty} dE\, \rho(E)\, e^{-\beta(E-E_4)} && (3.82)
\end{aligned}$$

We expand the spectral function in the vicinity of the nearer band edge, E_4:

$$\begin{aligned}
\rho(E) &= \frac{2E^2 - (E_3^2 + E_4^2) + \lambda^2 Z}{2\pi\sqrt{(E^2 - E_3^2)(E^2 - E_4^2)}} && (3.83)\\
&\sim \frac{1}{2\pi} \frac{E_4^2 - E_3^2 + \lambda^2 Z}{\sqrt{2E_4(E_4^2 - E_3^2)}} \frac{1}{\sqrt{E - E_4}} + O(\sqrt{E - E_4}) && (3.84)
\end{aligned}$$

Thus,

$$\Psi \sim \Psi_{T=0} - T^{3/2} \sqrt{\frac{\lambda}{2\pi}}\, f_4(\tilde{\nu})\, e^{-\beta(E_4-\mu)} \qquad (3.85)$$

where

$$f_4(\tilde{\nu}) = \frac{1}{\sqrt{\tilde{\nu}}} \left(1 - \frac{\mathbf{E}(\tilde{\nu})}{\mathbf{K}(\tilde{\nu})}\right) \qquad (3.86)$$

We now minimize Ψ with respect to λ and $\tilde{\nu}$, keeping the leading small T corrections to the $T = 0$ results of the previous section. We find, after some straightforward algebra,

$$\begin{aligned}
\mu(\tilde{\nu}, T) &\sim \frac{2\mathbf{E}(\tilde{\nu})}{\pi\sqrt{\tilde{\nu}}} - \sqrt{\frac{2T}{\pi}} \frac{(1-\tilde{\nu})\mathbf{K}(\tilde{\nu})}{\tilde{\nu}^{3/4}} \exp\left[-\beta\left(\frac{1}{\sqrt{\tilde{\nu}}}\left(1 - \frac{2\mathbf{E}(\tilde{\nu})}{\pi}\right)\right)\right]\\
\lambda(\tilde{\nu}, T) &\sim \frac{1}{\sqrt{\tilde{\nu}}} - \sqrt{\frac{\pi T}{2}} \frac{1}{\tilde{\nu}^{3/4}} \exp\left[-\beta\left(\frac{1}{\sqrt{\tilde{\nu}}}\left(1 - \frac{2\mathbf{E}(\tilde{\nu})}{\pi}\right)\right)\right] && (3.87)
\end{aligned}$$

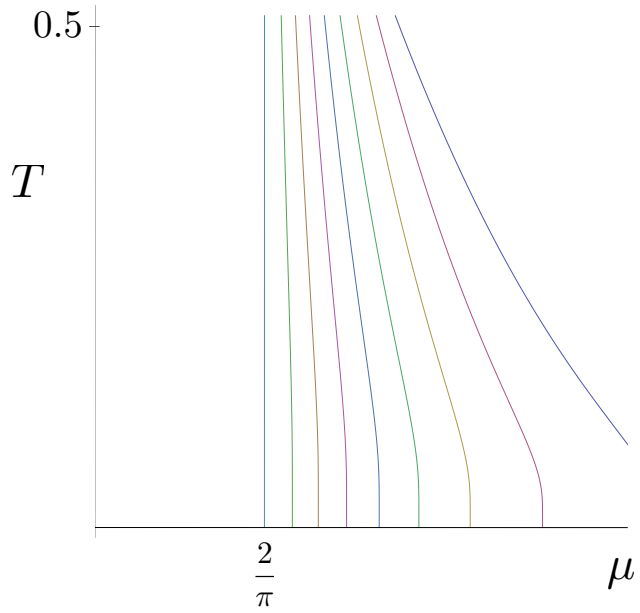

Fig. 3.6: Plots of the $\mu(T)$ for various values of $\tilde{\nu}$ in leading small T behavior.

These small T corrections are plotted in Figure 3.6, and are in very good agreement with the numerical results found in [22], and plotted in Figure 3.4. Already these corrections indicate the existence of a crystalline phase in which the condensate scale λ and the period (set by the elliptic parameter ν) are dependent on *both* T and μ. This is in contrast to the phase diagram of the NJL_2 model, shown in Figure 3.2, where the phase transition line is only a function of T, and the scale parameter λ is independent of the chemical potential μ. With this perspective we can trace this fundamental difference in the phase diagrams directly to the fundamental difference between the discrete and continous chiral symmetry of the two models.

3.5 All orders Ginzburg Landau expansion

In this Section we present another perspective on our solution, in order to illustrate what aspects might possibly be extended to the search of inhomogeneous phases in higher dimensional models. While a direct application of the resolvent approach, or the inverse scattering approach, to higher dimensions is problematic, one approach that can be straightforwardly generalized to higher dimensions consists of the Ginzburg-Landau expansion of the effective action. In this approach, one expands the free energy corresponding to the effective action (2.3) in powers of the static condensate Δ [i.e, the order parameter] and its spatial derivatives. Using the relation (2.19) between the spectral function $\rho(E)$ and the trace of the resolvent, we write the free energy density (per flavor) as

$$\Psi(x) = \frac{1}{\pi\beta}\int_{-\infty}^{\infty} dE\, \mathcal{I}m\left[\mathrm{tr}_D\, R(x; E + i\epsilon)\right] \ln\left(1 + e^{-\beta(E-\mu)}\right) \tag{3.88}$$

Thus, the information regarding the condensate which is carried by the resolvent and thermodynamic information which is carried by the Fermi factor are explicitly separated. Usually, it is impossible to evaluate this local density of states exactly. However, an asymptotic expansion of $R(x; E)$ can always be obtained from a Laplace transform of the heat kernel expansion, leading to

$$R(x; E) = \frac{1}{2}\sum_{n=0}^{\infty} \frac{r_n(x)}{E^n} \tag{3.89}$$

We stress that such an expansion can be derived in any dimension, not just in $1 + 1$ dimensions. This is because the heat kernel expansion is known in any

dimension. However, in $1+1$ dimensions we now have the luxury of having found an exact solution to the gap equation. In this Section we compare this exact solution with the Ginzburg-Landau expansion, and show in explicit detail how the gap equation for the inhomogeneous condensate is solved order-by-order in this Ginzburg-Landau expansion. The underlying reason is that both GN_2 and NJL_2 models are associated with particular integrable hierarchies whose the conservation equations are identified as the Ginzburg-Landau equations, as shown below.

In $1+1$ dimensions, including the Hartree-Fock double-counting correction, and renormalizing, leads to the standard Ginzburg-Landau expansion of the NJL_2 effective Lagrangian, the low order terms of which are

$$\begin{aligned}\mathcal{L}_{\mathrm{GL}} &= \alpha_0+\alpha_2|\Delta|^2+\alpha_3\,\mathcal{I}m\left[\Delta(\Delta')^*\right]+\alpha_4\left[|\Delta|^4+|\Delta'|^2\right]\\ &\quad+\alpha_5\,\mathcal{I}m\left[\left(\Delta''-3|\Delta|^2\Delta\right)(\Delta')^*\right]\\ &\quad+\alpha_6\left[2|\Delta|^6+8|\Delta|^2|\Delta'|^2+2\mathrm{Re}\left((\Delta')^2(\Delta^*)^2\right)+|\Delta''|^2\right]+\ldots \qquad (3.90)\end{aligned}$$

The low order terms are relatively simple, but high orders rapidly become cumbersome. The coefficients $\alpha_n(T,\mu)$ are known functions of temperature and chemical

potential. For example, in $1+1$ dimensions [55, 56]

$$\begin{aligned}
\alpha_0 &= -\frac{\pi^2 T^2}{6} - \frac{\mu^2}{2\pi} \\
\alpha_2 &= \frac{1}{2\pi}\left[\ln(4\pi T) + \mathrm{Re}\,\psi\left(\frac{1}{2} + i\frac{\beta\mu}{2\pi}\right)\right] \\
\alpha_3 &= -\frac{1}{2^3\pi^2 T}\mathcal{I}m\,\psi^{(1)}\left(\frac{1}{2} + i\frac{\beta\mu}{2\pi}\right) \\
\alpha_4 &= -\frac{1}{2^6\pi^3 T^2}\mathrm{Re}\,\psi^{(2)}\left(\frac{1}{2} + i\frac{\beta\mu}{2\pi}\right) \\
\alpha_5 &= \frac{1}{2^8\pi^4 3\,T^3}\mathcal{I}m\,\psi^{(3)}\left(\frac{1}{2} + i\frac{\beta\mu}{2\pi}\right) \\
\alpha_6 &= \frac{1}{2^{12}\pi^5 3\,T^4}\mathrm{Re}\,\psi^{(4)}\left(\frac{1}{2} + i\frac{\beta\mu}{2\pi}\right)
\end{aligned} \tag{3.91}$$

Here $\psi^{(k)}$ denotes the k^{th} derivative of the Euler digamma function $\psi(z) = d\ln\Gamma(z)/dz$.

In higher dimensions, an analogous Ginzburg-Landau expansion can be derived. The form of the $\alpha_n(T,\mu)$ is different, but known, and the form of the spatial terms $r_n(x)$ is different, but computable. In this section we consider how the NJL_2 model gap equation for inhomogeneous condensates looks in terms of the Ginzburg-Landau expansion. We first present a simple recursive way to generate the expansion to all orders, and then we show how the gap equation is solved order by order. A closely related expansion, the derivative [or gradient] expansion, which is an expansion just in powers of derivatives, but including all orders in powers of the condensate, is considered in [26].

The two key ingredients of our analysis are the asymptotic large energy expansion (3.89) (also known as the heat kernel expansion) of the resolvent $R(x;E)$

and the Eilenberger equation (2.24). In particular, the Eilenberger equation generates a nontrivial recursion relation between the terms in the heat kernel expansion. It is more convenient to define (as in [26])

$$g(x;E) \equiv R(x;E)\,\sigma_3 \tag{3.92}$$

In terms of g, the Eilenberger equation (2.24) reads

$$g' = iE[\sigma_3, g] + i[J, g] \quad , \quad J \equiv \begin{pmatrix} 0 & -\Delta \\ \Delta^* & 0 \end{pmatrix} \tag{3.93}$$

We now define an asymptotic expansion for g

$$g(x;E) = -\frac{i}{2}\sum_{n=0}^{\infty} \frac{g_n(x)}{E^n} \qquad , \qquad g_n(x) \equiv \begin{pmatrix} c_n(x) & -d_n(x) \\ d_n^*(x) & -c_n(x) \end{pmatrix} \tag{3.94}$$

The factor $-i$ comes from the large E expansion of $\mathcal{N}(E)$, as is already clear from the constant Δ case in (2.29), which also tells us that $g_0 = \sigma_3$. The Eilenberger equation implies the simple recursion formula for the $g_n(x)$:

$$g_n'(x) = i[\sigma_3, g_{n+1}(x)] + i[J(x), g_n(x)] \tag{3.95}$$

The determinant condition $\det g = \frac{1}{4}$ fixes the c_n in terms of the d_n:

$$\begin{aligned}
c_0 &= 1 \\
c_1 &= 0 \\
c_2 &= \frac{1}{2}|d_1|^2 \\
c_3 &= \frac{1}{2}\left(d_2 d_1^* + d_1 d_2^*\right) \\
c_4 &= -\frac{1}{8}|d_1|^4 + \frac{1}{2}|d_2|^2 + \frac{1}{2}\left(d_3 d_1^* + d_1 d_3^*\right) \\
c_5 &= -\frac{1}{4}|d_1|^2\left(d_2 d_1^* + d_1 d_2^*\right) + \frac{1}{2}\left(d_2 d_3^* + d_3 d_2^*\right) + \frac{1}{2}\left(d_4 d_1^* + d_1 d_4^*\right) \\
&\vdots
\end{aligned} \tag{3.96}$$

So, given $g_0 = \sigma_3$, we learn from (3.96) that $c_1 = 0$. Then the Eilenberger recursion equation (3.95) determines $d_1 = \Delta$, so that $g_1(x) = J(x)$. Next, knowing d_1, we learn from (3.96) that $c_2 = \frac{1}{2}|\Delta|^2$, and from the recursion equation (3.95), we find that $d_2 = -\frac{i}{2}\Delta'$. Iterating this procedure we find the off diagonal terms to be:

$$\begin{aligned}
d_0 &= 0 \\
d_1 &= \Delta \\
d_2 &= -\frac{i}{2}\Delta' \\
d_3 &= -\frac{1}{4}\left(\Delta'' - 2|\Delta|^2\Delta\right) \\
d_4 &= \frac{i}{8}\left(\Delta''' - 6|\Delta|^2\Delta'\right) \\
d_5 &= \frac{1}{16}\left(\Delta^{(\mathrm{iv})} - 8|\Delta|^2\Delta'' - 2\Delta^2\Delta^{*\prime\prime} - 4|\Delta'|^2\Delta - 6\Delta^*\Delta'^2 + 6|\Delta|^4\Delta\right) \\
&\vdots
\end{aligned} \tag{3.97}$$

Similarly the diagonal terms are:

$$\begin{aligned} c_0 &= 1 \\ c_1 &= 0 \\ c_2 &= \frac{1}{2}|\Delta|^2 \\ c_3 &= \frac{1}{2}\mathcal{I}m\left(\Delta'\Delta^*\right) \\ c_4 &= \frac{1}{8}\left(3|\Delta|^4 + 3|\Delta'|^2 - \left(|\Delta|^2\right)''\right) \\ c_5 &= \frac{1}{8}\mathcal{I}m\left(\Delta\Delta^{*'''} + \Delta''\Delta^{*\prime} + 6|\Delta|^2\Delta'\Delta^*\right) \\ &\vdots \end{aligned} \tag{3.98}$$

The spectral function is expressed in terms of the trace of the resolvent:

$$\operatorname{tr} R(x;E) = -i\sum_{n=0}^{\infty}\frac{c_n(x)}{E^n} \tag{3.99}$$

Then the Ginzburg-Landau expansion (3.90) is obtained by inserting (3.99) into (3.88) and performing the energy integrals:

$$\Psi_{GL} = \int dx \sum_{n=0}^{\infty}\alpha_n(T,\mu)\, c_n[\Delta,\Delta',...] \tag{3.100}$$

with the c_ns given in (3.98), Renormalization affects the first two terms, and the

others follow from the integrals ($n > 2$) [57]:

$$\begin{aligned}
\alpha_n(T,\mu) &= \frac{1}{\beta\pi}\int_{-\infty}^{\infty} dE\, \mathcal{I}m\left(\frac{-i}{(E+i\epsilon)^n}\right)\log\left(1+e^{-\beta(E-\mu)}\right) \\
&= \begin{cases} \frac{(-1)^{(n-2)/2}\beta^{n-2}}{(2\pi)^{n-1}(n-1)!}\,\mathrm{Re}\,\psi^{(n-2)}\left(\frac{1}{2}+i\frac{\beta\mu}{2\pi}\right) & , \quad \text{n even} \\ \\ \frac{(-1)^{(n-1)/2}\beta^{n-2}}{(2\pi)^{n-1}(n-1)!}\,\mathcal{I}m\,\psi^{(n-2)}\left(\frac{1}{2}+i\frac{\beta\mu}{2\pi}\right) & , \quad \text{n odd} \end{cases}
\end{aligned} \tag{3.101}$$

The Ginzburg-Landau equations follow from truncating the sum (3.100) at some order N and minimizing it in the function space.

$$\frac{\delta}{\delta\Delta^*}\sum_{n=0}^{N}\int dx\alpha_n(T,\mu)\, c_n[\Delta,\Delta',...] = 0 \tag{3.102}$$

In general this leads to a nonlinear differential equation of order $N-2$. This can directly be seen from noticing that α_n, Δ and Ψ_{GL} have mass dimensions $2-n$, 1 and 2 respectively. In a generic $1+1$ dimensional model, it is almost impossible to study these differential equations beyond numerical means to obtain information about the possible inhomogeneous phases near the tricritical point. However, the fact that the gap equation is soluble in NJL_2 and GN_2 models translates into a set of special properties of the corresponding Ginzburg-Landau equations. In fact, for NJL_2 , they coincide with the conservation equations of a hierarchy of differential equations known as the Ablowitz, Kaup, Newell, Segur (AKNS) hierarchy [58, 59].

A characteristic feature of integrable hierarchies is the existence of an infinite set of Lax pairs [60], Q_N and H. The operator H generates evolution with respect to a parameter t via $\frac{d}{dt} = [\,, H]$ and Q_Ns are the conserved quantities of the

hierarchy:

$$[Q_N, H] = 0 \tag{3.103}$$

In our case H is the BdG Hamiltonian (2.10) and Q_Ns can be constructed as follows. We first define:

$$q_n = i \sum_{k=0}^{n} g_{n-k}(x) H^k \tag{3.104}$$

where g_ns are the coefficients of the heat kernel expansion defined in (3.94). Using the recursion relation for g_n (3.95) we find:

$$[g_{n-k}, H] = \begin{pmatrix} 0 & 2d_{n+1-k} \\ -2d^*_{n+1-k} & 0 \end{pmatrix} - \begin{pmatrix} 0 & 2d_{n-k} \\ -2d^*_{n-k} & 0 \end{pmatrix} H \tag{3.105}$$

Then if we compute $[q_n, H]$, only the $k = 0$ term in the sum over k survives:

$$\begin{aligned} [q_n, H] &= i \sum_{k=0}^{n} [g_{n-k}, H] \\ &= \begin{pmatrix} 0 & 2id_{n+1} \\ -2id^*_{n+1} & 0 \end{pmatrix} \end{aligned} \tag{3.106}$$

Finally, we define the operator Q_N to be the linear combination of q_n with $n \in 0, 1, ...N$.

$$Q_N = \sum_{n=0}^{N} \gamma_{N-n} q_n \tag{3.107}$$

Without loss of generality, we can set the coefficient $\gamma_0 = 1$. The N^{th} conservation equation $[Q_N, H] = 0$ therefore is an N^{th} order differential equation:

$$d_{N+1} + \gamma_1 d_N + ... + \gamma_N d_1 = 0 \tag{3.108}$$

This hierarchy of differential equations is known as the AKNS hierarchy. The first few equations of the hierarchy are:

$$
\begin{aligned}
N=0 \quad &: \quad \Delta = 0 \quad , \\
N=1 \quad &: \quad -\frac{i}{2}\Delta' + \gamma_1 \Delta = 0 \quad , \\
N=2 \quad &: \quad -\frac{1}{4}(\Delta'' - 2|\Delta|^2\Delta) - \gamma_1 \frac{i}{2}\Delta' + \gamma_2 \Delta = 0 \quad , \\
N=3 \quad &: \quad \frac{i}{8}(\Delta''' - 6|\Delta|^2\Delta') - \gamma_1 \frac{1}{4}(\Delta'' - 2|\Delta|^2\Delta) - \gamma_2 \frac{i}{2}\Delta' + \gamma_3 \Delta = 0 \quad , \\
N=4 \quad &: \quad \frac{1}{16}\left(\Delta^{(\mathrm{iv})} - 8|\Delta|^2\Delta'' - 2\Delta^2\Delta^{*\prime\prime} - 4|\Delta'|^2\Delta - 6\Delta^*\Delta'^2 + 6|\Delta|^4\Delta\right) \\
&\qquad + \gamma_1 \frac{i}{8}(\Delta''' - 6|\Delta|^2\Delta') - \gamma_2 \frac{1}{4}(\Delta'' - 2|\Delta|^2\Delta) - \gamma_3 \frac{i}{2}\Delta' + \gamma_4 \Delta = 0 \\
&\vdots
\end{aligned}
\tag{3.109}
$$

To relate the AKNS hierarchy explicitly with the Ginzburg Landau expansion, we go back to the free energy (3.88) which can be written, after an integration by parts, as:

$$
\Psi = \frac{1}{\pi}\int_{-\infty}^{\infty} \frac{dE}{1+e^{\beta(E-\mu)}} \mathrm{tr}_{D,x}\, \ln(\gamma^0(E-H)) \tag{3.110}
$$

The gap equation then is:

$$
0 \;=\; \frac{\delta\Psi}{\delta\Delta^*} = \frac{1}{\pi}\int_{-\infty}^{\infty} \frac{dE}{1+e^{\beta(E-\mu)}} \mathrm{tr}_D\, \ln\left(\gamma^0(1+\gamma^5)\frac{1}{E-H}\right) \tag{3.111}
$$

This is of course the generalization of the standard gap equation (2.4) for nonzero T and μ. Now, using the heat kernel expansion (3.94) and the energy integrals (3.101) we can show that:

$$
\frac{\delta\Psi}{\delta\Delta^*} = \sum_{n=2}^{\infty} \alpha_n(T,\mu)\frac{n-1}{2} d_{n-1} \tag{3.112}
$$

which implies a remarkable property of the hierarchy:

$$\frac{\delta}{\delta\Delta^*}\int dx\, c_n[\Delta,\Delta',...] = \frac{n-1}{2} d_{n-1}[\Delta,\Delta',...] \tag{3.113}$$

This identity maps the N^{th} Ginzburg-Landau equation (3.102) to the $(N-2)^{th}$ AKNS equation

$$\frac{\delta}{\delta\Delta^*}\int dx \sum_{n=2}^{N} \alpha_n(T,\mu) c_n = \sum_{n=2}^{N} \alpha_n(T,\mu) d_{n-1} = 0 \tag{3.114}$$

The coefficients γ_n, are now expressed as the T, μ dependent coefficients α_n. Therefore, at the end of the minimization, all of the properties of the solutions Δ, which are encoded in these coefficients, are expressed in terms of the physical parameters T and μ.

Another crucial property of the AKNS hierarchy is that any solution Δ that satisfies the N^{th} AKNS equation automatically satisfies *all the higher order equations*. This can be seen from the recursion relation (3.95). In particular, notice that the 2^{nd} AKNS equation (3.109) is exactly the Nonlinear Schrödinger equation (2.31) that was associated with the NJL_2 gap equation. This recursion property of the hierarchy shows that the solutions of the NLSE solves the gap equation (3.102) order by order in the Ginzburg-Landau expansion regardless of which order we truncate. In fact, the solutions of the AKNS equations (3.109) of any order are known (see eg. [59, 61]) and expressed as hyper-elliptic functions. Remarkably, they define potentials whose spectra have only a finite number of bands. The solution of the N^{th} AKNS equation has $2N$ real parameters which can

be identified with the band edges in the corresponding fermion energy spectrum.

Now, the recursion relation can be understood physically as follows: The most general solution of order N has N gaps (or $2N$ band edges) in its energy spectrum. However there exists a particular solution in which two of the band edges are equal and there are $N-1$ gaps in the spectrum. Therefore it is the most general solution of order $N-1$. Reading it backwards; the most general solution of an arbitrary order N is always a particular solution of *all* the higher orders.

In the GN_2 model the order parameter Δ is real and all the odd terms in (3.98) vanish. The corresponding hierarchy generated by these coefficients is the modified Korteweg-de Vries (mKdV) hierarchy. The mKdV hierarchy is obtained from the KdV hierarchy [62] by writing the potential V as $V = \Delta \pm \Delta'$, and re expressing everything in terms of Δ. This transformation is known as the Miura transformation [63], and its origin is clear from the BgD equation (2.11) for the real condensate Δ. Since it is a particular subset of the AKNS hierarchy, all the properties of AKNS that we discussed above hold also for mKdV. The associated solutions have a symmetric energy spectrum due to the discrete chiral symmetry as explained in section 3.1. Hence the solution of N^{th} mKdV equation has N bands in the energy spectrum which are symmetric around zero and characterized by N parameters.

In the rest of this section, we investigate the Ginzburg-Landau expansions of the NJL_2 and GN_2 at models next-to-leading order.

3.5.1 Ginzburg-Landau expansion for the NJL_2 model

The "tricritical" point is defined as the point where the two lowest nontrivial coefficients, $\alpha_2(T,\mu)$ and $\alpha_3(T,\mu)$, vanish:

$$\alpha_2(T,\mu) = \alpha_3(T,\mu) = 0 \qquad \Rightarrow \qquad T_{\rm tc} = 0.566 \quad , \quad \mu_{\rm tc} = 0 \tag{3.115}$$

The first nontrivial order, to $\mathrm{O}(\alpha_3)$, the grand potential:

$$\Psi_{\rm GL} = \alpha_0 + \alpha_2|\Delta|^2 + \alpha_3\,\mathcal{I}m(\Delta'\Delta^*) \tag{3.116}$$

leads to the GL equation:

$$\Delta' - i\frac{\alpha_2}{\alpha_3}\Delta = 0 \quad \Rightarrow \quad \Delta = \lambda\,\exp\left[i\frac{\alpha_2}{\alpha_3}\,x\right] \tag{3.117}$$

But on this solution, the second and third term cancel each other and the grand potential is $\Psi_{\rm GL} = \alpha_0$, even though this condensate is crystalline. Thus, the phase diagram is simply that of a massless phase. The only thing we learn at this level of the GL expansion is the existence of the tricritical point at $T = 0.5669$ and $\mu = 0$.

Going to the next non-trivial order beyond the level defining the tricritical point, namely to $\mathrm{O}(\alpha_4)$, we obtain the GL equation of NLSE form:

$$\Delta'' - 2|\Delta|^2\Delta - i\frac{\alpha_3}{\alpha_4}\Delta' - \frac{\alpha_2}{\alpha_4}\Delta = 0 \tag{3.118}$$

Adapting the solution in Section 2.4, we can write the general solution as

$$\Delta = -\lambda\frac{\sigma(\lambda x + i\mathbf{K}' - i\theta/2)}{\sigma(\lambda x + i\mathbf{K}')\sigma(i\theta/2)}\exp\left[i\lambda x(-i\zeta(i\theta/2)) + i\theta\eta_3/2 + iqx\right] \tag{3.119}$$

which satisfies

$$-\Delta'' + 2\Delta|\Delta|^2 = -2i\,q\,\Delta' + (-3\lambda^2\mathcal{P}(i\theta/2) - q^2)\Delta \tag{3.120}$$

Identifying the terms with the NLSE equation we deduce:

$$\begin{aligned} q &= \frac{\alpha_3}{2\alpha_4} \\ \lambda^2 &= \left(-\frac{\alpha_2}{2\alpha_4}\left[1 - \frac{\alpha_3^2}{4\alpha_2\alpha_4}\right]\right)\left(\frac{2}{-3\mathcal{P}(i\theta/2)}\right) \end{aligned} \tag{3.121}$$

Notice that in the GL approach, we get explicit expressions for the dependence of the solution's parameters in terms of T and μ. Note that $(-\mathcal{P}(i\theta/2)) \geq 0$. Thus, this inhomogeneous crystal condensate only makes sense in regions of the (T, μ) plane where $\left(-\frac{\alpha_2}{\alpha_4}\left[1 - \frac{\alpha_3^2}{4\alpha_2\alpha_4}\right]\right) \geq 0$.

Now evaluating the averaged potential on this solution, we find

$$\begin{aligned} \langle\Psi\rangle_{\rm GL}^{\rm crystal} &= \alpha_0 + \left[-\frac{\alpha_2^2}{4\alpha_4}\left(1 - \frac{\alpha_3^2}{4\alpha_2\alpha_4}\right)^2\right]\left[\frac{4}{9}\left(1 + \frac{\nu^2 - \nu + 1}{9\mathcal{P}(i\theta/2)^2} + \frac{2}{\mathcal{P}(i\theta/2)}\frac{\eta}{\mathbf{K}}\right)\right] \\ &\equiv \alpha_0 + \left[-\frac{\alpha_2^2}{4\alpha_4}\left(1 - \frac{\alpha_3^2}{4\alpha_2\alpha_4}\right)^2\right] F(\nu, \theta) \end{aligned} \tag{3.122}$$

We note that $0 \leq F(\nu, \theta) \leq 1$. This factorization of the dependence on θ and ν, which are the distinguishing parameters of the twisted kink crystal (the twist and period), reflects the fact that only a particular form of the phase is favored. Depending on the sign of α_4 it is either the configuration with $F(\theta, \nu) = 1$ or the the massless phase with $F(\theta, \nu) = 0$. The twisted kink phase where $0 < F(\theta, \nu) < 1$ is completely eliminated. We now show that the favored inhomogeneous phase

is indeed the spiral:

$$\Delta^{\text{spiral}} = \lambda\, e^{iqx} \tag{3.123}$$

With this spiral ansatz we find

$$\langle\Psi\rangle_{\text{GL}}^{\text{spiral}} = \alpha_0 + \lambda^2\alpha_2 - q\lambda^2\alpha_3 + (\lambda^4 + q^2\lambda^2)\alpha_4 \tag{3.124}$$

Minimizing with respect to q we find $q = \alpha_3/2\alpha_4$. It is worth to mention that in the region where GL expansion is valid (i.e. $\mu = 0$, $T_{\text{tc}} = 0.566$), q has the expansion:

$$q = 2\mu + 0.77\frac{\mu^3}{T^2} + O(\mu^5) \tag{3.125}$$

which is in agreement with the exact solution with $q = 2\mu$. Further minimizing with respect to λ^2 we find

$$\lambda^2 \;=\; \left(-\frac{\alpha_2}{2\alpha_4}\left[1 - \frac{\alpha_3^2}{4\alpha_2\alpha_4}\right]\right) \tag{3.126}$$

which should be compared with (3.121). Furthermore, evaluating the averaged potential on this spiral condensate we find

$$\langle\Psi\rangle_{\text{GL}}^{\text{spiral}} \;=\; \alpha_0 + \left[-\frac{\alpha_2^2}{4\alpha_4}\left(1 - \frac{\alpha_3^2}{4\alpha_2\alpha_4}\right)^2\right] \tag{3.127}$$

Notice that this grand potential is the same as (3.122) with $F(\theta,\nu) = 1$. Furthermore from (3.127) we see that $\alpha_4(T,\mu) > 0$ for the spiral to have a lower free energy. This condition is constrained by the condition $\lambda^2 > 0$ in (3.126). These two conditions lead to the phase diagram illustrated in Figure 3.7.

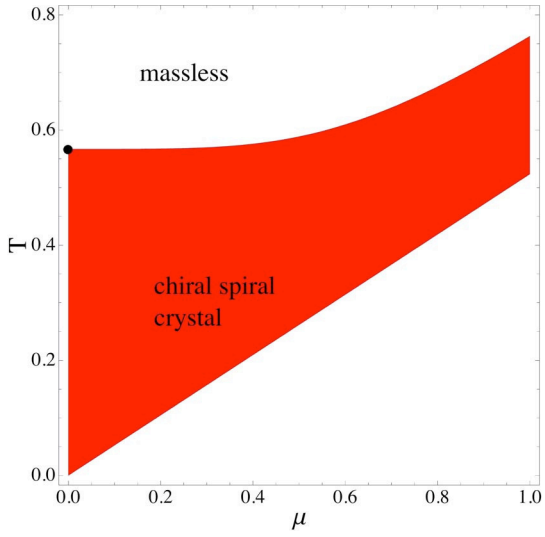

Fig. 3.7: The phase diagram of the NJL_2 model, based on a Ginzburg-Landau expansion to $O(\alpha_4)$.

As a result the Ginzburg-Landau analysis confirms once again that the chiral spiral is the thermodynamically preferred form of the inhomogeneous condensate, in the applicable part of the phase diagram. The general pattern is simple: to first nontrivial order $O(\alpha_3)$, we see the existence of the spiral phase as a solution of the GL equations, however it is not favored to this order. It is the next order of the GL expansion [i.e., one step beyond the order that defines the tricritical point] where we see that the spiral phase is favored. Going to even higher orders of the GL expansion, the crystalline region grows, and eventually covers the entire region given by the exact numerics, as shown in Figure 3.2.

We now analyse the Ginzburg-Landau expansion of the GN_2 model and demonstrate that the same pattern we described above also appears there.

3.5.2 Ginzburg-Landau expansion for the GN_2 model

We start with the grand potential density:

$$\begin{aligned}\Psi_{\rm GL} &= \alpha_0 + \alpha_2\phi^2 + \alpha_4\left(\phi^4 + \phi'^2 - \frac{1}{3}\left(\phi^2\right)''\right) \\ &\quad +\alpha_6\left(2\phi^6 + 10\phi^2\phi'^2 + \phi''^2 - \left(\phi^4 + (\phi')^2 - \frac{1}{5}\left(\phi^2\right)''\right)''\right) \\ &\quad +\ldots \end{aligned} \tag{3.128}$$

The tricritical point is defined as the point where the first two nontrivial coefficients, $\alpha_2(T,\mu)$ and $\alpha_4(T,\mu)$ vanish:

$$\alpha_2(T,\mu) = \alpha_4(T,\mu) = 0 \qquad \Rightarrow \qquad T_{\rm tc} = 0.318329 \quad , \quad \mu_{\rm tc} = 0.608221 \tag{3.129}$$

Here we see that the absence of the odd terms due to the real order parameter in the Ginzburg-Landau expansion leads to a completely different tricritical point for the GN_2 model. This is another outcome of the discrete chiral symmetry which is the ultimate reason why the order parameter is real. As mentioned above, the expansion to $O(\alpha_2)$ yields no information. The next nontrivial order, to $O(\alpha_4)$, leads to the following GL equation, which is a special case of the NLSE (3.118)

$$\phi'' - 2\phi^3 - \frac{\alpha_2}{\alpha_4}\phi = 0 \tag{3.130}$$

The general solution can be written as

$$\phi = \lambda\sqrt{\nu}\,{\rm sn}(\lambda x;\nu) \quad \Leftrightarrow \quad \phi'' - 2\phi^3 + (1+\nu)\lambda^2\,\phi = 0 \tag{3.131}$$

with the identification of the scale parameter λ as

$$\lambda^2 = \left(-\frac{\alpha_2}{\alpha_4}\right)\left(\frac{1}{1+\nu}\right) \tag{3.132}$$

Since $\frac{1}{1+\nu} \geq 0$, this expression tells us that this inhomogeneous solution only makes sense in regions of the (T,μ) plane where $\left(-\frac{\alpha_2}{\alpha_4}\right) \geq 0$. Using the following identities satisfied by the solution in (3.131)

$$\left(\phi'\right)^2 = \phi^4 - (1+\nu)\lambda^2\phi^2 + \nu\,\lambda^4 \tag{3.133}$$

$$\left(\phi^2\right)'' = 6\phi^4 - 4(1+\nu)\lambda^2\,\phi^2 + 2\nu\,\lambda^4 \tag{3.134}$$

we can write the grand potential density to this order as

$$\begin{aligned}\Psi_{\rm GL} &= \alpha_0 + \alpha_2\phi^2 + \alpha_4\left(\frac{1}{3}(1+\nu)\lambda^2\phi^2 + \frac{1}{3}\nu\,\lambda^4\right) \\ &= \alpha_0 + \frac{2}{3}\alpha_2\,\phi^2 + \frac{\nu}{3(1+\nu)^2}\,\frac{\alpha_2^2}{\alpha_4}\end{aligned} \tag{3.135}$$

Here we have used the above expression (3.132) for λ^2. Averaging over one period, we use $\langle\phi^2\rangle = \lambda^2(1-\mathbf{E}(\nu)/\mathbf{K}(\nu))$, and again using (3.132) we find

$$\begin{aligned}\langle\Psi\rangle_{\rm GL}^{\rm crystal} &= \alpha_0 + \left(-\frac{\alpha_2^2}{4\alpha_4}\right)\left[\frac{4}{1+\nu}\left(\frac{2+\nu}{3(1+\nu)} - \frac{2}{3}\frac{\mathbf{E}(\nu)}{\mathbf{K}(\nu)}\right)\right] \\ &\equiv \alpha_0 + \left(-\frac{\alpha_2^2}{4\alpha_4}\right)F(\nu)\end{aligned} \tag{3.136}$$

Note that the function $F(\nu)$ is a smooth function interpolating monotonically between $F(0) = 0$ and $F(1) = 1$. This is very similar to the expression in the NJL_2 case (3.122). We have written $\langle\Psi\rangle_{\rm GL}^{\rm crystal}$ like this in order to compare with the homogeneous ansatz: $\phi = \lambda$. Then

$$\langle\Psi\rangle_{\rm GL}^{\rm homogeneous} = \alpha_0 + \alpha_2\lambda^2 + \alpha_4\lambda^4 \tag{3.137}$$

Minimizing with respect to λ^2, we obtain the condition $\lambda^2 = -\alpha_2/(2\alpha_4)$, and at this minimum

$$\langle\Psi\rangle_{\rm GL}^{\rm homogeneous} = \alpha_0 + \left(-\frac{\alpha_2^2}{4\alpha_4}\right) \tag{3.138}$$

Therefore, we can write

$$\langle\Psi\rangle_{\rm GL}^{\rm homogeneous} - \langle\Psi\rangle_{\rm GL}^{\rm crystal} = \left(-\frac{\alpha_2^2}{4\alpha_4}\right)[1 - F(\nu)] \tag{3.139}$$

An important observation is that at the values of $\nu = 1$ and $\nu = 0$, the minimized grand potential reduces to that of the homogeneous and the massless condensates (recall $\mathbf{E}/\mathbf{K}(\nu = 1) = 0, \mathbf{E}/\mathbf{K}(\nu = 0)$=1):

$$\begin{aligned} \langle\Psi\rangle_{\rm GL}^{\rm crystal}(\nu = 1) &= \alpha_0 + \left(-\frac{\alpha_2^2}{4\alpha_4}\right) = \langle\Psi\rangle_{\rm GL}^{\rm homogenous} \\ \langle\Psi\rangle_{\rm GL}^{\rm crystal}(\nu = 0) &= \alpha_0 = \langle\Psi\rangle_{\rm GL}^{\rm massless} \end{aligned} \tag{3.140}$$

This behavior is depicted in Figure 3.8, where the grand potential of the crystal condensate lies between that of the massless and massive homogeneous phases, interpolating between them as a function of ν. Minimizing with respect to ν pushes us to the massive homogeneous phase in the blue region, but to the massless homogeneous phase in the white region. Thus, at this order of the GL expansion, even though the solution to the GL equation has the form of a crystalline condensate, the thermodynamic minimum is a constant condensate, either zero or non-zero, but always constant. We now show that this picture changes significantly at the next order.

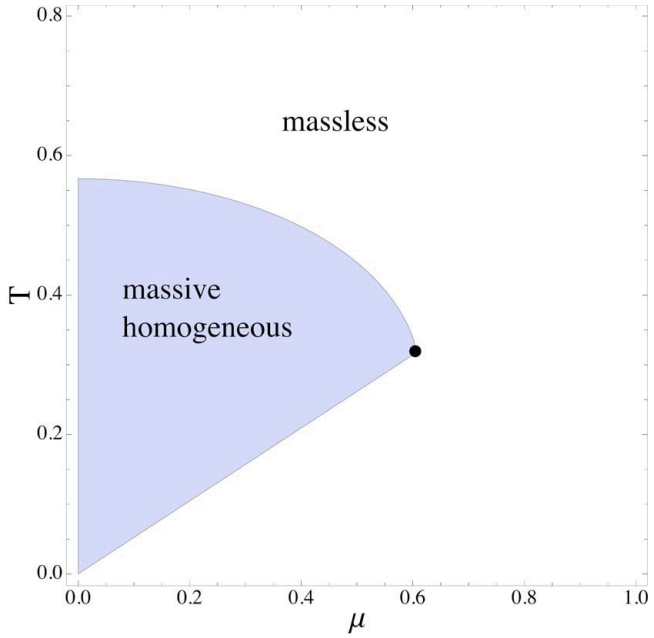

Fig. 3.8: The phase diagram of the GN_2 model, based on a Ginzburg-Landau expansion to the lowest nontrivial order: $O(\alpha_4)$.

Going to the next non-trivial order beyond the level defining the tricritical point, we expand the grand potential density in powers of the real condensate field ϕ and its derivatives [we drop the total derivative terms as these are not important for this argument]:

$$\Psi_{\rm GL} = \alpha_0 + \alpha_2\phi^2 + \alpha_4(\phi^4 + \phi'^2) + \alpha_6(2\phi^6 + 10\phi^2\phi'^2 + \phi''^2) \qquad (3.141)$$

The GL equation is now a fourth-order equation:

$$\left(\phi'''' - 10\phi^2\phi'' - 10\phi(\phi')^2 + 6\phi^5\right) + \frac{\alpha_4}{\alpha_6}\left(-\phi'' + 2\phi^3\right) + \frac{\alpha_2}{\alpha_6}\phi = 0 \qquad (3.142)$$

The simplest solution is a homogeneous condensate, $\phi = \lambda$, with massless and

massive solutions:

$$\begin{aligned} \lambda &= 0 \qquad \text{(massless homogeneous phase)} \\ \lambda^4 + \frac{\alpha_4}{3\alpha_6}\lambda^2 + \frac{\alpha_2}{6\alpha_6} &= 0 \quad \Rightarrow \quad \lambda_\pm^2 = -\frac{\alpha_4}{6\alpha_6}\left(1 \pm \sqrt{1 - \frac{6\alpha_2\alpha_6}{\alpha_4^2}}\right) \\ & \qquad \text{(massive homogeneous phase)} \end{aligned} \tag{3.143}$$

The general solution to (3.142) is very complicated, but we can use the inhomogeneous solution to the NLSE

$$\phi = \lambda\sqrt{\nu}\,\mathrm{sn}(\lambda\, x, \nu) \tag{3.144}$$

A similar idea was used in an analogous condensed matter model in [35]. This solution satisfies the nonlinear equations:

$$\begin{aligned} -\phi'' + 2\phi^3 &= (1+\nu)\lambda^2\phi \\ \left(\phi'''' - 10\phi^2\phi'' - 10\phi(\phi')^2 + 6\phi^5\right) &= (\nu^2 + 4\nu + 1)\lambda^4\phi \end{aligned} \tag{3.145}$$

Thus, comparing with the GL equation (3.142), we see that ϕ satisfies the GL equation (3.142) provided we identify:

$$\lambda^4 + \frac{\nu+1}{(\nu^2+4\nu+1)}\frac{\alpha_4}{\alpha_6}\lambda^2 + \frac{1}{(\nu^2+4\nu+1)}\frac{\alpha_2}{\alpha_6} = 0 \tag{3.146}$$

This condition leads to two solutions

$$\lambda_\pm^2 = -\frac{\nu+1}{2(\nu^2+4\nu+1)}\frac{\alpha_4}{\alpha_6}\left(1 \pm \left(1 - \frac{4(\nu^2+4\nu+1)}{(\nu+1)^2}\frac{\alpha_2\alpha_6}{\alpha_4^2}\right)^{1/2}\right) \tag{3.147}$$

Evaluated on the crystalline solution, the grand potential is

$$\begin{aligned} \langle\Psi\rangle_{\mathrm{GL}} &= \alpha_0 + \lambda^2\alpha_2\left(1 - \frac{\mathbf{E}}{\mathbf{K}}\right) + \frac{\lambda^4\alpha_4}{3}\left(1 + 2\nu - (1+\nu)\frac{\mathbf{E}}{\mathbf{K}}\right) \\ &\quad + \frac{\lambda^6\alpha_6}{5}\left(3\nu^2 + 6\nu + 1 - (\nu^2+4\nu+1)\frac{\mathbf{E}}{\mathbf{K}}\right) \end{aligned} \tag{3.148}$$

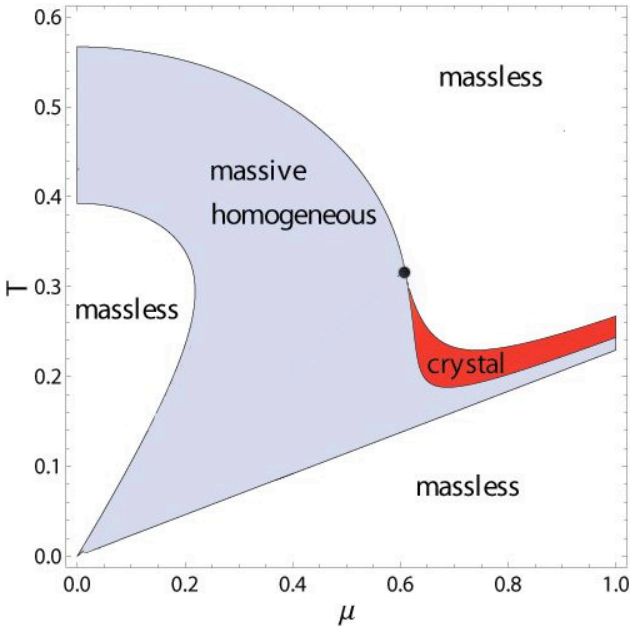

Fig. 3.9: The phase diagram of the GN_2 model, based on a Ginzburg-Landau expansion to the lowest nontrivial order: $O(\alpha_6)$.

This is just a function of T and μ (through the α's) and the elliptic parameter ν, because λ is given by the solutions in (3.147). We can therefore evaluate the grand potential throughout the (T, μ) plane and ask where it is lower than the grand potential of the homogeneous phase. The result is shown in Figure 3.9, which shows the existence of a crystalline phase in a small region in the vicinity of the tricritical point. This is a region in which the grand potential of the crystalline condensate is lower than that of the massless or massive homogeneous condensate. On the upper edge, $\nu = 0$ and the scale of the crystalline condensate vanishes as it reduces to a massless phase; on the lower edge, $\nu = 1$, and the period of the

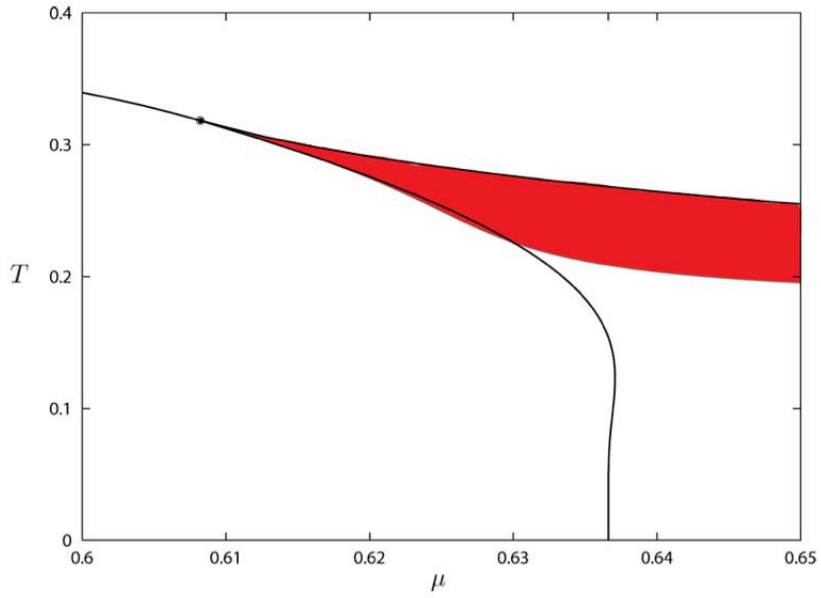

Fig. 3.10: A close-up view of the crystalline region in Fig. 3.9

crystalline condensate diverges as it reduces to a homogeneous massive phase. The form of this region matches very well with the full crystalline region, near the tricritical point, as shown by the close-up view in Figure 3.10. Especially, the agreement is excellent near the tricritical point and near the LOFF boundary with the massless phase. Going to higher orders of the GL expansion, this crystalline region grows, and eventually covers the entire region given by the exact numerics [22].

Consequently, we see the same general pattern in the GL expansion as in the NJL_2 case. To the first nontrivial order where the tricritical point is defined, we see the inhomogeneous crystal phase as a solution yet it is not favored in the phase diagram. When we go to the next nontrivial order, we start to see the

crystal phase in the phase diagram. The region in which it is favored approaches the exact result as we take into account more orders in the Ginzburg-Landau expansion.

3.6 An overview of phase diagrams

After a detailed study of the phase diagrams of NJL_2 and GN_2 systems, that are associated with discrete and continuous chiral symmetries, we now focus on the underlying physical mechanism that shapes these phase diagrams. It can be summarized as a combination of the Peierls instability and chiral symmetry breaking. The Peierls instability [64] is a famous result concerning one dimensional crystals, stating that at small enough temperatures opening a gap in the energy spectrum around the Fermi point, such that all the filled states are below the band and all the empty states are above, is energetically favorable compared to having no gap. Qualitatively, the existence of the gap decreases the energy of all the filled states hence the total free energy. In a chain type crystal at half filling, the gap is generated by a small displacement of the every second crystal site by an small (with respect to lattice size) amount δ. This shift generates a term (see the second reference in [64])

$$-\delta^2 \ln(\delta) \tag{3.149}$$

in the free energy, where δ is proportional to the width of the gap. We see that this is exactly the $\lambda^2 \ln \lambda$ term in the free energy (3.42) where λ is again the width of

the gap, measured in the units of the dynamically generated mass. Therefore the dynamical mass generation can be interpreted as another realization of the Peierls instability, generalized to a continuous system rather than a discrete lattice.

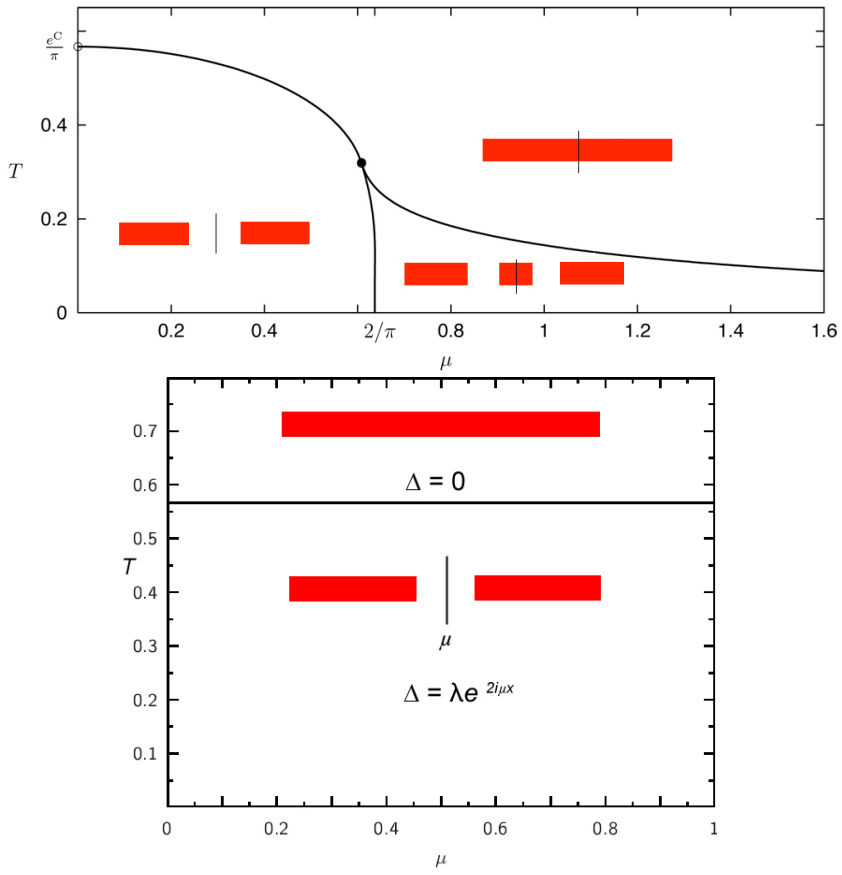

Fig. 3.11: The energy spectra of the phases in GN_2 and NJL_2 models

At nonzero chemical potential, the fermion mass gap is not centered around the Fermi point anymore. The crucial difference between the GN_2 and NJL_2 models occurs at nonzero μ. In the GN_2 model, due to the discrete chiral symmetry, the energy spectrum has to be symmetric around zero (see Section 3.1) and the only way to open a gap around a nonzero energy value is to open *two* gaps placed

symmetrically around zero. This configuration is precisely the real kink crystal described in Section 2.4.4. However it does not necessarily lead to a minimum free energy for all μ. Therefore there is a competition between the homogeneous phase with one gap around zero and crystal phase with two gaps. In fact, the crystal phase is only favored above a critical chemical potential $\mu_c = \frac{2}{\pi}$. Physically this μ_c is the mass of the dynamically generated baryon [10, 19, 50] in the theory. Also because of the effect of the lower gap on the density of states, the upper gap is not exactly centered around μ, but slightly closer to the upper band (see Fig 3.5). In the NJL_2 model, the continuous chiral symmetry allows one to shift the energy spectrum by an arbitrary amount q. Therefore it is always possible to open a gap around μ and this is precisely what happens (see Section 3.2.1). The corresponding configuration is the chiral spiral. In both of the models above a critical temperature, the entropy dominates. Combined with the asymptotic freedom, the the favored phase therefore, is the massless, free fermion where the chiral symmetry is restored.

As a result, the underlying mechanism behind the phase diagrams of GN_2 and NJL_2 models is a generalized form of the Peierls instability where the gap is formed through chiral symmetry breaking. The form of the chiral symmetry has a direct impact on the phase diagram. Moreover, this argument suggests that the formation of spiral phases in 1+1 dimensional fermion systems is generic. In fact, recent studies showed that this is indeed the case, and certain models

such as the 't Hooft model [65] or the proposed "quarkyonic" phase [45, 46] of the cold, dense QCD at large N_c limit host chiral spiral phases. The quarkyonic phase is described by a quark fermi sea with confined excitations in the region $\mu >> \Lambda_{QCD} >> \mathrm{M_{Debye}}$. The dynamics of the Fermi surface leads to a factorized gluon propagator since the contribution transverse momentum transfer ($\sim \Lambda_{QCD}$) to the quark free energy is negligible compared to the longitudinal one ($\sim \mu$). Therefore one ends up with an effectively 1+1 dimensional system whose ground state is a chiral spiral [46]. Additionally, a spiral phase in $\mathrm{SU(2)_R \times SU(2)_L}$ symmetric $\mathrm{NJL_2}$ model with isospin chemical potential [66] is also recently been found [67].

As mentioned, the $\mathrm{GN_2}$ model can be realized as the continuum limit of certain one dimensional polymer chains [29] or spin Peierls cuprates [31] where the discrete chiral symmetry breaking corresponds to dimerization. The role of chemical potential is played by the external magnetic field which creates an imbalance between spin up and down electrons. There also exist inhomogeneous superconductors [32, 33, 34, 35, 36]. where the gap formation is due to BCS pairing. In all these materials, the Peierls instability is observed. Next, we apply this reasoning to study dense quark matter under a strong magnetic field where the dimensional reduction form 3+1 to 1+1 dimensions is due to strong magnetic field that causes the transverse degrees of freedom to "freeze" in the lowest Landau level.

Chapter 4

Chiral magnetic spiral

In the previous chapter we have showed that, below a critical temperature, the ground state of the NJL_2 model at nonzero density is a spiral with a phase equal to the chemical potential, and further argued that this is a generic phenomenon in 1+1 dimensional systems with continuous chiral symmetry at nonzero density. In this section, we apply this reasoning to quark matter in the presence of a strong magnetic field which induces a dimensional reduction mechanism from 3+1 to 1+1 dimensions. In particular we revisit the Chiral Magnetic Effect from this dimensionally reduced picture using our results regarding thermal properties of 1+1 dimensional systems with chiral U(1) symmetry, summarized in Section 3.6. The work discussed in this chapter is published as [14].

Recently, the STAR Collaboration at the Relativistic Heavy Ion Collider reported [68, 69] observation of charge-dependent azimuthal correlations, representing evidence for the Chiral Magnetic Effect (CME) [70, 71, 72, 73, 74] in QCD coupled to electromagnetism. The essence of the effect is the generation of electric current along the direction of an external magnetic field in the presence of topo-

logically nontrivial gauge field configurations creating a local imbalance between left and right chiralities. The colliding positively charged ions generate, at early times, a very strong magnetic field, $eB \sim m_\pi^2$ [72, 75], that inside the produced quark-gluon matter is directed perpendicular to the reaction plane of the collision. Topological fluctuations in the produced matter (for recent specific realizations, see [76, 77]) then induce the experimentally measured charge asymmetry with respect to the reaction plane that fluctuates on an event-by-event basis.

The CME has been studied also in lattice gauge theory, and evidence for charge separation in a magnetic field has been found both in quenched calculations [78] and in calculations with dynamical light quarks [79]. At finite baryon density, there is a closely related phenomenon of chiral separation (flow of axial current) along the direction of the magnetic field [80, 81, 82]. Very recently, it has been found [83] that the vacuum of the theory in the confined, chirally broken phase develops a finite electric conductivity along the direction of a sufficiently strong external magnetic field. A natural question arises about the nature of the low frequency mode capable of transporting the charge current in the vacuum.

The two important physical effects are the lowest Landau level (LLL) projection induced by the strong magnetic field, which leads to an effective reduction of the system to 1+1 dimensions, as in the physics of magnetic catalysis of symmetry breaking [84, 85], and the topological charge fluctuations of the QCD vacuum, which induce local regions of chirality of zero modes.

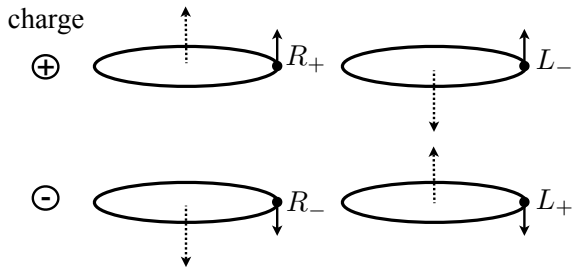

Fig. 4.1: Sketch of the effect of the strong magnetic field on the various spinors.

The effect of the strong magnetic field (directed upward in these figures) on the various spinor basis elements is shown in Figure 4.1. The circles denote the cyclotron orbits, the spin direction is denoted by solid arrows, and the direction of momentum by dotted arrows. $R_\pm$ and $L_\pm$ label right- and left-handed chirality with $\pm$ direction of momentum along the B field. The upper row, labeled on the left with a circled + sign, corresponds to positive charge in the lowest Landau level projection of spins aligned along the B field, while the lower row, labeled on the left with a circled $-$ sign, corresponds to negative charge in the lowest Landau level projection of spins anti-aligned with the B field.

There are three important spinor bases relevant to our discussion: a chirality basis, a spin basis and a momentum direction basis, because of the roles played by topological charge fluctuations, Zeeman splitting, and the dimensional reduction due to lowest Landau level projection. We consider a strong (and approximately uniform) magnetic field B along the x^3 direction, and use Dirac matrices ($j =$

$1, 2, 3$)

$$\gamma^0 = \begin{pmatrix} 0 & \mathbf{1} \\ \mathbf{1} & 0 \end{pmatrix} \quad \gamma^j = \begin{pmatrix} 0 & -\sigma^j \\ \sigma^j & 0 \end{pmatrix} \quad \gamma^5 = \begin{pmatrix} \mathbf{1} & 0 \\ 0 & -\mathbf{1} \end{pmatrix} \tag{4.1}$$

We decompose the 4-component spinor in terms of eigenstates of the chiral projectors, $P_{R,L} = \frac{1}{2}(\mathbf{1} \pm \gamma^5)$, the spin projectors $P_{\uparrow,\downarrow} = \frac{1}{2}(\mathbf{1} \pm \Sigma^3)$, and the momentum direction projectors $P_{+,-} = \frac{1}{2}(\mathbf{1} \pm \gamma^0\gamma^3)$. The longitudinal spin operator is $\Sigma^3 = \gamma^0\gamma^3\gamma^5 = \mathrm{diag}(\sigma^3, \sigma^3)$, and the helicity operator is $\gamma^0\gamma^3 = \mathrm{diag}(\sigma^3, -\sigma^3)$. We can write the 4-component spinor field as

$$\Psi = \Big(R_+, R_-, L_-, L_+\Big)^T \tag{4.2}$$

Define the following 2 component spinors, eigenspinors of chirality, spin and momentum direction, respectively:

$$\begin{aligned} \mathcal{R} &= \begin{pmatrix} R_+ \\ R_- \end{pmatrix} \qquad \mathcal{L} = \begin{pmatrix} L_+ \\ L_- \end{pmatrix} \\ \phi_\uparrow &= \begin{pmatrix} R_+ \\ L_- \end{pmatrix} \qquad \phi_\downarrow = \begin{pmatrix} L_+ \\ R_- \end{pmatrix} \\ \eta_+ &= \begin{pmatrix} R_+ \\ L_+ \end{pmatrix} \qquad \eta_- = \begin{pmatrix} L_- \\ R_- \end{pmatrix} \end{aligned} \tag{4.3}$$

Then the axial current, $J_5^\mu = \bar{\Psi}\gamma^\mu\gamma^5\Psi$, can be decomposed in terms of 2-

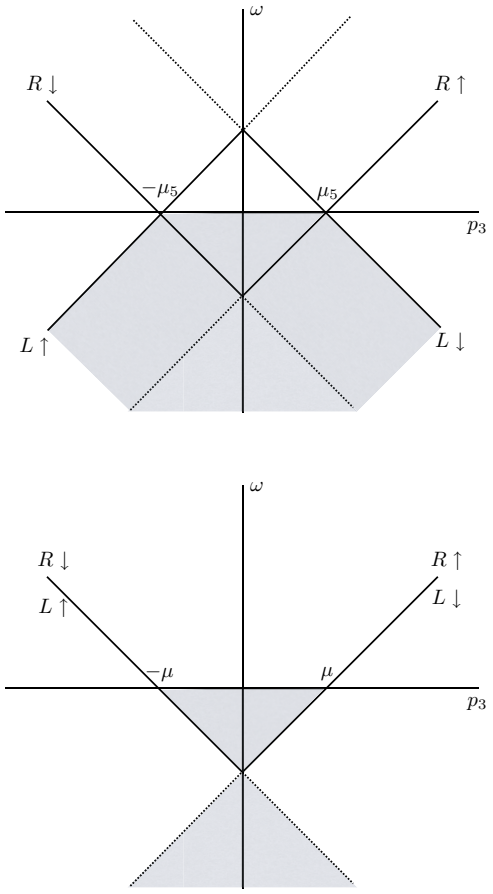

Fig. 4.2: The dispersion diagrams for the case of nonzero μ_5 (upper figure) and for nonzero μ (lower figure).

component spinors as follows:

$$\begin{aligned} J_5^0 &= \mathcal{R}^\dagger\mathcal{R} - \mathcal{L}^\dagger\mathcal{L} = -i\bar{\phi}_\uparrow\Gamma^z\phi_\uparrow + i\bar{\phi}_\downarrow\Gamma^z\phi_\downarrow \\ J_5^1 &= \bar{\mathcal{R}}\,\mathcal{R} + \bar{\mathcal{L}}\,\mathcal{L} = \bar{\phi}_\uparrow\phi_\downarrow + \bar{\phi}_\downarrow\phi_\uparrow \\ J_5^2 &= i\bar{\mathcal{R}}\,\Gamma^5\mathcal{R} - i\bar{\mathcal{L}}\,\Gamma^5\mathcal{L} = -i\bar{\phi}_\uparrow\phi_\downarrow + i\bar{\phi}_\downarrow\phi_\uparrow \\ J_5^3 &= \bar{\mathcal{R}}\,\Gamma^z\mathcal{R} - \bar{\mathcal{L}}\,\Gamma^z\mathcal{L} = \phi_\uparrow^\dagger\phi_\uparrow - \phi_\downarrow^\dagger\phi_\downarrow \end{aligned} \tag{4.4}$$

and the charge current, $J^\mu = \bar{\Psi}\gamma^\mu\Psi$, is decomposed:

$$\begin{aligned} J^0 &= \mathcal{R}^\dagger\mathcal{R} + \mathcal{L}^\dagger\mathcal{L} = \phi_\uparrow^\dagger\phi_\uparrow + \phi_\downarrow^\dagger\phi_\downarrow \\ J^1 &= \bar{\mathcal{R}}\,\mathcal{R} - \bar{\mathcal{L}}\,\mathcal{L} = -\bar{\phi}_\uparrow\Gamma^5\phi_\downarrow + \bar{\phi}_\downarrow\Gamma^5\phi_\uparrow \\ J^2 &= i\bar{\mathcal{R}}\,\Gamma^5\mathcal{R} + i\bar{\mathcal{L}}\,\Gamma^5\mathcal{L} = i\bar{\phi}_\uparrow\Gamma^5\phi_\downarrow + i\bar{\phi}_\downarrow\Gamma^5\phi_\uparrow \\ J^3 &= \bar{\mathcal{R}}\,\Gamma^z\mathcal{R} + \bar{\mathcal{L}}\,\Gamma^z\mathcal{L} = \bar{\phi}_\uparrow\Gamma^z\phi_\uparrow + \bar{\phi}_\downarrow\Gamma^z\phi_\downarrow \end{aligned} \tag{4.5}$$

Here we have defined the 2 dimensional gamma matrices as $\Gamma^0 = \sigma^1, \Gamma^z = -i\sigma^2, \Gamma^5 = \sigma^3$. Note that J^0, J_5^0, J^3 and J_5^3 are expressed in terms of 2d densities and currents for $\mathcal{R}$ and $\mathcal{L}$, while $J^\perp$ and $J_5^\perp$ are expressed in terms of 2d scalar and pseudoscalar condensates for $\mathcal{R}$ and $\mathcal{L}$.

The fillings of right- and left-handed levels are shown in Figure 4.2 for the cases of nonzero chiral chemical potential $\mu_5 = \mu_R = -\mu_L$, and for nonzero chemical potential $\mu = \mu_R = \mu_L$. Accounting for the appropriate branches of the excitations, the dispersion relation for $\mu_5 \neq 0$ is:

$$\begin{aligned} \mu_5 \neq 0 : R\uparrow\!: \omega = p_3 - \mu_5 \quad &, \quad L\uparrow\!: \omega = p_3 + \mu_5 \\ R\downarrow\!: \omega = -p_3 - \mu_5 \quad &, \quad L\downarrow\!: \omega = -p_3 + \mu_5 \end{aligned} \tag{4.6}$$

while for $\mu \neq 0$:

$$\begin{aligned} \mu \neq 0 : R\uparrow\!: \omega = p_3 - \mu \quad &, \quad L\uparrow\!: \omega = -p_3 - \mu \\ R\downarrow\!: \omega = -p_3 - \mu \quad &, \quad L\downarrow\!: \omega = p_3 - \mu \end{aligned} \tag{4.7}$$

For certain pairings, the up-moving and down-moving plane waves $e^{\pm ip_3 z}$ acquire a phase difference because of the chemical potential shift, which naturally leads

to the production of sinusoidal spatial modulations in the longitudinal direction. We show below that these modulations occur in the transverse components of the currents.

The key observation is that, after dimensional reduction, the $3+1$ dimensional spinor break down into two "flavors" of $1+1$ dimensional two component spinors $\mathcal{R}$ and $\mathcal{L}$. Also, in the previous section we argued that in a generic theory with continuous chiral symmetry and nonzero chemical potential, the ground state below the critical temperature is the chiral spiral. Therefore in the dimensionally reduced picture we expect $\mathcal{R}$ and $\mathcal{L}$ to develop chiral spiral phases. Then the renormalized number density (3.25), is automatically given by μ_f/π. We now investigate the cases with nonzero axial chemical potential μ_5 and quark chemical potential μ separately.

4.1 Nonzero chiral chemical potential $\mu_5 \neq 0$

To understand the implications of the chiral spiral for $3+1$ dimensions, consider first the effect of a nonzero chiral chemical potential $\mu_5 \neq 0$, corresponding to $\mu_R = \mu_5 = -\mu_L$. The fillings of the fermionic single-particle levels for massless $\mathcal{R}$ and $\mathcal{L}$ particles are depicted in Figure 4.2, using the dispersion relations in (4.6). The imbalance between right-handed and left-handed particles leads to the "chiral magnetic effect" [70, 71, 72, 73, 74], a charge separation along the direction of the magnetic field. For example, as depicted in Figure 4.1, in a region with a surplus of

right-handed zero modes, the positive charges necessarily have spin up due to the LLL projection, and hence have positive momentum, while negatively charged right-handed particles have spin down and hence negative momentum, thereby inducing a spatial separation of charge. This charge separation is associated with a nonzero expectation value, $\langle J^3 \rangle = \frac{eB}{2\pi}\frac{e\mu_5}{\pi}$, computed in [70, 73], reflecting the surplus of right-handed particles leading to a surplus of right-handed current along the $x^3 = z$ direction.

Moreover ,from the renormalized number density (3.25), we find $\rho_R = \frac{\mu_5}{\pi}$ and $\rho_L = -\frac{\mu_5}{\pi}$. Combined with the Landau degeneracy factor $\frac{eB}{2\pi}$, we find from (4.4) the nonzero expectation value $\langle J_5^0 \rangle = \frac{1}{2}\frac{eB}{2\pi}\frac{2e\mu_5}{\pi}$ [1] [73, 74], while from (4.5) we have $\langle J^0 \rangle = 0$. This is another way to understand the usual chiral magnetic effect, in a way that emphasizes the physical factorization into the product of a transverse Landau degeneracy factor and a longitudinal one-dimensional density-of-states factor.

Alternatively, this can also be understood as a dimensional reduction of the 3+1 dimensional chiral anomaly [86, 87, 88, 89] to the $1 + 1$ dimensional chiral anomaly, expressed in terms of the $1 + 1$ dimensional density and current. The

[1] In computing $\langle J_5^0 \rangle$ (analogously for $\langle J_5^3 \rangle$ with $\mu \neq 0$), there is an additional factor of $\frac{1}{2}$ coming from integrating over half of the momentum space, as is appropriate for the dispersion relations associated with the relevant pairing. For a comprehensive discussion see sections II and III B in [73].

3+1 dimensional chiral anomaly can be expressed as [74]:

$$\frac{dQ_5}{dt} \equiv \frac{d}{dt}\int d^3\vec{x}\langle J_5^0\rangle = \frac{e^2}{2\pi^2}\int d^3\vec{x}\,\vec{E}\cdot\vec{B} \tag{4.8}$$

Here, the electric field can be thought of generated by an adiabatic chiral chemical potential μ_5 with $E \sim \dot{\mu}_5/e$, consistent with the spectral flow picture. The the term $\int d^2x_\perp \frac{eB}{2\pi}$ is again recognized as the Landau degeneracy, leading to:

$$\frac{d}{dt}\langle J_5^0\rangle = \frac{eB}{2\pi}\frac{d}{dt}\left(\frac{\mu_5}{\pi}\right) \tag{4.9}$$

which reproduces the same result $\langle J_5^0\rangle = \rho_R - \rho_L = \frac{eB}{2\pi}\frac{\mu_5}{\pi}$ as above.

Our first new observation concerns the effect of a strong magnetic field and nonzero μ_5 on the *transverse* components of the axial and charge currents. In the longitudinal direction there is no effect on the axial current, $\langle J_5^3\rangle = 0$, because we assume the chirality imbalance occurs homogeneously (i.e., μ_5 is almost constant along the z axis). On the other hand, we find nonzero expectation values for the *transverse* components, $\langle J_5^\perp\rangle$ and $\langle J^\perp\rangle$, of both the axial and charge currents, and moreover these have a characteristic spiral dependence on the longitudinal coordinate, set by $2\mu_5$. To see this, recall that the dispersion relations for the massless fermions are linear (4.6), and the nonzero μ_5 represents an imbalance in the fillings of R and L fermion levels, as shown in Figure 4.2. The free part of the Lagrangian with nonzero μ_5 is:

$$\begin{aligned}\mathcal{L}_{\mu_5} &= iR_+^*\left(\partial_0+\partial_z-i\mu_5\right)R_+ + iR_-^*\left(\partial_0-\partial_z-i\mu_5\right)R_- \\ &\quad + iL_+^*\left(\partial_0+\partial_z+i\mu_5\right)L_+ + iL_-^*\left(\partial_0-\partial_z+i\mu_5\right)L_-\end{aligned} \tag{4.10}$$

Referring to Figure 4.2, pairing occurs at the Fermi surface between $\mathcal{R}$ particles with $p_3 \sim \mu_5$ and $\mathcal{R}$ holes with $p_3 \sim -\mu_5$, and between $\mathcal{L}$ particles with $p_3 \sim -\mu_5$ and $\mathcal{L}$ holes with $p_3 \sim \mu_5$. Thus the condensates $\bar{\mathcal{R}}\,\mathcal{R}$, $\bar{\mathcal{R}}\,i\Gamma^5\mathcal{R}$, $\bar{\mathcal{L}}\,\mathcal{L}$ and $\bar{\mathcal{L}}\,i\Gamma^5\mathcal{L}$ appearing in $J^\perp$ and $J_5^\perp$ have momentum dependences displaced by $\pm\mu_5$, leading to

$$\begin{aligned}
\langle J^1\rangle &= C^2\cos(2\mu_5\, z - \phi_R) - D^2\cos(2\mu_5\, z + \phi_L) \\
\langle J^2\rangle &= -C^2\sin(2\mu_5\, z - \phi_R) + D^2\sin(2\mu_5\, z + \phi_L) \\
\langle J_5^1\rangle &= C^2\cos(2\mu_5\, z - \phi_R) + D^2\cos(2\mu_5\, z + \phi_L) \\
\langle J_5^2\rangle &= -C^2\sin(2\mu_5\, z - \phi_R) - D^2\sin(2\mu_5\, z + \phi_L)
\end{aligned} \tag{4.11}$$

for some constants C and D, and relative phases ϕ_R and ϕ_L. This is consistent with the generation of chiral spiral behavior of the chiral condensates of $\mathcal{R}$ and $\mathcal{L}$ spinors.

4.2 Nonzero chemical potential $\mu \neq 0$

Now consider the opposite situation where we have a particle-hole imbalance due to a real chemical potential μ. So, we take $\mu_5 = 0$ but $\mu \neq 0$, with $\mu_R = \mu = \mu_L$. Then, according to [80, 81, 82], there is a net flow of chirality along the direction of the magnetic field, characterized by $\langle J_5^3\rangle \neq 0$. This effect can be easily understood from (4.4) by noticing that $\langle J_5^3\rangle \neq 0$ is the difference between the spin densities. Indeed, a direct LLL computation [80, 85] shows that $\langle J_5^3\rangle = \frac{eB}{2\pi}\frac{e\mu}{\pi}$, in agreement

with the $1+1$ dimensional charge condensate argument given above that $\rho_f = \mu_f/\pi$. In this case, as opposed to the charge separation effect when $\mu_5 \neq 0$, for nonzero μ there is a separation of chirality. On the other hand, with nonzero μ, if we consider the charge current we find $\langle J^3 \rangle = 0$, while $\langle J^0 \rangle$ is nonzero. This is again due to assuming μ is almost constant along z, inside the collision region. The imbalance between holes and quarks is homogeneous, resulting in vanishing current. Our second new result is that the *transverse* components of the axial and charge currents develop a similar spiral inhomegeneity, now characterized by μ. Once again, the physical origin of the spiral dependence is the relation between the energy imbalance and the momentum imbalance through the dispersion relations for one-dimensional massless fermions. The free part of the Lagrangian with nonzero μ is:

$$\begin{aligned} \mathcal{L}_\mu &= iR_+^* \left(\partial_0 + \partial_z - i\mu\right) R_+ + iR_-^* \left(\partial_0 - \partial_z - i\mu\right) R_- \\ &\quad + iL_+^* \left(\partial_0 + \partial_z + i\mu\right) L_+ + iL_-^* \left(\partial_0 - \partial_z + i\mu\right) L_- \end{aligned} \tag{4.12}$$

Referring to Figure 4.2, pairing occurs at the Fermi surface between $\mathcal{R}$ particles with $p_3 \sim \mu$ and $\mathcal{R}$ holes with $p_3 \sim -\mu$, and between $\mathcal{L}$ particles with $p_3 \sim -\mu$ and $\mathcal{L}$ holes with $p_3 \sim \mu$. Thus the condensates $\bar{\mathcal{R}}\,\mathcal{R}$, $\bar{\mathcal{R}}\, i\Gamma^5 \mathcal{R}$, $\bar{\mathcal{L}}\,\mathcal{L}$ and $\bar{\mathcal{L}}\, i\Gamma^5 \mathcal{L}$

appearing in $J^{\perp}$ and $J_5^{\perp}$ have momentum dependence displaced by $\pm\mu$, leading to

$$\begin{aligned}
\langle J^1 \rangle &= C^2 \cos(2\mu z - \phi_R) - D^2 \cos(2\mu z - \phi_L) \\
\langle J^2 \rangle &= -C^2 \sin(2\mu z - \phi_R) - D^2 \sin(2\mu z - \phi_L) \\
\langle J_5^1 \rangle &= C^2 \cos(2\mu z - \phi_R) + D^2 \cos(2\mu z - \phi_L) \\
\langle J_5^2 \rangle &= -C^2 \sin(2\mu z - \phi_R) + D^2 \sin(2\mu z - \phi_L)
\end{aligned} \tag{4.13}$$

As before, this spiral behavior follows immediately from the dimensionally reduced picture, once we have an imbalance, which is here set by μ. This also implies that with both μ_5 and μ being nonzero, we predict spiral condensates for the transverse components of both the axial and charge currents, with the wavenumbers being determined by both μ and μ_5.

In heavy ion collisions, the chiral magnetic spiral can induce both out-of-plane and in-plane fluctuating charge asymmetries (the separation of out-of-plane and in-plane fluctuations has been performed recently [90] on the basis of STAR data [68, 69]). In the absence of topological fluctuations ($\mu_5 = 0$), at finite baryon density ($\mu \neq 0$), and in the chirally broken phase, the current of charge has only transverse components, and the charge asymmetry will fluctuate only in-plane. It should be kept in mind that the presence of magnetic field increases the chiral transition temperature [84]. If topological fluctuations are present in the chirally broken phase (e.g. due to the presence of meta-stable η' domains [91]), the CME current can be carried by the chiral magnetic spiral. The chiral magnetic spiral

has also been seen in a holographic study [92] in the framework of Sakai-Sugimoto model of holographic QCD.

Chapter 5

Conclusions

In this dissertation we have studied the two dimensional Nambu-Jona-Lasinio and Gross Neveu models at finite temperature and chemical potential. Both of these models exhibit chiral and translational symmetry breaking at sufficiently low temperatures. We further showed that the phase diagrams of NJL_2 and GN_2 models are vastly different which we explained by the difference in the symmetry breaking pattern; namely continuous vs. discrete chiral symmetry. The NJL_2 model has a spiral phase with constant charge density whose amplitude depends on the temperature and phase is linear in the chemical potential, as opposed to the homogeneous and crystalline phases in the GN_2 model. We argued that the spiral phase of NJL_2 is a generic feature of two dimensional systems exhibiting chiral U(1) symmetry breaking and constructed a simple physical picture explaining the ubiquity of the spiral phase based on a generalized form of the Peierls instability. Indeed, there are various examples [46, 65, 66] supporting this argument. As a phenomenological application of this result, we developed an alternative way to derive various properties of quark matter under a strong magnetic field [73, 81]

and proposed a possible explanation of the observed out-of-plane and in-plane correlations in heavy ion collisions [68, 69]. Our proposal regarding heavy ion collisions is further supported by a holographic calculation [92].

The computational tools that we used were based on an inhomogeneous ansatz for the Gorkov resolvent. This ansatz allowed the functional gap equation to be reduced to an ordinary differential equation, which was furthermore soluble. We presented the most general solution, the twisted kink crystal, and showed that all the previously known solutions can be obtained as various limiting cases of this most general solution. We also studied the properties of the corresponding spinor solutions such as the charge density and axial anomaly. In particular, the axial anomaly in the NJL_2 system vanishes as a result of the inhomogeneous gap equation leading to a constant charge density.

These one dimensional models are somewhat special, due to the rich integrability structure underlying their gap equation, and we showed that this is also reflected in the associated Ginzburg-Landau expansions of the models by presenting the mechanism that made it possible to solve the Ginzburg-Landau equations to all orders. We found that in both the NJL_2 and GN_2 models the crystalline region appears at the order of the Ginzburg-Landau expansion *one step beyond* the first nontrivial order, which is used to identify the relevant tricritical point. On the other hand, the Ginzburg-Landau approach for a generic system does not necessarily rely on an integrability structure. It would be in-

teresting to try to extend some of these ideas to higher dimensions, for example for higher dimensional Gross-Neveu or Nambu-Jona Lasinio models [36, 93], or more ambitiously to search for crystalline condensates in QCD or QCD models [94, 95, 96, 97, 98, 99, 100]. It would also be interesting to study the NJL_2 system on the lattice, complementing the GN_2 work of [50, 51], and the recent Monte Carlo formulations in [52, 53, 54].

Appendix A

Resolvent of a Dirac system, and the Eilenberger equation

In this appendix we summarize the derivation of the Dikii-Eilenberger equation (2.24) for the diagonal resolvent of a Dirac system. The interested reader is urged to consult also references [28, 27], and Appendix B of the first paper in [26]. Here we sketch the key features of the argument, for the sake of being more self-contained.

The important idea is simple. Recall that in one dimension, for a Schrödinger-like Sturm-Liouville operator, it is well known that the Green's function can be written in terms of a product of two independent solutions, normalized by their Wronskian [102]. An analogous construction exists for a one dimensional Dirac operator [28, 27, 26]. Furthermore, in the Sturm-Liouville case, the coincident-point limit $R(x, x; E)$ satisfies a differential equation, known as the Gel'fand-Dik'ii equation , just by virtue of being written as a product of solutions to the original differential equation [102]. Likewise, for a Dirac system, the coincident-point limit $R(x, x; E)$ also satisfies an equation, just by virtue of being expressed in terms of solutions to the original differential equation. This equation is the Dik'ii-

Eilenberger equation (2.24). The technical difference from the Gel'fand-Dik'ii equation arises because the Dirac operator is *first-order in derivatives* and because it is a 2×2 *matrix operator*.

So, consider two independent spinor solutions $\psi_{1,2}$ of the BdG equation $H\psi = E\psi$ in (2.11), where H is the 2×2 matrix first-order differential operator in (2.10). Then we can write the resolvent (also a 2×2 matrix) as

$$R(x,y;E) = \begin{cases} \psi_1(x)R(y) \quad , \quad x < y \\ \\ \psi_2(x)L(y) \quad , \quad x > y \end{cases} \tag{A.1}$$

The row-vector functions $R(y)$ and $L(y)$ are determined by demanding that $R(x,y;E)$ satisfy

$$(H - E)\, R(x,y;E) = \delta(x-y) \tag{A.2}$$

Integrating this first-order differential equation across the point $x = y$, we learn that

$$R(x,y;E) = \begin{cases} \frac{1}{iW}\psi_1(x)\psi_2^T(y)\,\sigma_1 \quad , \quad x < y \\ \\ \frac{1}{iW}\psi_2(x)\psi_1^T(y)\,\sigma_1 \quad , \quad x > y \end{cases} \tag{A.3}$$

where the Wronskian W is the scalar function $W(\psi_1,\psi_2) = i\psi_1^T\sigma_2\psi_2$. The coincident-point limit $x = y$ is given by an averaged limit as [see (2.25)]:

$$R(x;E) = \frac{1}{2iW}\left(\psi_1(x)\psi_2^T(x) + \psi_2(x)\psi_1^T(x)\right)\sigma_1 \tag{A.4}$$

Now, express the BdG equation (2.11) as

$$\psi' = i \begin{pmatrix} E & -\Delta \\ \Delta^* & -E \end{pmatrix} \psi \quad , \quad \psi'^T = i\psi^T \begin{pmatrix} E & \Delta^* \\ -\Delta & -E \end{pmatrix} \tag{A.5}$$

Then, differentiating (A.4) once with respect to x, using the fact that each of ψ_1 and ψ_2 satisfies the BdG equation (2.11) in the form (A.5), we arrive immediately at the Dik'ii-Eilenberger equation (2.24). Furthermore, if we write $\psi_1 = (u_1, v_1)^T$, and $\psi_2 = (u_2, v_2)^T$, then (A.4) says that

$$R(x;E) = \frac{1}{2i(u_1 v_2 - u_2 v_1)} \begin{pmatrix} u_1 v_2 + u_2 v_1 & 2u_1 u_2 \\ 2v_1 v_2 & u_1 v_2 + u_2 v_1 \end{pmatrix} \tag{A.6}$$

Thus, the algebraic conditions (2.22) and (2.23) follow. The hermiticity condition (2.21) is less immediately obvious, because this depends on E and W. However, it is clear from the definition of the resolvent that $R(x;E) = \langle x|1/(H-E)|x\rangle$ is hermitean for real E. The appropriate hermiticity properties are studied in more detail in [28, 26, 27], and can also be seen from the result for the constant Δ case (2.29), and the $i\,\epsilon$ condition used to define the spectral function (2.19).

Appendix B

Some useful properties of elliptic functions

In this appendix we collect some basic facts and nontrivial identities for Weierstrass elliptic functions that are used repeatedly in this dissertation, in order to make the dissertation more self-contained. These functions play a special role because the self-consistent condensate $\Delta(x)$ and the spinor solutions $\psi(x)$ to the Bogoliubov-de Gennes equation are all expressed in terms of these functions. There are many good books on elliptic functions. Excellent classical references are [101, 102]. We also found [104, 103] to be particularly useful. Very roughly speaking, the Weierstrass elliptic functions are doubly-periodic extensions of standard trigonometric functions:

$$\begin{aligned} \sin(z) &\leftrightarrow \sigma(z) \\ \cot(z) = \frac{d}{dz}\ln\sin(z) &\leftrightarrow \zeta(z) = \frac{d}{dz}\ln\sigma(z) \\ \frac{1}{\sin^2(z)} = -\frac{d}{dz}\cot(z) &\leftrightarrow \mathcal{P}(z) = -\frac{d}{dz}\zeta(z) \end{aligned} \tag{B.1}$$

The trigonometric functions have periodicity properties along the real z axis, but the Weierstrass functions are *doubly* (quasi-)periodic. They are specified by the

real and imaginary (half-)periods, ω_1 and ω_3. It is standard to define also ω_2 by $\omega_1 + \omega_2 + \omega_3 = 0$. Then the Weierstrass sigma function is quasi-periodic under shifts by $2\omega_i$:

$$\sigma(z + 2\omega_i) = -e^{2\eta_i(z+\omega_i)}\sigma(z) \quad , \quad i = 1, 2, 3 \quad . \tag{B.2}$$

Here $\eta_i \equiv \zeta(\omega_i)$. In general, ω_1 and ω_3 define a fundamental parallelogram characterizing the doubly-periodic nature of the Weierstrass functions. We choose a fundamental rectangle, with $\omega_1 = \mathbf{K}(\nu)$ and $\omega_3 = i\,\mathbf{K}' \equiv i\,\mathbf{K}(1-\nu)$. The periods are then parametrized by the elliptic parameter ν that takes values in $[0, 1]$. At the limits ν=0 and $\nu = 1$, the Jacobi elliptic function reduce to trigonometric and hyperbolic functions respectively. Physically, they interpolate between kink-like solutions and sinusoidal ones.

The Weierstrass functions are then related to the Jacobi elliptic functions as follows. We define

$$\sigma_i(z) = e^{-\eta_i z}\frac{\sigma(z + \omega_i)}{\sigma(\omega_i)} \tag{B.3}$$

and Jacobi's elliptic functions can be constructed from their ratios,

$$\mathrm{sn}(z) = \frac{\sigma(z)}{\sigma_3(z)} \quad ; \quad \mathrm{cn}(z) = \frac{\sigma_1(z)}{\sigma_3(z)} \quad ; \quad \mathrm{dn}(z) = \frac{\sigma_2(z)}{\sigma_3(z)} \tag{B.4}$$

where the Jacobi functions have elliptic parameter ν and the Weierstrass functions have periods $\omega_1 = \mathbf{K}(\nu)$ and $\omega_3 = i\mathbf{K}'(\nu)$.

Weierstrass's zeta function is defined as the logarithmic derivative of the

sigma function:

$$\zeta(z) = \frac{d}{dz}\ln(\sigma(z)) = \frac{\sigma'(z)}{\sigma(z)} \tag{B.5}$$

From (B.2) it is clear that ζ is also quasi periodic

$$\zeta(z + 2\omega_i) = 2\eta_i + \zeta(z) \qquad ; \quad i = 1, 2, 3 \quad . \tag{B.6}$$

Here η_i is given by the zeta function evaluated on the periods $z = \omega_i$:

$$\zeta(\omega_i) = \eta_i \tag{B.7}$$

Finally, the Weierstrass $\mathcal{P}$ function is defined as:

$$\mathcal{P}(z) = -\frac{d\zeta(z)}{dz} \tag{B.8}$$

$\mathcal{P}$ is doubly periodic, with periods $2\omega_1$, $2\omega_3$:

$$\mathcal{P}(z + 2\omega_i) = \mathcal{P}(z) \qquad ; \quad i = 1, 2, 3 \quad . \tag{B.9}$$

Another important property of $\mathcal{P}$ is that it satisfies the differential equation

$$\begin{aligned} \mathcal{P}'^2(z) &= 4\mathcal{P}^3(z) - g_2 P(z) - g_3 \\ &\equiv 4\left(\mathcal{P}(z) - e_1\right)\left(\mathcal{P}(z) - e_2\right)\left(\mathcal{P}(z) - e_3\right) \end{aligned} \tag{B.10}$$

This equation is the one satisfied by the amplitude squared of the condensate, following from the nonlinear Schrödinger equation. The constants g_2 and g_3 in (B.10) are known as the *invariants* and they are parameters depending on the periods. Similarly for the e_i, with $e_1 + e_2 + e_3 = 0$, and $g_2 = -4(e_1e_2 + e_2e_3 + e_1e_3)$

and $g_3 = 4e_1e_2e_3$. With our choice of periods, these can be related to the Jacobi elliptic parameter ν as:

$$e_1 = \frac{1}{3}(2-\nu) \quad ; \quad e_2 = \frac{1}{3}(2\nu - 1) \quad ; \quad e_1 = -\frac{1}{3}(1+\nu) \quad . \tag{B.11}$$

Just as the trigonometric and hyperbolic functions satisfy addition and product formulae, so too do the elliptic functions. Indeed, these elliptic identities generate all others as special cases. Here we list some of the important addition formulas for σ, ζ and $\mathcal{P}$ that we have used throughout the dissertation. References [103, 104] are particularly good concerning these identities.

$$\frac{\sigma(u+v)\sigma(u-v)}{\sigma^2(u)\sigma^2(v)} = -\mathcal{P}(u) + \mathcal{P}(v) \tag{B.12}$$

$$\frac{\sigma(u+v)\sigma(u-v)\sigma(2x)}{\sigma(u+x)\sigma(u-x)\sigma(v+x)\sigma(v-x)} = \zeta(u+x) - \zeta(u-x) - \zeta(v+x) + \zeta(v-x) \tag{B.13}$$

$$[\zeta(u+v) - \zeta(u) - \zeta(v)]^2 = \mathcal{P}(u+v) + \mathcal{P}(u) + \mathcal{P}(v) \tag{B.14}$$

$$\zeta(u+v) - \zeta(u-v) - 2\zeta(v) = \frac{\mathcal{P}'(v)}{\mathcal{P}(v) - \mathcal{P}(u)} \tag{B.15}$$

References

[1] D. J. Gross, F. Wilczek, "Asymptotically Free Gauge Theories. 1," Phys. Rev. **D8**, 3633-3652 (1973). H. D. Politzer, "Reliable Perturbative Results for Strong Interactions?," Phys. Rev. Lett. **30**, 1346-1349 (1973).

[2] J. D. Bjorken, "Asymptotic Sum Rules at Infinite Momentum," Phys. Rev. **179**, 1547-1553 (1969).

[3] K. Rajagopal and F. Wilczek, "The condensed matter physics of QCD," in *At the Frontier of Particle Physics / Handbook of QCD*, M. Shifman, ed., (World Scientific, 2001); arXiv:hep-ph/0011333.

E. V. Shuryak, "Quantum Chromodynamics and the Theory of Superdense Matter," Phys. Rept. **61**, 71-158 (1980), *The QCD vacuum, hadrons and superdense matter*, (World Scientific, 2004)

J. I. Kapusta, "Quantum Chromodynamics at High Temperature," Nucl. Phys. **B148**, 461-498 (1979).

D. J. Gross, R. D. Pisarski, L. G. Yaffe, "QCD and Instantons at Finite Temperature," Rev. Mod. Phys. **53**, 43 (1981)

R. Casalbuoni and G. Nardulli, "Inhomogeneous superconductivity in con-

densed matter and QCD," Rev. Mod. Phys. **76**, 263 (2004) [arXiv:hep-ph/0305069].

[4] Z. Fodor, S. D. Katz, "Lattice determination of the critical point of QCD at finite T and mu," JHEP **0203**, 014 (2002). [hep-lat/0106002]. F. Karsch, "Lattice QCD at high temperature and density," Lect. Notes Phys. **583**, 209-249 (2002). [hep-lat/0106019].

[5] P. de Forcrand, O. Philipsen, "The QCD phase diagram for small densities from imaginary chemical potential," Nucl. Phys. **B642**, 290-306 (2002). [hep-lat/0205016].

[6] M. A. Stephanov, K. Rajagopal, E. V. Shuryak, "Signatures of the tricritical point in QCD," Phys. Rev. Lett. **81**, 4816-4819 (1998). [hep-ph/9806219].

[7] P. Kovtun, D. T. Son, A. O. Starinets, "Viscosity in strongly interacting quantum field theories from black hole physics," Phys. Rev. Lett. **94**, 111601 (2005). [hep-th/0405231].

[8] M. G. Alford, A. Schmitt, K. Rajagopal, T. Schafer, "Color superconductivity in dense quark matter," Rev. Mod. Phys. **80**, 1455-1515 (2008). [arXiv:0709.4635 [hep-ph]].

[9] Y. Nambu and G. Jona-Lasinio, "Dynamical model of elementary particles based on an analogy with superconductivity," Phys. Rev. **122**, 345 (1961);

"Dynamical model of elementary particles based on an analogy with superconductivity. II," Phys. Rev. **124**, 246 (1961).

[10] D. J. Gross and A. Neveu, "Dynamical Symmetry Breaking In Asymptotically Free Field Theories," Phys. Rev. D **10**, 3235 (1974).

[11] G. Basar and G. V. Dunne, "Self-consistent crystalline condensate in chiral Gross-Neveu and Bogoliubov-de Gennes systems," Phys. Rev. Lett. **100**, 200404 (2008) [arXiv:0803.1501 [hep-th]].

[12] G. Basar and G. V. Dunne, "A Twisted Kink Crystal in the Chiral Gross-Neveu model," Phys. Rev. D **78**, 065022 (2008) [arXiv:0806.2659 [hep-th]].

[13] G. Basar, G. V. Dunne and M. Thies, "Inhomogeneous Condensates in the Thermodynamics of the Chiral NJL(2) model," Phys. Rev. D **79**, 105012 (2009) [arXiv:0903.1868 [hep-th]].

[14] G. Basar, G. V. Dunne and D. E. Kharzeev, "Chiral Magnetic Spiral," Phys. Rev. Lett. **104**, 232301 (2010) [arXiv:1003.3464 [hep-ph]].

[15] G. 't Hooft, "A Planar Diagram Theory for Strong Interactions," Nucl. Phys. **B72**, 461 (1974)

[16] S. Coleman, *Aspects of Symmetry*, Cambridge University Press (1988)

[17] P.C. Hohenberg, "Existence of Long-Range Order in One and Two Dimensions," Phys. Rev. **158**, 383 (1967)

N.D. Mermin, H. Wagner, "Absence of Ferromagnetism or Antiferromagnetism in One- or Two-Dimensional Isotropic Heisenberg Model," Phys. Rev. Lett. **17**, 11331136 (1966)

S. Coleman, "There are no Goldstone bosons in two dimensions," Commun. Math. Phys. **31**, 259 (1973)

[18] E. Witten, "Chiral Symmetry, The 1/N Expansion, And The SU(N) Thirring Model," Nucl. Phys. B **145**, 110 (1978);

[19] R. F. Dashen, B. Hasslacher and A. Neveu, "Semiclassical Bound States In An Asymptotically Free Theory," Phys. Rev. D **12**, 2443 (1975).

[20] S. S. Shei, "Semiclassical Bound States In A Model With Chiral Symmetry," Phys. Rev. D **14**, 535 (1976).

[21] J. Feinberg and A. Zee, "Dynamical Generation of Extended Objects in a 1 + 1 Dimensional Chiral Field Theory: Non-Perturbative Dirac Operator Resolvent Analysis," Phys. Rev. D **56**, 5050 (1997) [arXiv:cond-mat/9603173]; "Generalized supersymmetric quantum mechanics and reflectionless fermion bags in 1+1 dimensions," [arXiv:hep-th/0109045], in Olshanetsky, M. (ed.) et al. *Multiple facets of quantization and supersymmetry* (World Scientific, 2002). J. Feinberg, "All about the static fermion bags in the Gross-Neveu model," Annals Phys. **309**, 166 (2004) [arXiv:hep-th/0305240].

[22] M. Thies, "Analytical solution of the Gross-Neveu model at finite density," Phys. Rev. D **69**, 067703 (2004) [arXiv:hep-th/0308164]; O. Schnetz, M. Thies and K. Urlichs, "Phase diagram of the Gross-Neveu model: Exact results and condensed matter precursors," Annals Phys. **314**, 425 (2004) [arXiv:hep-th/0402014]. "From relativistic quantum fields to condensed matter and back again: Updating the Gross-Neveu phase diagram," J. Phys. A **39**, 12707 (2006) [arXiv:hep-th/0601049].

[23] P. G. de Gennes, *Superconductivity of Metals and Alloys* (Addison-Wesley, Redwood City, CA, 1989).

[24] T. Matsubara, "A New Approach to Quantum-Statistical Mechanics," Prog. Theor. Phys. **14**, 351 (1955)

[25] G. Eilenberger, "Transformation of Gorkov's Equation for Type II Superconductors into Transport Like Equations", Z. Phys. **214**, 195 (1968).

[26] I. Kosztin, S. Kos, M. Stone and A. J. Leggett, "Free energy of an inhomogeneous superconductor: A wave-function approach", Phys. Rev. B **58**, 9365 (1998); S. Kos and M. Stone, "Gradient expansion for the free energy of a clean superconductor ", Phys. Rev. B **59**, 9545 (1999).

[27] L. A. Dickey, *Soliton Equations and Hamiltonian Systems*, (World Scientific, Singapore, 1991).

[28] D. Waxman, "The Fredholm Determinant For A Dirac Hamiltonian With A Topological Mass Term," Annals Phys. **241**, 285 (1995).

[29] B. Horovitz, "Soliton Lattice in Polyacetylene, Spin-Peierls Systems, and Two-Dimensional Sine-Gordon Systems", Phys. Rev. Lett. **46**, 742 (1981). S. A. Brazovskii, S. A. Gordynin, and N. N. Kirova, "Exact solution of the Peierls model with an arbitrary number of electrons in the unit cell", Pis. Zh. Eksp. Teor. Fiz. **31**, 486 (1980) [JETP Lett. **31**, 456 (1980)]; "Excitons, polarons and bipolarons in conducting polymers", Pis. Zh. Eksp. Teor. Fiz. **33**, 6 (1981) [JETP Lett. **33**, 4 (1981)]; S. A. Brazovskii, N. N. Kirova and Matveenko, "Peierls effect in conducting polymers", Zh. Eksp. Teor. Fiz. **86**, 743 (1984) Sov. Phys. JETP **59**, 434 (1984). A. J. Heeger, S. Kivelson, J. R. Schrieffer and W. P. Su, "Solitons in conducting polymers," Rev. Mod. Phys. **60**, 781 (1988). D. K. Campbell and A. R. Bishop, "Soliton Excitations In Polyacetylene And Relativistic Field Theory Models," Nucl. Phys. B **200**, 297 (1982).

[30] J.P, Boucher, and L.P. Regnault "The Inorganic Spin-Peierls Compound $CuGeO_3$. J. Phys. I France **6** (1996) 1939-1966

[31] J. Hofmann, "Dimensional reduction in quantum field theories at finite temperature and density," Phys. Rev. **D82**, 125027 (2010). [arXiv:1009.4071 [hep-th]].

[32] J. Bar-Sagi and C. G. Kuper, "Self-Consistent Pair Potential in an Inhomogeneous Superconductor", Phys. Rev. Lett. **28** 1556 (1972).

[33] J. Mertsching and H. J. Fischbeck, "The incommensurate Peierls phase of the quasi-dimensional Frohlich model with a nearly half-filled band", Phys. Stat. Sol. B **103**, 783 (1981).

[34] K. Machida and H. Nakanishi, "Superconductivity under a ferromagnetic molecular field", Phys. Rev. B **30**, 122 (1984).

[35] A. I.Buzdin and V. V. Tugushev, "Phase diagrams of electronic and superconducting transitions to soliton lattice states", Zh. Eksp. Teor. Fiz. **85**, 735 (1983), [Sov. Phys. JETP **58**, 428 (1983)]; A. I.Buzdin and S. V. Polonskii, "Nonuniform State in quasi-1D superconductors", Zh. Eksp. Teor. Fiz. **93**, 747 (1987), [Sov. Phys. JETP **66**, 422 (1988)].

[36] D. Nickel and M. Buballa, "Solitonic ground states in (color-) superconductivity," Phys. Rev. D **79**, 054009 (2009) [arXiv:0811.2400 [hep-ph]]; D. Nickel, "How many phases meet at the chiral critical point?," Phys. Rev. Lett. **103**, 072301 (2009) [arXiv:0902.1778 [hep-ph]]; "Inhomogeneous phases in the Nambu-Jona-Lasino and quark-meson model," Phys. Rev. D **80**, 074025 (2009) [arXiv:0906.5295 [hep-ph]].

[37] A. I. Larkin and Y. N. Ovchinnikov, "Nonuniform state of superconductors", Zh. Eksp. Teor. Fiz. **47**, 1136 (1964) [Sov. Phys. JETP **20**, 762 (1965)];

P. Fulde and R. A. Ferrell, "Superconductivity in a Strong Spin-Exchange Field", Phys. Rev. **135**, A550 (1964).

[38] R. Jackiw and C. Rebbi, "Solitons With Fermion Number 1/2," Phys. Rev. D **13**, 3398 (1976). J. Goldstone and F. Wilczek, "Fractional Quantum Numbers On Solitons," Phys. Rev. Lett. **47**, 986 (1981). A. J. Niemi and G. W. Semenoff, "Fermion Number Fractionization In Quantum Field Theory," Phys. Rept. **135**, 99 (1986).

[39] A. O. Smirnov, "The Dirac Operator with Elliptic Potential", Sbornik Math **186**, 1213 (1995).

[40] K. Ohwa, "Crystalline ground state in chiral Gross-Neveu and Cooper pair models at finite densities," Phys. Rev. D **65**, 085040 (2002) [arXiv:hep-ph/0111074].

[41] A. Neveu and N. Papanicolaou, "Integrability Of The Classical Scalar And Symmetric Scalar-Pseudoscalar Contact Fermi Interactions In Two-Dimensions," Commun. Math. Phys. **58**, 31 (1978).

[42] A. Klotzek and M. Thies, "Kink dynamics, sinh-Gordon solitons and strings in AdS(3) from the Gross-Neveu model," J. Phys. A **43**, 375401 (2010) [arXiv:1006.0324 [hep-th]].

[43] G. Basar, G. V. Dunne, "Gross-Neveu Models, Nonlinear Dirac Equations, Surfaces and Strings," JHEP **1101**, 127 (2011). [arXiv:1011.3835 [hep-th]]

[44] F. Karbstein and M. Thies, "Divergence of the axial current and fermion density in Gross-Neveu models," Phys. Rev. D **76**, 085009 (2007) [arXiv:0706.0424 [hep-th]].

[45] L. McLerran, R. D. Pisarski, "Phases of cold, dense quarks at large N(c)," Nucl. Phys. **A796**, 83-100 (2007). [arXiv:0706.2191 [hep-ph]].

[46] T. Kojo, Y. Hidaka, L. McLerran, R. D. Pisarski, "Quarkyonic Chiral Spirals," Nucl. Phys. **A843**, 37-58 (2010). [arXiv:0912.3800 [hep-ph]]. T. Kojo, R. D. Pisarski, A. M. Tsvelik, "Covering the Fermi Surface with Patches of Quarkyonic Chiral Spirals," Phys. Rev. **D82**, 074015 (2010). [arXiv:1007.0248 [hep-ph]].

[47] V. Schon and M. Thies, "Emergence of Skyrme crystal in Gross-Neveu and 't Hooft models at finite density," Phys. Rev. D **62**, 096002 (2000) [arXiv:hep-th/0003195]; "2D model field theories at finite temperature and density," [arXiv:hep-th/0008175], in Shifman, M. (ed.), *At the frontier of particle physics*, Vol. 3 (World Scientific).

[48] U. Wolff, "The phase diagram of the infinite-N Gross-Neveu Model at finite temperature and chemical potential", Phys. Lett. **157B**, 303 (1985).

[49] T. F. Treml, "Dynamical Mass Generation In The Gross-Neveu Model At Finite Temperature And Density," Phys. Rev. D **39**, 679 (1989).

[50] F. Karsch, J. B. Kogut and H. W. Wyld, "The Gross-Neveu Model At Finite Temperature And Density," Nucl. Phys. B **280**, 289 (1987).

[51] P. de Forcrand and U. Wenger, "New baryon matter in the lattice Gross-Neveu model," PoS **LAT2006**, 152 (2006) [arXiv:hep-lat/0610117].

[52] M. Limmer, C. Gattringer and V. Hermann, "Fermion loop simulations in 2–d lattice theories – results and limitations," PoS **LAT2007**, 268 (2007) [arXiv:0710.2794 [hep-lat]].

[53] U. Wolff, "Cluster simulation of relativistic fermions in two space-time dimensions," Nucl. Phys. B **789**, 258 (2008) [arXiv:0707.2872 [hep-lat]].

[54] K. Langfeld, G. Dunne, H. Gies and K. Klingmuller, "Worldline Approach to Chiral Fermions," PoS **LAT2007**, 202 (2007) [arXiv:0709.4595 [hep-lat]]. "Worldline Monte Carlo for fermion models at large N_f", to appear.

[55] C. Boehmer, M. Thies and K. Urlichs, "Tricritical behavior of the massive chiral Gross-Neveu model," Phys. Rev. D **75**, 105017 (2007) [arXiv:hep-th/0702201].

[56] A. I. Buzdin and H. Kachkachi, "Generalized Ginzburg-Landau theory for nonuniform FFLO superconductors", Phys. Lett. A **225**, 341 (1997).

[57] K. Urlichs, unpublished notes (2007).

[58] M. J. Ablowitz, D. J. Kaup, A. C. Newell and H. Segur, "The Inverse scattering transform fourier analysis for nonlinear problems," Stud. Appl. Math. **53**, 249 (1974).

[59] F. Correa, G. V. Dunne, M. S. Plyushchay, "The Bogoliubov/de Gennes system, the AKNS hierarchy, and nonlinear quantum mechanical supersymmetry," Annals Phys. **324**, 2522-2547 (2009). [arXiv:0904.2768 [hep-th]].

[60] P. D. Lax, "Integrals Of Nonlinear Equations Of Evolution And Solitary Waves," Commun. Pure Appl. Math. **21**, 467 (1968).

[61] F. Gesztesy and H. Holden, *Soliton Equations and their Algebro-Geometric Solutions*, (Cambridge University Press, 2003).

[62] D.J. Korteweg and F. de Vries, ''On the Change of Form of Long Waves Advancing in a Rectangular Canal, and on a New Type of Long Stationary Waves," Philos. Mag. **39**, 422-443, (1895).

[63] R.M. Miura, "Korteweg-de Vries Equation and Generalizations. I. A Remarkable Explicit Nonlinear Transformation," J. Math. Phys. **9**, 1202-1204, (1968).

[64] R. Peierls, *The Quantum Theory of Solids* (Oxford, 1955), *More Surprises in Theoretical Physics* (Princeton, 1991)

[65] B. Bringoltz, "Chiral crystals in strong-coupling lattice QCD at nonzero chemical potential," JHEP **0703**, 016 (2007) [arXiv:hep-lat/0612010]. "Solving two-dimensional large-N QCD with a nonzero density of baryons and arbitrary quark mass," Phys. Rev. D **79**, 125006 (2009) [arXiv:0901.4035 [hep-lat]].

[66] D. Ebert, K. G. Klimenko, A. V. Tyukov and V. C. Zhukovsky, "Finite size effects in the Gross-Neveu model with isospin chemical potential," Phys. Rev. D **78**, 045008 (2008) [arXiv:0804.4826 [hep-ph]]; D. Ebert and K. G. Klimenko, "Pion condensation in the Gross-Neveu model with nonzero baryon and isospin chemical potentials," arXiv:0902.1861 [hep-ph].

[67] D. Ebert, N. V. Gubina, K. G. Klimenko, S. G. Kurbanov, V. C. .Zhukovsky, "Chiral density waves in the NJL_2 model with quark number and isospin chemical potentials,"

[68] B. I. Abelev *et al.* [STAR Collaboration], "Azimuthal Charged-Particle Correlations and Possible Local Strong Parity Violation," Phys. Rev. Lett. **103**, 251601 (2009) [arXiv:0909.1739 [nucl-ex]].

[69] B. I. Abelev *et al.* [STAR Collaboration], "Observation of charge-dependent azimuthal correlations and possible local strong parity violation in heavy ion collisions," arXiv:0909.1717 [nucl-ex].

[70] D. Kharzeev, "Parity violation in hot QCD: Why it can happen, and how to look for it," Phys. Lett. B **633**, 260 (2006) [arXiv:hep-ph/0406125].

[71] D. Kharzeev and A. Zhitnitsky, "Charge separation induced by P-odd bubbles in QCD matter," Nucl. Phys. A **797**, 67 (2007) [arXiv:0706.1026 [hep-ph]].

[72] D. E. Kharzeev, L. D. McLerran and H .J. Warringa, "The effects of topological charge change in heavy ion collisions: 'Event by event P and CP violation'," Nucl. Phys. A **803**, 227 (2008);

[73] K. Fukushima, D. E. Kharzeev and H. J. Warringa, "The Chiral Magnetic Effect," Phys. Rev. D **78**, 074033 (2008) [arXiv:0808.3382 [hep-ph]].

[74] D. E. Kharzeev, "Topologically induced local P and CP violation in QCD x QED," Annals Phys. **325**, 205 (2010) [arXiv:0911.3715 [hep-ph]].

[75] V. Skokov, A. Y. Illarionov and V. Toneev, "Estimate of the magnetic field strength in heavy-ion collisions," Int. J. Mod. Phys. A **24**, 5925 (2009) [arXiv:0907.1396 [nucl-th]].

[76] J. Liao and E. Shuryak, "Strongly coupled plasma with electric and magnetic charges," Phys. Rev. C **75**, 054907 (2007) [arXiv:hep-ph/0611131].

[77] M. N. Chernodub, A. D'Alessandro, M. D'Elia and V. I. Zakharov, "Thermal

monopoles and selfdual dyons in the Quark-Gluon Plasma," arXiv:0909.5441 [hep-ph].

[78] P. V. Buividovich, M. N. Chernodub, E. V. Luschevskaya and M. I. Polikarpov, "Numerical evidence of chiral magnetic effect in lattice gauge theory," Phys. Rev. D **80**, 054503 (2009) [arXiv:0907.0494 [hep-lat]].

[79] M. Abramczyk, T. Blum, G. Petropoulos and R. Zhou, "Chiral magnetic effect in 2+1 flavor QCD+QED," arXiv:0911.1348 [hep-lat].

[80] D. T. Son and A. R. Zhitnitsky, "Quantum anomalies in dense matter," Phys. Rev. D **70**, 074018 (2004) [arXiv:hep-ph/0405216].

[81] M. A. Metlitski and A. R. Zhitnitsky, "Anomalous axion interactions and topological currents in dense matter," Phys. Rev. D **72**, 045011 (2005) [arXiv:hep-ph/0505072].

[82] D. T. Son and P. Surowka, "Hydrodynamics with Triangle Anomalies," Phys. Rev. Lett. **103**, 191601 (2009) [arXiv:0906.5044 [hep-th]].

[83] P. V. Buividovich, M. N. Chernodub, D. E. Kharzeev, T. Kalaydzhyan, E. V. Luschevskaya and M. I. Polikarpov, 'Magnetic-Field-Induced insulator-conductor transition in SU(2) quenched lattice gauge theory," arXiv:1003.2180 [hep-lat].

[84] V. P. Gusynin, V. A. Miransky and I. A. Shovkovy, "Dimensional reduction

and catalysis of dynamical symmetry breaking by a magnetic field," Nucl. Phys. B **462**, 249 (1996) [arXiv:hep-ph/9509320].

[85] E. V. Gorbar, V. A. Miransky and I. A. Shovkovy, "Chiral asymmetry of the Fermi surface in dense relativistic matter in a magnetic field," Phys. Rev. C **80**, 032801 (2009) [arXiv:0904.2164 [hep-ph]].

[86] S. L. Adler, "Axial vector vertex in spinor electrodynamics," Phys. Rev. **177**, 2426 (1969).

[87] J. S. Bell and R. Jackiw, "A PCAC puzzle: $\pi^0 \to \gamma\gamma$ in the sigma model," Nuovo Cim. A **60**, 47 (1969).

[88] R. Jackiw, "Topological Investigations Of Quantized Gauge Theories," in Les Houches Summer School, *Relativity Grops and Topology*, B. S. DeWitt and R. Stora (Eds) (North-Holland, 1984).

[89] H. B. Nielsen and M. Ninomiya, "Adler-Bell-Jackiw Anomaly And Weyl Fermions In Crystal," Phys. Lett. B **130**, 389 (1983).

[90] A. Bzdak, V. Koch, J. Liao, "Remarks on possible local parity violation in heavy ion collisions," arXiv:0912.5050 [nucl-th].

[91] D. Kharzeev, R. D. Pisarski and M. H. G. Tytgat, "Possibility of spontaneous parity violation in hot QCD," Phys. Rev. Lett. **81**, 512 (1998) [arXiv:hep-ph/9804221].

[92] K. -Y. Kim, B. Sahoo, H. -U. Yee, "Holographic chiral magnetic spiral," JHEP **1010**, 005 (2010). [arXiv:1007.1985 [hep-th]].

[93] K. G. Klimenko, "Phase Structure Of Generalized Gross-Neveu Models," Z. Phys. C **37**, 457 (1988); S. Hands, A. Kocic and J. B. Kogut, "The Four Fermi Model In Three-Dimensions At Nonzero Density And Temperature," Nucl. Phys. B **390**, 355 (1993) [arXiv:hep-lat/9206024].

[94] R. Casalbuoni, R. Gatto, N. Ippolito, G. Nardulli and M. Ruggieri, "Ginzburg-Landau approach to the three flavor LOFF phase of QCD," Phys. Lett. B **627**, 89 (2005) [Erratum-ibid. B **634**, 565 (2006)] [arXiv:hep-ph/0507247].

[95] M. Mannarelli, K. Rajagopal and R. Sharma, "Testing the Ginzburg-Landau approximation for three-flavor crystalline color superconductivity," Phys. Rev. D **73**, 114012 (2006) [arXiv:hep-ph/0603076].

[96] I. R. Klebanov, "Nuclear Matter In The Skyrme Model," Nucl. Phys. B **262**, 133 (1985).

[97] A. S. Goldhaber and N. S. Manton, "Maximal Symmetry Of The Skyrme Crystal," Phys. Lett. B **198**, 231 (1987).

[98] A. D. Jackson and J. J. M. Verbaarschot, "Phase structure of the Skyrme model," Nucl. Phys. A **484**, 419 (1988); L. Castillejo, P. S. J. Jones,

A. D. Jackson, J. J. M. Verbaarschot and A. Jackson, "Dense Skyrmion Systems," Nucl. Phys. A **501**, 801 (1989).

[99] N. S. Manton and P. M. Sutcliffe, "Skyrme crystal from a twisted instanton on a four torus," Phys. Lett. B **342**, 196 (1995) [arXiv:hep-th/9409182].

[100] B. Bringoltz, "Chiral crystals in strong-coupling lattice QCD at nonzero chemical potential," JHEP **0703**, 016 (2007) [arXiv:hep-lat/0612010].

[101] I. Abramowitz and I. Stegun, *Handbook of mathematical functions*, (Dover, New York, 2000).

[102] E. T. Whittaker and G. N. Watson, *Modern Analysis*, (Cambridge University Press, 1962).

[103] N. I. Akhiezer, *Elements of the theory of elliptic functions*, (American Mathematical Society Translations, Providence, 1980).

[104] D. F. Lawden, *Elliptic Functions and Applications*, (Springer-Verlag, New York, 1980).